

Spring 2010

Volatile organic compounds in the New England troposphere: Atmospheric chemistry and measurement techniques

Jesse L. Ambrose

University of New Hampshire, Durham

Follow this and additional works at: <https://scholars.unh.edu/dissertation>

Recommended Citation

Ambrose, Jesse L., "Volatile organic compounds in the New England troposphere: Atmospheric chemistry and measurement techniques" (2010). *Doctoral Dissertations*. 580.
<https://scholars.unh.edu/dissertation/580>

This Dissertation is brought to you for free and open access by the Student Scholarship at University of New Hampshire Scholars' Repository. It has been accepted for inclusion in Doctoral Dissertations by an authorized administrator of University of New Hampshire Scholars' Repository. For more information, please contact nicole.hentz@unh.edu.

VOLATILE ORGANIC COMPOUNDS IN THE NEW ENGLAND TROPOSPHERE:
ATMOSPHERIC CHEMISTRY AND MEASUREMENT TECHNIQUES

BY

JESSE L. AMBROSE

B.S., Chemistry, University of New Hampshire, 2004

DISSERTATION

Submitted to the University of New Hampshire

in Partial Fulfillment of

the Requirements for the Degree of

Doctor of Philosophy

in

Chemistry

May, 2010

UMI Number: 3470087

All rights reserved

INFORMATION TO ALL USERS

The quality of this reproduction is dependent upon the quality of the copy submitted.

In the unlikely event that the author did not send a complete manuscript and there are missing pages, these will be noted. Also, if material had to be removed, a note will indicate the deletion.



UMI 3470087

Copyright 2010 by ProQuest LLC.

All rights reserved. This edition of the work is protected against unauthorized copying under Title 17, United States Code.



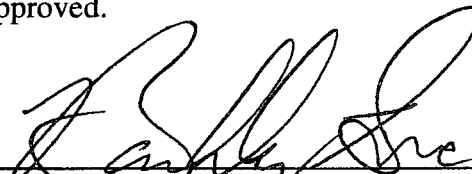
ProQuest LLC
789 East Eisenhower Parkway
P.O. Box 1346
Ann Arbor, MI 48106-1346

ALL RIGHTS RESERVED

c 2010

Jesse L. Ambrose

This dissertation has been examined and approved.



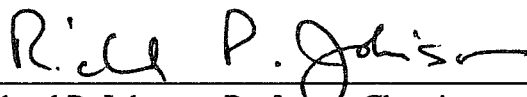
Dissertation Director, Barkley C. Sive, Research
Associate Professor, Climate Change Research
Center



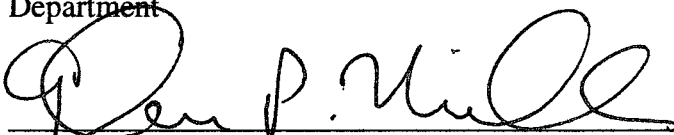
Howard R. Mayne, Professor, Chemistry
Department



Robert W. Talbot, Director, Climate Change
Research Center



Richard P. Johnson, Professor, Chemistry
Department



Glen P. Miller, Professor, Chemistry Department

December 10, 2009

Date

ACKNOWLEDGMENTS

Financial support for this work was provided through the Office of Oceanic and Atmospheric Research at the National Oceanic and Atmospheric Administration under grants #NA04OAR4600154, #NA05OAR4601080 and #NA06OAR4600189. Additional support was provided thorough the University of New Hampshire Chemistry Department under the Ingram Award and through the UNH College of Engineering and Physical Sciences under the John B. and Martha M. W. Zocchi Scholarship and the John H. Smith Scholarship.

I thank my advisors, Dr. Sive and Dr. Mayne, for their generosity, patience and enthusiasm. I am honored to have had the opportunity to participate in their research and will always be grateful for their mentorship and their friendship.

I also thank my family, especially my parents, for their support and encouragement of all my endeavors.

TABLE OF CONTENTS

ACKNOWLEDGMENTS.....	iv
LIST OF TABLES.....	ix
LIST OF FIGURES.....	x
ABSTRACT.....	xii

CHAPTER	PAGE
---------	------

INTRODUCTION.....	1
I. NIGHTTIME NITRATE RADICAL CHEMISTRY AT APPLIEDORE ISLAND, MAINE.....	3
I.1. Introduction.....	3
I.2. Experimental Methods.....	6
I.2.1. Trace Gas Measurements.....	7
I.2.2. Analysis Methods.....	9
I.3. Results and Discussion.....	12
I.3.1. Kinetic Comparison of Gas-Phase Nighttime NO ₃ Loss Processes....	12
I.3.2. Nocturnal Chemistry Case Studies.....	15
I.3.2.1. Clean Marine Flow on July 13 and 14.....	15
I.3.2.2. Polluted Continental Outflow on July 11.....	16
I.3.2.3. Polluted Continental Outflow on July 16.....	18

I.3.2.4.	Polluted and Biogenic Continental Outflow on July 25...	20
I.3.3.	Measured versus Calculated NO ₃ Time Series Profiles.....	22
I.3.4.	Heterogeneous Nighttime NO ₃ Loss: Uptake of N ₂ O ₅ by Aerosols/Ocean Surface.....	24
I.3.5.	Daytime versus Nighttime NO _x Removal.....	29
I.4.	Summary.....	31
II.	INTERCOMPARISON OF GC-FID AND PTR-MS TOLUENE MEASUREMENTS.....	34
II.1.	Introduction.....	34
II.2.	Methods.....	37
II.2.1.	Experimental.....	37
II.2.2.	Calculations.....	41
II.3.	Results and Discussion.....	44
II.3.1.	Monoterpene Distributions.....	44
II.3.2.	GC-FID/PTR-MS Toluene Field Intercomparison.....	48
II.3.3.	Sources of Interference from Monoterpene Fragmentation.....	50
II.3.3.1.	Reactions with H ₃ O ⁺	52
II.3.3.2.	Reactions with O ₂ ⁺ and NO ⁺	55
II.3.4.	Sources of Interference from Monoterpene Oxidation Products.....	57
II.3.4.1.	Ozonolysis Products.....	58
II.3.4.2.	Photooxidation products.....	59
II.3.5.	Additional Contributions to PTR-MS Signal at <i>m/z</i> = 93.....	63
II.3.5.1.	Chloroacetone.....	64
II.3.5.2.	Proton-bound Ethanol Dimer ((EtOH) ₂ + H) ⁺	65
II.4.	Summary.....	65

III. DEVELOPMENT OF A GAS CHROMATOGRAPHIC SYSTEM FOR MEASUREMENT OF HYDROGEN CYNAIDE IN THE LOWER ATMOSPHERE.....	69
III.1. Introduction.....	69
III.2. Experimental.....	72
III.2.1. Measurement Site Location.....	72
III.2.2. Configuration of the GC-FTD Instrument.....	73
III.2.3. Instrument Development.....	76
III.2.3.1. PDHID Experiments.....	76
III.2.3.2. FID Experiments.....	77
III.2.3.3. Preparation of an Acetonitrile Qualitative Standard.....	78
III.3. Results and Discussion.....	79
III.3.1. Sample Dehumidification and Enrichment.....	79
III.3.2. Results with PDHID and FID.....	81
III.3.2.1. Response Comparison between PDHID and FID.....	81
III.3.2.2. Response of the PDHID to Permanent Gases.....	83
III.3.2.3. Blank Measurement with PDHID.....	84
III.3.2.4. Long Term Stability of PDHID Response.....	86
III.3.3. Results with FTD.....	88
III.3.3.1. Dependence of Response on Detector Bead Voltage.....	88
III.3.3.2. Response Comparison and MDL.....	89
III.3.3.3. Carrier Gas Flow Rate.....	90
III.3.3.4. Influence of Injection Parameters on HCN Chromatographic Analysis.....	90
III.3.3.5. Ambient Air Analysis with GC-FTD Instrument.....	91

III.3.3.6. Qualitative Identification of Acetonitrile (CH ₃ CN) in Ambient Air Samples.....	92
III.4. Summary.....	93
LIST OF REFERENCES.....	144

LIST OF TABLES

1. Measurement details for atmospheric observations at AI during the ICARTT campaign.....	96
2. Rate data applicable to nighttime gas-phase NO ₃ chemistry and pertaining to the chemical variables monitored at AI during the ICARTT campaign.....	97
3. Comparison between rates of NO _x loss and HNO ₃ production from NO ₃ and N ₂ O ₅ mechanisms for selected times during the ICARTT campaign.....	99
4. Operational and quality parameters for analytical systems operated at THF during summer 2004 and from which measurements were used in this work.....	100
5. Comparison between monoterpene emission fluxes calculated by <i>Geron et al.</i> [2000] for forestland encompassing the THF site and relative monoterpene abundances from mixing ratios measured by GC-FID at THF between July 24 and August 15, 2004.....	101
6. Measured retention times for C ₉ –C ₁₁ hydrocarbons in the THF GC system primary working standard that eluted between nonane and undecane on the VF-5ms column together with predicted retention times for several additional monoterpenes.....	102
7. Quantitative comparison of GC-FID and PTR-MS toluene measurements for different monoterpene fragmentation corrections applied to the PTR-MS data.....	103
8. Comparison of reported yields of <i>m/z</i> = 93 fragment ions associated with analysis of monoterpenes by PTR-MS and SIFT-MS.....	104
9. Comparison of PTR-MS operating parameters employed at THF during summer of 2004 and in selected studies reported in the literature.....	105
10. Comparison of reported yields of <i>m/z</i> = 93 fragment ions associated with analysis of monoterpene oxidation products by PTR-MS and SIFT-MS.....	106
11. Operational protocol of the GC-FTD instrument.....	107
12. Sample volumes (at standard temperature and pressure) required to yield HCN masses greater than the PDHID, FID and FTD MDL.....	108

LIST OF FIGURES

1. Time series of selected trace gases measured between noon on July 8 and noon on July 28.....	110
2. Relative biogenic reactivity calculated for the nighttime hours between 21:00 on July 8 and 05:00 on July 28.....	111
3. Absolute reactivity of DMS, monoterpenes and isoprene calculated for the nighttime hours between 21:00 on July 8 and 05:00 on July 28.....	112
4. HYSPLIT trajectories for selected case study periods.....	113
5. Atmospheric composition and chemistry on the night of July 11.....	114
6. Atmospheric composition and chemistry on the night of July 16.....	115
7. Atmospheric composition and chemistry on the night of July 25.....	116
8. Measured versus calculated NO ₃ mixing ratios.....	117
9. Average relative contributions of gas-phase and heterogeneous mechanisms to NO _x removal for the period July 8–28.....	118
10. Linear correlation between elution order (retention time) and boiling point for C ₉ –C ₁₁ compounds in the THF GC system primary working standard that eluted from the VF-5ms column between nonane and undecane.....	119
11. Portion of a chromatogram from the THF GC system primary working standard...	120
12. Portion of a chromatogram recorded at THF at 04:23 on August 3 during a period of enhanced monoterpene mixing ratios.....	121
13. Comparison of trends in the mixing ratios of α -pinene and an unidentified (UnID) compound (assumed to be C ₁₀) during the period from 12:00 on August 2 to 12:00 on August 3.....	122
14. Time series of monoterpenes, $J(\text{NO}_2)$ and wind speed measured at THF from 22:00 on July 24 to 06:00 on August 15.....	123
15. Time series of toluene measured by GC-FID and PTR-MS during the period between 22:00 on July 24 to 06:00 on August 15.....	124

16. Linear correlation between toluene measurements by GC-FID and PTR-MS.....	125
17. Comparison between values of $\epsilon_{\text{PTR-MS}}$ and Δ_{Mon} for merged GC-FID, PTR-MS data for the period from 22:00 on July 24 to 06:00 on August 15.....	126
18. Schematic of the GC-FTD system.....	127
19. Schematic of the instrument configurations employed for development of HCN sampling and detection schemes.....	128
20. Schematic of the instrument configuration used for preliminary testing of both the PDHID and FTD.....	129
21. Water vapor trapping efficiency in the sample dehumidification loop as a function of T1 temperature.....	130
22. HCN trapping efficiency as a function of sample enrichment loop temperature.....	131
23. Chromatograms recorded with the PDHID for blank and standard samples prepared with the Cryofocus System.....	132
24. Configurations of standard dilution system used for blank response attribution.....	133
25. Comparison of measured blank HCN chromatographic peak areas with those calculated using an HCN desorption model.....	134
26. Observed variation in PDHID response as a function of sample injection number..	135
27. Response of the FTD to HCN as a function of bead voltage.....	136
28. Carrier gas flow rate measurements.....	137
29. Comparison between standard chromatograms recorded over a range of injection temperatures.....	138
30. Chromatographic peak areas measured for standard samples analyzed during a period of continuous operation between April 2 and 9, 2009.....	139
31. De-trended measurements from Figure 30.....	140
32. Calibration curve constructed from de-trended standard and blank measurements made between April 2 and 9, 2009.....	141
33. Time series of ambient HCN VMR measured between April 2 and 9, 2009.....	142
34. Qualitative identification of CH_3CN in ambient air.....	143

ABSTRACT

VOLATILE ORGANIC COMPOUNDS IN THE NEW ENGLAND TROPOSPHERE: ATMOSPHERIC CHEMISTRY AND MEASUREMENT TECHNIQUES

by

Jesse L. Ambrose

University of New Hampshire, May, 2010

Atmospheric measurements made at Appledore Island, Maine were used to investigate nighttime nitrate radical (NO_3) chemistry and its significance for the nitrogen oxides ($\text{NO}_x = \text{NO} + \text{NO}_2$) budget in the Gulf of Maine region during the summer of 2004 International Consortium for Atmospheric Research on Transport and Transformation field campaign. Removal of NO_x was strongly dependent on reactions of NO_3 with biogenic volatile organic compounds and the fate of dinitrogen pentoxide (N_2O_5). For three case studies, temporal profiles of NO_3 were calculated from measured parameters. Comparisons between measured and calculated NO_3 mixing ratios highlighted significant uncertainties in the kinetic parameters governing gas-phase and heterogeneous N_2O_5 hydrolysis. Removal of NO_x was estimated to be $\sim 11 \text{ ppbv day}^{-1}$, with nighttime chemical pathways contributing $\sim 50\%$.

Atmospheric measurements made at the AIRMAP atmospheric monitoring station Thompson Farm (THF) during summer, 2004 were used to test the specificity of a proton transfer reaction-mass spectrometer (PTR-MS) for atmospheric toluene measurements under conditions often dominated by biogenic emissions. Quantitative estimates were

made of potential interferences in the PTR-MS toluene measurements related to sampling and analysis of monoterpenes, including fragmentation of the monoterpenes and some of their primary carbonyl oxidation products in the PTR-MS drift tube. The analysis supported only minor interferences from the investigated fragmentation sources, suggesting that toluene can be reliably quantified by PTR-MS with the operating parameters used, under the ambient compositions probed. This work extends the range of field conditions under which PTR-MS validation studies have been conducted.

A GC instrument was developed for measurement of hydrogen cyanide (HCN) in the lower atmosphere. Its major features include a cold temperature analyte enrichment system, a robust porous polymer stationary phase capillary column and a flame thermionic detector. The instrument was deployed for a 1 week period in April, 2009 at THF. Measured HCN mixing ratios ranged between 0.07(3) and 0.33(3) ppbv, with significant temporal variability, and appeared to agree well with previous tropospheric measurements. Long term, in-situ atmospheric measurement of HCN is necessary to characterize the regional HCN budget and reduce uncertainty in the global budget. Few such measurements have been demonstrated at present.

INTRODUCTION

The troposphere extends from Earth's surface to the tropopause, the boundary at ~12 km altitude (at mid-latitudes) between the troposphere and stratosphere [*Brasseur and Schimel*, 1999]. Its compositional complexity and direct interaction with Earth's surface make the troposphere a particularly challenging and exciting area for atmospheric investigation. The lower troposphere, consisting of the first few km above the surface and often referred to as the planetary boundary layer (PBL) [*Brasseur et al.*, 1999], is directly impacted by most of the natural and anthropogenic sources that emit trace gases and aerosols to the atmosphere. It is also the region where issues of air quality, including photochemical smog, ozone and fine particulate matter pollution are most relevant. Beyond their effects on human health many of the trace species emitted to the atmosphere at Earth's surface also influence regional and global climate [*IPCC*, 2007].

Our knowledge of the composition and chemistry of the troposphere is far from complete [*Goldstein and Galbally*, 2007; *Heald et al.*, 2008]. Continued effort is necessary to accurately describe the present composition of the troposphere, the temporal evolution of tropospheric composition and the corresponding climate responses and feedbacks. Such work is critically needed to address both current and possible future deleterious anthropogenic modifications of air quality and climate. Two important current directions in atmospheric research, relevant to the composition and chemistry of the troposphere, include (1) describing the budgets of the primary oxidants, the hydroxyl radical (OH), ozone (O₃) and the nitrate radical (NO₃) [*Brown et al.*, 2006a,b; *Rohrer and*

Berresheim, 2006], and (2) developing measurement techniques for the multitude of trace atmospheric constituents [*Apel et al., 2003a; Sive et al., 2005; Sullivan and Prather, 2005; de Gouw and Warneke, 2007*].

The present work primarily concerns the abundances, chemistry and accurate quantitative measurement of selected volatile organic compounds in the PBL at the University of New Hampshire's AIRMAP atmospheric monitoring stations, Thompson Farm (THF) and Appledore Island (AI). Three separate projects were carried out and are described in the following chapters. For the first project (Chapter I) an extensive set of atmospheric observations made during the summer of 2004 International Consortium for Atmospheric Research on Transport and Transformation field campaign was used to describe nighttime NO_3 chemistry at AI. For the second (Chapter II) atmospheric observations at THF were used to quantify potential interferences in measurement of toluene by proton transfer reaction-mass spectrometry related to sampling of biogenic monoterpene compounds. Finally, Chapter III describes the development of a gas-chromatographic instrument for measurement of hydrogen cyanide.

CHAPTER I.

NIGHTTIME NITRATE RADICAL CHEMISTRY

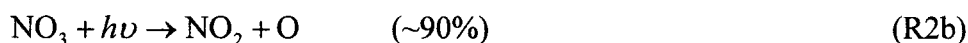
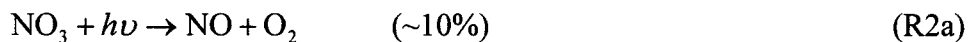
AT APPLEDORE ISLAND, MAINE

I.1. Introduction

The hydroxyl radical (OH), nitrate radical (NO₃) and ozone molecule (O₃) are the most important gas phase oxidants of volatile organic compounds (VOCs) and nitrogen oxides (NO_x = NO + NO₂) in the troposphere. Both OH and O₃ have primary photochemical sources, and OH is the most important daytime oxidant. NO₃ is produced exclusively by the reaction of NO₂ with O₃,



and is highly photo-labile with limited oxidative capacity during the daytime due to rapid photolysis via

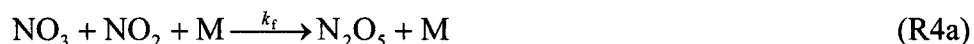


and reaction with NO,



[Atkinson, 2000; Geyer *et al.*, 2001; Geyer and Platt, 2002; Brown *et al.*, 2003a]. At night, the production rate of NO₃ far exceeds that of OH, and NO₃ is generally several orders of magnitude more reactive toward VOCs and NO_x than O₃ [e.g., Atkinson, 2000].

During the nighttime, NO₃ is directly removed from the atmosphere by reactions with VOCs and NO. For saturated VOCs, dimethylsulfide (DMS), the oxygenated VOCs (OVOCs), and aromatics, NO₃-initiated degradation proceeds mostly via hydrogen-atom abstraction to generate nitric acid (HNO₃) and peroxy radicals. For unsaturated VOCs including isoprene, the alkenes and monoterpenes, reaction with NO₃ proceeds mostly via initial NO₃ addition at unsaturated sites with the initial products being nitrooxy peroxy radicals. Biogenic VOCs, such as isoprene, monoterpenes and DMS [Allan *et al.*, 2000; Geyer *et al.*, 2001; Warneke *et al.*, 2004; Aldener *et al.*, 2006] are particularly important reactants for NO₃. Because NO is rapidly oxidized to NO₂ by reaction with O₃ after dark [Allan *et al.*, 2000], it is generally an important reactant for NO₃ only in the proximity of sources [Platt and Janssen, 1995; Brown *et al.*, 2003a; Stutz *et al.*, 2004]. Also important to nighttime NO₃ chemistry is the reversible reaction of NO₃ with NO₂ to generate dinitrogen pentoxide (N₂O₅),

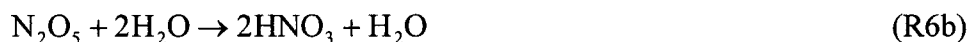


where k_f and k_r are the rate coefficients for reactions (R4a) and (R4b), respectively. The NO₃-NO₂-N₂O₅ system equilibrates rapidly after dark [Atkinson, 2000; Geyer *et al.*, 2001; Brown *et al.*, 2003b]. The removal of N₂O₅ is generally expected to be governed by heterogeneous chemistry (i.e., reaction of N₂O₅ on or within aerosol particles),



and likely depends strongly on aerosol composition [e.g., Folkers, *et al.*, 2003; Hallquist *et al.*, 2003; Thornton *et al.*, 2003; Thornton and Abbatt, 2005; Brown *et al.*, 2006a].

Gas-phase reactions of N₂O₅ with water vapor have also been demonstrated [*Wahner et al.*, 1998],



although their overall importance in the chemistry of the atmosphere remains a topic of considerable uncertainty [*Heintz et al.*, 1996; *Martinez et al.*, 2000; *Atkinson et al.*, 2004; *Stutz et al.*, 2004; *Aldener et al.*, 2006; *Brown et al.*, 2006a].

The reactivity of NO₃ can influence nighttime and early morning abundances of VOCs and NO_x, and thus photochemical production of O₃. How efficiently NO₃ mediates the removal of VOCs and NO_x from the atmosphere depends strongly on the abundance of NO_x [*Platt and Janssen*, 1995] and the sinks for N₂O₅ [*Brown et al.*, 2003a; *Warneke et al.*, 2004; *Brown et al.*, 2006b]. Accordingly, nighttime NO₃ chemistry is significantly different in urban versus rural and continental versus marine environments, and varies considerably with season of the year [*Platt and Janssen*, 1995; *Heintz et al.*, 1996; *Geyer and Platt*, 2002; *Vrekoussis et al.*, 2007].

The New England (NE) coastal marine boundary layer (MBL) is a unique environment for studying nighttime NO₃ chemistry. It is a corridor for mixing of air masses of both marine and continental origin, and consequently ambient conditions vary from those characteristic of the remote Atlantic to being dominated by strong continental biogenic and anthropogenic sources. Measurements of NO₃ in this region were previously limited to the 2002 New England Air Quality Study [*Brown et al.*, 2004; *Warneke et al.*, 2004; *Aldener et al.*, 2006], which demonstrated that during the summer months nighttime NO₃ chemistry competes with daytime OH chemistry in controlling the

NO_x budget [*Brown et al.*, 2004] and isoprene oxidation [*Warneke et al.*, 2004]. The nighttime abundances of NO₃ and monoterpenes were also closely coupled [*Warneke et al.*, 2004; *Aldener et al.*, 2006]. Hydrolysis of N₂O₅ and reactions of NO₃ with VOCs were shown to contribute roughly equally to nighttime NO₃ removal [*Aldener et al.*, 2006].

In this study we utilize measurements of a suite of trace gasses, including NO₂, NO₃, O₃, and VOCs, and relevant meteorological parameters within the coastal Gulf of Maine MBL at the University of New Hampshire (UNH) AIRMAP Observing Station on Appledore Island (AI) (<http://www.airmap.unh.edu>) during the 2004 International Consortium for Atmospheric Research on Transport and Transformation (ICARTT). (See *Fehsenfeld et al.* [2006] for an overview of the ICARTT campaign.) Our goals were to quantify the gas-phase chemistry that governed the observed nocturnal behavior of NO₃ and to estimate the contribution of heterogeneous N₂O₅ chemistry to NO₃ and NO_x removal.

I.2. Experimental Methods

Routine measurements of CO, NO, and O₃ at AI, ME (42° 59' 13"N, 70° 36' 55"W) have been made seasonally (May to October) from the top story (~40 m asl) of a World War II-era surveillance tower since 2002 as part of the UNH AIRMAP Observing Network. The tower was equipped for measurements of an extensive suite of chemical parameters for the ICARTT campaign. The subset of measurements incorporated into this analysis, together with the experimental details of the instrumentation deployed

during ICARTT, is summarized in Table 1. Additionally, meteorological variables were monitored at the National Data Buoy Center Coastal-Marine Automated Network station (IOSN3) on White Island (42° 58' 00"N, 70° 37' 24"W, 15 m asl) [National Data Buoy Center, 2004] located 2.3 km southeast of AI. Backward air mass trajectories were simulated at Plymouth State University using the NOAA HYSPLIT model, initiated from AI and run for 24 hrs (<http://pscwx.plymouth.edu/ICARTT/archive.html>). The trajectories were used to provide qualitative descriptions of the mesoscale dynamics accompanying the trace gas observations.

I.2.1. Trace Gas Measurements

Air samples were collected hourly between July 2 and August 13, 2004 for C₂–C₁₀ non-methane hydrocarbons (NMHCs), C₁–C₂ halocarbons, C₁–C₅ alkyl nitrates, selected OVOCs, CO₂, and CH₄. During the sampling period a single head metal bellows pump (MB-302MOD, Senior Flexonics, Sharon, MA) continuously drew ambient air from ~40 m asl through a ~20 m × 6.35 mm I.D. stainless steel inlet line. Samples were collected in evacuated (10⁻² mbar) 2 l electropolished stainless steel canisters and pressurized to 3.4 bar. Filled canisters were returned to the UNH Climate Change Research Center every 4 days and their contents were analyzed by gas chromatography using flame ionization and electron capture detection in conjunction with quadrupole mass spectrometry. Detailed discussions of the UNH canister sampling and analysis protocols are provided by *Sive et al.* [2005] and *Zhou et al.* [2005].

In addition to chromatographic analysis, Proton Transfer Reaction-Mass Spectrometry (PTR-MS) was used to provide high frequency measurements of several groups of isomeric NMHCs, certain individual OVOCs, DMS, and acetonitrile from July 1 to August 12 (Table 1). The PTR-MS sampled air that was continuously drawn through a 30.5 m × 9.525 mm I.D. PFA Teflon® tube from the same height as the canister pump inlet. The flow rate through the sample line was $\sim 75 \text{ l min}^{-1}$, resulting in a $\sim 2 \text{ s}$ residence time. A sub-stream of fast flowing air off the main sample line was sent directly to the PTR-MS. The PTR-MS was operated with a drift tube pressure of 2 mbar and a drift voltage of 600 V while continuously stepping through a series of 30 masses. Of the 30 masses monitored, 6 masses were used for diagnostic purposes while the other 24 masses corresponded to the VOCs of interest. The dwell time for each of the 24 masses was 20 s, yielding a total measurement cycle of $\sim 10 \text{ min}$. The system was zeroed every 2.5 hrs for 4 cycles by diverting the flow of ambient air through a heated catalytic converter (0.5% Pd on alumina at 450° C) to oxidize the VOCs and determine system background signals.

Calibrations for the PTR-MS system were conducted using three different high-pressure cylinders containing synthetic blends of selected NMHCs and OVOCs at the part per billion by volume (ppbv) level (Apel-Reimer Environmental, Inc.). Each of the cylinders used in the calibrations had an absolute accuracy of $< \pm 5\%$ for all gases. Using methods similar to those described by *Apel et al.* [1998], standards were diluted to atmospheric mixing ratios (ppbv to pptv levels) with catalytic converter prepared zero air adjusted to maintain the humidity of the sampled air. Calibrations were conducted periodically to monitor PTR-MS performance and quantify the mixing ratios of target

gases. Additionally, mixing ratios for each gas were calculated by using the normalized counts per second which were obtained by subtracting out the non-zero background signal for each compound.

Long-Path (LP) Differential Optical Absorption Spectroscopy (DOAS) was used to measure a suite of inorganic gases, including NO₂ and NO₃, and formaldehyde [*Alicke et al.*, 2002]. The retroreflector array was installed (~15 m asl) on the White Island lighthouse, 2.3 km from AI. Spectra were recorded from the tower's third floor (~40 m asl) over a 4.6 km path length [*Pikelnaya et al.*, 2007]. The DOAS system was operated from July 8 to August 11 although spectra were often not obtainable during periods of persistent fog and/or precipitation.

I.2.2. Analysis Methods

In this paper we use an incremental approach to determine the respective importance of gas-phase and heterogeneous mechanisms in nighttime NO₃ chemistry at AI. This section describes our treatment of gas-phase NO₃ chemistry. The potential importance of heterogeneous chemistry is discussed separately in Section I.3.4. Table 2 lists the measured NO₃ reactants along with the kinetic data for their corresponding reactions. Kinetic data for additional reactions considered in this study are also given in Table 2. The pseudo first-order loss rate coefficient (hereinafter referred to as the loss efficiency) for removal of NO₃ via its reaction with trace gas *i*, k'_i (s⁻¹), is given by the product of the reaction rate coefficient, $k_{(\text{NO}_3+i)}$, and the concentration of *i*:

$$k'_i = k_{(\text{NO}_3+i)} \cdot [i] \quad (1)$$

$$k'_T = \sum_{i=1}^N k'_i \quad (2)$$

where k'_T (s^{-1}) is the total loss efficiency for the removal of NO_3 by all N reactive gases. (The term k'_i will also be described as the reactivity of i .) Because N_2O_5 was not measured, its contribution to NO_3 removal was estimated by assuming equilibrium with NO_2 and NO_3 during the nighttime hours:

$$K_{\text{eq}}(T) = \frac{[\text{N}_2\text{O}_5]}{[\text{NO}_2][\text{NO}_3]} = \frac{k_f}{k_r} \quad (3)$$

The errors incurred by this approximation are expected to be minimal under most conditions observed at AI. For instance, for average conditions encountered at AI (see below) with $[\text{O}_3] \approx 40$ ppbv, relative humidity (RH) $\approx 90\%$, loss efficiencies for NO_3 and N_2O_5 of $\sim 7 \times 10^{-3}$ and $\sim 5 \times 10^{-4} s^{-1}$, respectively, and the chemistry represented as described by *Brown et al.* [2003b; equations (4) and (5)], simple box model calculations demonstrated that ambient N_2O_5 would have been 95% of its equilibrium value within ~ 15 min of an instantaneous sunset, with starting concentrations of NO_3 and N_2O_5 equal to zero. Furthermore, recent simultaneous field measurements of O_3 , NO_2 , NO_3 , and N_2O_5 showed good agreement between measured N_2O_5 mixing ratios and those calculated assuming equilibrium among the nitrogen oxides [*Brown et al.*, 2003a]. In our analysis, the uncertainty in k_r (average value of $\sim 20\%$) made the dominant contribution to the uncertainty in K_{eq} [*Atkinson et al.*, 2004]; together the uncertainties in the measurements of NO_2 ($\sim 20\%$) and NO_3 ($\sim 40\%$) made a greater contribution to the overall uncertainty ($\sim 60\%$) in the calculated N_2O_5 mixing ratios. The NO_3 loss efficiency with respect to the reactions of N_2O_5 with water vapor, $k'_{(\text{H}_2\text{O}(\text{g}) + \text{N}_2\text{O}_5)}$, was determined as

$$k'_{(\text{H}_2\text{O}(\text{g}) + \text{N}_2\text{O}_5)} \equiv k'_{\text{indirect}} = (k_{6a} + k_{6b} \cdot [\text{H}_2\text{O}]) \cdot K_{\text{eq}} \cdot [\text{NO}_2][\text{H}_2\text{O}] \quad (4)$$

where the rate coefficients k_{6a} and k_{6b} correspond with reactions (R6a) and (R6b), respectively, and $[H_2O]$ is the atmospheric water vapor concentration. The NO_3 loss rate with respect to sink (i.e., loss pathway) j , $L_j(NO_3)$, is the product of the loss efficiency for sink j and the NO_3 concentration; the total loss rate via gas-phase (homogeneous) sinks, $L_{\text{hom}}(NO_3)$, is given by

$$L_{\text{hom}}(NO_3) = \sum_{j=1}^K L_j(NO_3) = (k'_T + k'_{\text{indirect}}) \cdot [NO_3] = k'_{\text{hom}} \cdot [NO_3] \quad (5)$$

where the summation is over all K gas-phase sinks. The total rate of gas-phase nighttime NO_x removal is given by

$$L(NO_x)_{\text{night}} = L_T(NO_3) + 2 \cdot L_{\text{indirect}}(NO_3) \quad (6)$$

where the factor of 2 appears in front of the N_2O_5 -mediated NO_3 loss rate because N_2O_5 contains two equivalents of NO_x . Daytime NO_x removal results primarily from the reaction of NO_2 with OH,



with a rate given by

$$L(NO_x)_{\text{day}} \cong k_{(NO_2+OH)} \cdot [NO_2][OH] \quad (7)$$

[Brown *et al.*, 2004]. During the ICARTT campaign, OH concentrations were calculated following the parameterization of *Ehhalt and Rohrer* [2000] as discussed by *Keene et al.* [2007]. The NO_3 production rate, $P(NO_3)$, was calculated from the measured mixing ratios of NO_2 and O_3 and the corresponding rate coefficient (Table 2):

$$P(NO_3) = k_{(NO_2+O_3)}(T) \cdot [NO_2][O_3] \quad (8)$$

The total rate of the NO_3 concentration change, $d[NO_3]/dt$, can be approximated as

$$\frac{d[\text{NO}_3]}{dt} = P(\text{NO}_3) - k'_{\text{hom}} \cdot [\text{NO}_3] \quad (9)$$

If the terms $P(\text{NO}_3)$ and k'_{hom} in equation (9) are constant, the concentration of NO_3 at any arbitrary time t , $[\text{NO}_3]_t$ is given by:

$$[\text{NO}_3]_t = \frac{P(\text{NO}_3) - [(P(\text{NO}_3) - k'_{\text{hom}} \cdot [\text{NO}_3]_0) \cdot \exp(-k'_{\text{hom}} \cdot t)]}{k'_{\text{hom}}} \quad (10)$$

where $[\text{NO}_3]_0$ is the initial NO_3 concentration. Since these terms do in fact vary, the time dependence of $[\text{NO}_3]_t$ was obtained by propagating equation (10) for short intervals, updating the values of $P(\text{NO}_3)$ and k'_{hom} at every time step. For this investigation, equation (10) was used to calculate nocturnal NO_3 mixing ratio profiles with the initial condition $[\text{NO}_3]_{0=21:00} = 0$. For clarity in presentation of our results, we utilized U.S. east coast local time (Eastern Daylight Time), which is UT - 4 hours.

I.3. Results and Discussion

I.3.1. Kinetic Comparison of Gas-Phase Nighttime NO_3 Loss Processes

Time series of NO_3 , its precursors NO_2 and O_3 , biogenic VOCs, and selected anthropogenic tracer species are presented in Figure 1 for July 8–28, 2004, where the thickened lines correspond to measurements during the nighttime hours (21:00–05:00). Highly variable conditions were experienced at AI, as the site was frequently impacted by continental outflow comprised of both anthropogenic and biogenic emissions [*Chen et al.*, 2007]. The mixing ratios of NO_2 , NO_3 , isoprene, DMS, and the monoterpenes varied over wide ranges from below their limit of detection (LOD) to 19.6, 0.073, 0.85, 0.33,

and 0.62 ppbv, respectively. The average NO₃ mixing ratio was ~10 pptv (see below), which appears to agree well with the observations of *Warneke et al.* [2004] in this region during July and August, 2002. By comparison, the average summertime NO₃ mixing ratio on the island of Crete in the East Mediterranean Sea during the years 2001–2003 was ~6 pptv [*Vrekoussis et al.*, 2007]. *Allan et al.* [2000] measured NO₃ mixing ratios up to 40 and 20 pptv in the northeast Atlantic at Mace Head, Ireland during July and August, 1996 and at Tenerife Island off the coast of northwestern Africa during June and July, 1997, respectively. Average NO₃ mixing ratios during several nights in June, 1995 at a coastal site in north Norfolk, England [*Allan et al.*, 1999] ranged between ~4 and 25 pptv. Average NO₃ mixing ratios in summer 1993 at a rural site on Rügen Island in the Baltic Sea [*Heintz et al.*, 1996] ranged between 6 and 10 pptv. During several nights in August and September, 2000, at a suburban continental site outside the city center of Houston, TX, *Stutz et al.* [2004] observed NO₃ mixing ratios typically <10 pptv with a maximum of ~60 pptv. *Geyer et al.* [2001] observed similar values during July and August, 1998 at a suburban site near Berlin, Germany. During July and August, 1990 at a suburban site in the San Joaquin Valley, CA *Smith et al.* [1995] observed average and maximum NO₃ mixing ratios of ~2 and 80 pptv respectively.

The time series shown in Figure 2 presents the ratio of the total reactivity of biogenic compounds, $k'_{\text{biogenics}}$, to the total reactivity of all VOCs, k'_{VOCs} . The average ratio during the time period from July 8–28 was 0.91 ± 0.14 , emphasizing the dominance of biogenic VOC reactivity. The alkenes appeared to be the next most important class of VOCs for nighttime NO₃ removal, but on average they accounted for <10% of the VOC

reactivity during the night. The OVOCs, aromatics and alkanes each accounted for <1% of the VOC reactivity during the night.

The relative contribution of the individual biogenic VOCs to the overall NO₃ loss rate was evaluated, including $k'_{\text{monoterpenes}}$, k'_{DMS} and k'_{isoprene} (Figure 3). Of the biogenically derived compounds measured at AI, DMS appeared to be the dominant NO₃ reactant. Average values of $k'_i/k'_{\text{biogenics}}$, where $i = \text{DMS, isoprene and monoterpenes}$, were 0.56 ± 0.36 , 0.18 ± 0.21 and 0.26 ± 0.30 respectively. When they were above the LOD, monoterpenes generally accounted for a large fraction of the NO₃ nightly loss, but due to their continental origin they appeared at AI only during time periods influenced by strong offshore flow. This occurred ~30% of the time during the ICARTT study period [Chen *et al.*, 2007].

Assuming equilibrium conditions for the NO₂-NO₃-N₂O₅ system, the NO₃ and N₂O₅ mixing ratios should be nearly equal when NO₂ mixing ratios are several ppbv for the average conditions encountered at AI ($T = 290 \pm 2$ K, NO₃ = 0.011 ± 0.013 ppbv, and NO₂ = 4.0 ± 4.2 ppbv). Our calculations suggest that removal of NO₃ via gas-phase reactions of N₂O₅ was frequently comparable in magnitude to NO₃ removal with VOCs, indicating $k'_{\text{VOCs}} \approx k'_{\text{indirect}}$. The average values of $k'_{\text{indirect}}/k'_{\text{hom}}$ and $k'_{\text{VOCs}}/k'_{\text{hom}}$ were 0.42 ± 0.26 and 0.58 ± 0.27 respectively, indicating that these two pathways were, in fact, comparable sinks for NO₃.

Whereas the reactions of NO₃ with VOCs remove NO₃ and NO_x at the same rate, hydrolysis of N₂O₅ is two times more efficient than NO₃-related mechanisms for NO_x removal because two equivalents of NO_x are associated with N₂O₅. The average rate of NO_x loss via reactions of N₂O₅ with H₂O(g) was estimated to be 0.36 ± 0.41 ppbv hr⁻¹

compared to a NO_x loss rate of $0.12 \pm 0.11 \text{ ppbv hr}^{-1}$ through reactions of NO_3 with VOCs.

I.3.2. Nocturnal Chemistry Case Studies

The following discussion focuses on trace gas measurements from several nights during July 8–28, 2004. Backward air mass trajectories were used for qualitative source region identification, while trace gas measurements and relevant gas-phase kinetics were used to explain important features of nighttime NO_3 chemistry.

The selected case studies illustrate the role of nighttime NO_3 chemistry over a range of conditions at AI, including periods of Atlantic aged marine flow (July 13 and 14), polluted continental outflow (July 11 and 16), and polluted continental/biogenic outflow (July 25). For each case study we examined the relative levels of pollutants and estimated the transport pathway, calculated the mixing ratio of N_2O_5 , and subsequently assessed the NO_3/NO_x loss rates due to reaction with marine and terrestrial biogenic VOCs.

I.3.2.1. Clean Marine Flow on July 13 and 14.

The lowest trace gas levels during the nighttime hours of the ICARTT campaign were measured on July 13 and 14. Backward trajectories for these two nights (Figures 4a and 4b) indicate that prior to their arrival at AI, the air masses resided over the Atlantic Ocean for $>24 \text{ hr}$ [Keene *et al.*, 2007]. Overall, the trace gas mixing ratios were

characteristic of relatively clean conditions, exhibiting no recent anthropogenic influences. For example, average mixing ratios of toluene, ethyne and *o*-xylene on the night of July 13 were 0.008 ± 0.002 , 0.288 ± 0.051 and 0.015 ± 0.002 ppbv respectively and on the night of July 14 were 0.009 ± 0.003 , 0.105 ± 0.011 and 0.015 ± 0.003 ppbv. By comparison, for the nighttime hours (21:00–05:00) between July 8 and 28, the average mixing ratios of these three gases were 0.157 ± 0.151 , 0.360 ± 0.231 and 0.031 ± 0.018 ppbv.

During both nights NO_2 mixing ratios were sub-ppbv and NO_3 was below its LOD of 3.4 pptv. The relatively low abundances of NO_3 presumably resulted from correspondingly low levels of NO_x coupled with high levels of DMS. Mixing ratios of DMS were elevated to >0.20 ppbv, while isoprene remained <0.025 ppbv and the monoterpenes were below their LODs (Figure 1). Throughout both nights, DMS mixing ratios exhibited increasing trends while oxidant concentrations remained low. The average values of $k'_{\text{DMS}}/k'_{\text{VOCs}}$ were 0.970 ± 0.004 and 0.948 ± 0.014 on the two nights respectively, indicating that reaction of NO_3 with DMS was the dominant gas-phase mechanism for removal of NO_3 .

I.3.2.2. Polluted Continental Outflow on July 11.

Trace gas measurements and backward trajectories on July 11 (Figure 4c) suggest that AI was impacted by polluted continental air masses characterized by average mixing ratios of toluene, ethyne and *o*-xylene of 0.39 ± 0.13 , 0.69 ± 0.21 and 0.057 ± 0.012 ppbv respectively (Figure 5a). These levels were 2 to 5-fold higher compared to the nights of

July 13 and 14. In addition, the average mixing ratios of NO_2 and NO_3 were elevated by more than an order of magnitude to 12 ± 6 ppbv and 7 ± 3 pptv respectively. Backward trajectories indicate that during daytime on July 11 the air mass descended to the southeast of AI enroute from over northeastern Maine and then circled back to AI from the south (Figure 4c). The air mass appeared to traverse the Boston metropolitan area at approximately 20:00 and was subsequently transported to AI in <6 hours. The mixing ratios for most of the anthropogenic tracers increased throughout the night, corresponding to continuous continental outflow of urban pollutants which seemingly fumigated the MBL surrounding AI.

The calculated reactivities of biogenic VOCs closely tracked the measured mixing ratios of NO_3 around the midnight hours (Figures 5b and 5c). Between 23:00 and 01:00, NO_3 mixing ratios increased by about a factor of six while biogenic reactivity decreased ~8-fold. The loss rate of isoprene with NO_3 was >20 times faster than with O_3 during this time period, indicating that the observed removal of isoprene most likely resulted from reaction with NO_3 . On this night it appears that isoprene was the most important NO_3 reactant, and the attendant reduction in biogenic reactivity was mostly caused by its removal from 0.53 ppbv at 23:00 to 0.06 ppbv at 01:00.

The contribution to k'_{hom} from the reactions of N_2O_5 increased significantly from sunset to sunrise. As illustrated in Figure 5c, this trend was driven mostly by the increase in NO_2 mixing ratios, which shifted the nitrogen oxides equilibrium toward N_2O_5 . The reaction of N_2O_5 with $\text{H}_2\text{O}(\text{g})$ generally becomes more important with increasing relative humidity or decreasing temperature; however, both of these variables were relatively constant in this case. After midnight, k'_{hom} was apparently dominated by reactions of

N_2O_5 , such that during the remainder of the evening NO_3 chemistry should have been primarily generating HNO_3 . At 01:00, NO_2 mixing ratios were 11.0 ppbv resulting in a gas-phase HNO_3 production rate of 0.54 ± 0.31 ppbv hr^{-1} . By 05:00 when NO_2 had increased to 18.4 ppbv, the rate of gas-phase HNO_3 production was increased to 1.1 ± 0.6 ppbv hr^{-1} . The corresponding rates of gas-phase NO_x loss were 0.58 ± 0.31 and 1.2 ± 0.6 ppbv hr^{-1} respectively. The gas-phase rates of HNO_3 production and NO_x loss at 01:00 and 05:00 are compared with the corresponding rates from heterogeneous N_2O_5 hydrolysis in Table 3. Despite increasing NO_2 mixing ratios, the NO_3 production rate remained roughly constant at 0.51 ± 0.12 ppbv hr^{-1} , resulting from the subsequent decrease in O_3 mixing ratios. Thus, it appears that the slight decreasing trend in the NO_3 mixing ratios after 01:00 resulted primarily from the increasing trend in the N_2O_5 loss rate.

I.3.2.3. Polluted Continental Outflow on July 16.

Polluted continental air masses characterized by average mixing ratios of toluene, ethyne and *o*-xylene of 0.36 ± 0.09 , 0.67 ± 0.19 and 0.040 ± 0.009 ppbv respectively impacted AI on July 16. For most of this night these anthropogenic marker species had decreasing trends in their mixing ratios (Figure 6a), suggesting a reduced influence of pollution sources at AI after dark. The 02:00 backward trajectory (Figure 4d) showed that the air mass originated over central New York State during the night of July 15 and was lofted to ~1 km altitude over northern Massachusetts during the day on July 16. By

sunset, the air mass appeared to be traveling several hundred meters above ground level and may have had minimal contact with the surface layer upwind of AI during the night.

Opposite trends in the biogenic reactivity and NO_3 concentrations were observed at both the beginning and end of this night (Figures 6b and 6c). Between 21:00 and 22:00, the biogenic reactivity decreased from $6 \pm 3 \times 10^{-3}$ to $1.5 \pm 0.7 \times 10^{-3} \text{ s}^{-1}$ while NO_3 mixing ratios increased from 4 to 21 pptv. These trends corresponded with decreases in isoprene and DMS mixing ratios from 0.280 to 0.062 ppbv and 0.044 to 0.019 ppbv, respectively. From 03:00 to 04:00 the NO_3 mixing ratio decreased from 19 to 4 pptv as the biogenic reactivity increased from $2.3 \pm 0.6 \times 10^{-3}$ to $8.1 \pm 1.9 \times 10^{-3} \text{ s}^{-1}$. Increases in the mixing ratios of α -pinene, β -pinene and camphene (from their LODs to 8, 45 and 44 pptv, respectively) comprised the dominant contribution to the biogenic reactivity. In this case a concurrent decrease in the NO_3 production rate, which was $<L_{\text{hom}}(\text{NO}_3)$ during this time period, appeared to contribute to the observed trend in NO_3 . Decreased production, coupled with a shift in loss mechanism also seemed to significantly reduce the rate of gas-phase NO_x loss from $1.0 \pm 0.2 \text{ ppbv hr}^{-1}$ (22:00–03:00) to $<0.4 \text{ ppbv hr}^{-1}$ (after 03:00).

The NO_3 loss frequency was probably controlled by N_2O_5 reactions between 22:00 and 03:00 (Figure 6b), when the ambient levels of the biogenic VOCs were relatively low. During this time period, the values of k'_{indirect} were on average roughly two times larger than the corresponding values of k'_{VOCs} , while the calculated N_2O_5 mixing ratios were approximately an order of magnitude greater than the measured NO_3 mixing ratios. The average contribution of N_2O_5 hydrolysis to gas-phase NO_x removal was $82 \pm 7\%$. The average contributions of gas-phase and heterogeneous mechanisms to

NO_x removal and HNO₃ production are compared in Table 3 for the periods from 22:00 to 03:00 and from 04:00 to 05:00. The general decreasing trend in the measured NO₃ mixing ratios appeared to result mostly from decreasing rates of production as the total gas-phase loss rate was relatively constant between 22:00 and 03:00 and exceeded $P(\text{NO}_3)$ during the interval 23:00 to 04:00. Because the NO₂ mixing ratios remained constant, the NO₃ trend closely followed that of O₃ (Figure 6c).

I.3.2.4. Polluted and Biogenic Continental Outflow on July 25.

Trace gas measurements during the night of July 25 indicate that AI experienced relatively clean conditions prior to 01:00, similar to those observed on the nights of July 13 and 14. This is supported by the low mixing ratios of anthropogenic tracers such as CO (<120 ppbv), toluene (<0.050 ppbv), ethyne (<0.150 ppbv), *o*-xylene (<LOD), and NO₂ (<3 ppbv) (Figure 7a). The influence of polluted continental outflow was first observed after 01:00, when O₃ and NO₃ concentrations decreased abruptly by 10 ppbv and 20 pptv respectively (Figure 7c). One hour prior to this, the mixing ratio of CO began to rise from 120 ppbv reaching 170 ppbv by 01:00. However, sharp increases in the mixing ratios of monoterpenes and aromatics were delayed until 02:00 (Figure 7a). Between 02:00 and 03:00, the CO mixing ratio increased by another 50 ppbv to 220 ppbv, NO₂ rose from 1.7 to 11.3 ppbv, isoprene from the LOD (0.002 ppbv) to 0.160 ppbv, and monoterpenes from 0.012 to 0.30 ppbv. By 04:00 the measured NO₂ mixing ratio had increased to 19.6 ppbv and all the alkenes and aromatic compounds listed in Table 2 were above their respective LODs. Finally, O₃ plummeted to ~4 ppbv by 04:00.

The transport patterns for both July 11 and 25 were strikingly similar (Figure 4, c and e) and the backward trajectories suggest that the air masses probably incorporated emissions from the urban coastal corridor stretching from Boston to southern Maine (Figure 4e). Winds were significantly weaker on July 25 ($1.3 \pm 0.5 \text{ m s}^{-1}$) compared to July 11 ($5.7 \pm 0.8 \text{ m s}^{-1}$), resulting in longer transport times to AI on July 25. The relatively stagnant conditions during the night of July 25 likely led to little influx of air masses with higher O_3 levels, and O_3 titration continued after 01:00, which prevented the NO_3 production rate from reaching even half the average value for the night of July 11. Relatively weak production, coupled with extraordinary enhancements of NO_3 reactants, particularly monoterpenes, suppressed NO_3 concentrations to below the LOD by 04:00. Conversely, higher levels of monoterpenes on this night than on both July 11 and 16 likely resulted in part from reduced production of NO_3 .

At 03:00 the rate of gas-phase NO_x removal reached a maximum of $0.83 \pm 0.21 \text{ ppbv hr}^{-1}$, which was $\sim 75\%$ of the average removal rate after 03:00 on July 12. However, after 03:00 on July 26 the removal rate was apparently dominated by the reactions of NO_3 with monoterpenes and would have decreased considerably due to the slow rate of NO_3 production. For instance, if the NO_3 mixing ratio was equal to half the LOD (1.7 pptv; probably a conservative lower limit) after 03:00, the rate of NO_x removal would have decreased to $<0.12 \text{ ppbv hr}^{-1}$ for the remainder of the night. The estimated contributions of gas-phase and heterogeneous mechanisms to NO_x removal and HNO_3 production at 03:00 are presented in Table 3.

I.3.3. Measured versus Calculated NO₃ Time Series Profiles

Figures 8a–c show comparisons between measured and calculated (Section I.2.2.) NO₃ mixing ratios for July 11, 16 and 25 respectively, where only gas-phase chemistry was considered. The calculated profiles reproduce the measurements within estimated uncertainties during most time intervals, indicating that gas-phase chemistry may have accounted for the majority of NO₃ loss. Assuming that uncertainties in the interpolated NO₃ production and loss rates are comparable to those of the hourly values, uncertainties in the calculated NO₃ mixing ratios for July 11, 16 and 25 ranged from 30–40%, 20–30% and 10–40% respectively.

Discrepancies between the measured and calculated values likely resulted mainly from the real temporal variability of the atmosphere not being captured in the hourly input values. For example, on the night of July 16, peak NO₂ mixing ratios were observed around 02:30, which slowed the overall decrease in the NO₃ production rate at the end of the night (Figure 8b). Thus, the calculated NO₃ values appeared to decrease faster than the measured ones after 02:00 due to coarse resolution that resulted in under-predicted NO₃ production between the hours of 02:00 and 03:00. Similarly, the peak in O₃ between 02:00 and 03:00 on July 26 was not captured in the calculated NO₃ production and caused the under-prediction of measured NO₃ during that time period. The calculated NO₃ mixing ratios appeared to more accurately reproduce the measurements on July 16 compared with July 11 and July 25, which is likely due to increased variability in chemical composition during the latter two nights. In general, the calculation was expected to perform less well when any of the input parameters, namely

the concentrations of NO₂ and O₃ and the value of k'_{hom} , varied nonlinearly between the hour steps. Furthermore, variations in the input parameters between measurements could not be fully captured in the calculation; they depended strongly on the distributions and strengths of upwind emissions sources, which were unknown.

Exclusion of heterogeneous chemistry from the determination of the overall NO₃ loss efficiency probably contributed to the systematic positive bias observed in the calculated values for the nights of July 11 and 16 (Figures 8a and 8b). For July 11, the bias was largest at the end of the night when N₂O₅ chemistry made the greatest contribution to the NO₃ loss efficiency. For July 16, the bias was largest at the beginning of the night when the calculation was most sensitive to the input parameters.

The night of July 25 was an exception in that the calculated NO₃ mixing ratios were generally negatively biased. This suggests that the total NO₃ loss efficiency derived from the measurements may have been larger than the average over the DOAS measurement path length. Between 21:00 and 01:00 α -pinene was near the LOD but made a significant contribution to the total NO₃ loss efficiency. Variability in the level of α -pinene between the LOD (0.002 ppbv) and 0.008 ppbv controlled much of the variability in the measured (relative standard deviation (RSD) = 80%) and calculated (RSD = 70%) NO₃ mixing ratios. A 50% variation in the α -pinene mixing ratios (~1–4 pptv) caused an average change in the calculated NO₃ mixing ratios of $24 \pm 9\%$. The details of this sensitivity to α -pinene may not have been captured well by the hourly hydrocarbon measurements.

Finally, disagreement between measured and calculated NO₃ mixing ratios would be expected if conditions at the point of the tower sampling inlets were in fact different

than the average over the DOAS path length. This could arise from spatial heterogeneity in the air masses influencing the region or from the influence of local emissions sources. Indeed, during ICARTT air mass heterogeneity on a scale as small as ~ 3 km, which is close to the maximum distance along the DOAS light path from the tower sampling inlets, was determined from inter-comparisons between the NOAA research vessel *Ronald H. Brown* (R/V *Brown*) and the AI DOAS system [Osthoff *et al.*, 2005]. However, O_3 measurements from the tower and the DOAS system generally tracked each other well, indicating the same air mass was usually being sampled. Times when local emissions could be clearly identified (these corresponded with nocturnal spikes in NO) were filtered out in our analysis.

I.3.4. Heterogeneous Nighttime NO_3 Loss: Uptake of N_2O_5 by Aerosols/Ocean

Surface

To estimate the contributions to NO_3 and NO_x removal of heterogeneous N_2O_5 chemistry (i.e., reaction (R5) and presumably also deposition of N_2O_5 to the ocean surface) the NO_3 loss efficiency with respect to heterogeneous N_2O_5 chemistry, k'_{het} , was first approximated based on discrepancies between the measured and calculated NO_3 mixing ratios for the nights of July 11 and 16 (Figures 8a and 8b, respectively). After midnight on July 11 (Figure 5b) and between 22:00 and 03:00 on the night of July 16 (Figure 6b) reactions of N_2O_5 potentially dominated NO_3/NO_x removal. During these time periods, with the exception of the period between 02:00 and 03:00 on July 17 (Section I.3.3), the systematic positive biases in the calculated NO_3 mixing ratios likely

resulted from the exclusion of heterogeneous chemistry in the calculations. By adding a term equal to an adjustable fraction of k'_{indirect} to the total NO_3 loss efficiency in equation (10), the value of k'_{het} was determined as the fraction of k'_{indirect} for which the average error between the calculated and measured NO_3 mixing ratios was minimized. The resulting ranges of $k'_{\text{het}}/k'_{\text{indirect}}$ (denoted as ρ_{het} hereinafter) were 0.3–0.4 and 0.2–0.3 for the nights of July 11 and 16 respectively. Figures 8d–f show comparisons between calculated and measured NO_3 mixing ratios for the nights of July 11, 16 and 25, respectively, where $0.2 \leq \rho_{\text{het}} \leq 0.4$. Again, the night of July 25 was the exception; agreement between the measured and calculated NO_3 mixing ratios was not improved by accounting for heterogeneous N_2O_5 chemistry. This was expected based on our discussion in Section I.3.3.

Aerosol properties as a function of size were measured in the Gulf of Maine aboard R/V *Brown* (data courtesy of T. Bates, NOAA Pacific Marine Environmental Laboratory (PMEL)). We utilized data obtained within a 50 km radius of AI (ship coordinate data courtesy of J. Johnson, NOAA PMEL) to better quantify heterogeneous removal of N_2O_5 by aerosols. The aerosol surface area density distributions suggested that aerosols with diameters $d < 1 \mu\text{m}$ accounted for $97 \pm 2\%$ of the total aerosol surface area density S_{a} . Average aerosol reaction probabilities γ were estimated using

$$\gamma = \frac{4 \cdot k'_{\text{het}}}{v \cdot S_{\text{a}} \cdot K_{\text{eq}} \cdot [\text{NO}_2]} \quad (11)$$

Here v is the mean molecular speed of N_2O_5 and values for k'_{het} were taken as derived above (i.e., $0.2 \leq \rho_{\text{het}} \leq 0.4$). Using the regionally averaged surface area density, S_{a} ($= 290 \pm 140 \mu\text{m}^2 \text{cm}^{-3}$), we obtained a range of 0.003 ± 0.001 to 0.019 ± 0.004 for γ . Note

the minimum and maximum derived average values of γ correspond with $\rho_{\text{het}} = 0.2$, $S_{\text{a}} = 430 \mu\text{m}^2 \text{cm}^{-3}$ and $\rho_{\text{het}} = 0.4$, $S_{\text{a}} = 150 \mu\text{m}^2 \text{cm}^{-3}$, respectively. This range compares favorably with previous work and properties of sub- μm aerosol observed at AI [Hallquist et al., 2000; Folkers et al., 2003; Hallquist et al., 2003; Thornton and Abbatt, 2005; Fischer et al., 2006; Keene et al., 2007].

Sub- μm aerosol at AI was reportedly acidic in general, with median pH values ≤ 1.6 and total acidity dominated by bisulfate anion (HSO_4^-) [Keene et al., 2007]. For N_2O_5 uptake on aqueous sub- μm sulfuric acid (H_2SO_4) aerosol under similar atmospheric environment, Hallquist et al. [2000] obtained the γ value of 0.033 ± 0.004 , which is close to the upper bound of our derived range of γ (~ 0.023).

It is suggested in several studies that increasing NO_3^- activity in aqueous sub- μm sodium nitrate ($\text{Na}\cdot\text{NO}_3$) aerosol [Hallquist et al., 2003] and adding surface active organic compounds to sub- μm aerosol [Folkers et al., 2003; Thornton and Abbatt, 2005] can reduce reactive uptake of N_2O_5 . In particular, Folkers et al. [2003] measured 3- to 7-fold reductions in γ upon exposure of aqueous ammonium bisulfate ($\text{NH}_4\cdot\text{HSO}_4$) aerosol to particle free ambient air. Since particulate nitrate (NO_3^-) loading in sub- μm aerosol size fractions was observed at AI in continental outflow during ICARTT [Fischer et al., 2006], values of $\gamma < 0.033$ seem to be highly reasonable. Our lower bound agrees favorably with the value of ~ 0.003 derived by Allan et al. [1999] and the one obtained by applying a sevenfold reduction to the γ of Hallquist et al. [2003].

The favorable agreement between the calculated and assumed γ values indicates that our derived range of ρ_{het} values is valid. However, it should be cautioned that the γ

values calculated in this study might represent upper limits since depositional loss of N_2O_5 was not accounted for. Over the derived range of ρ_{het} values, the rates of NO_3 and NO_x removal were on average $10 \pm 6\%$ to $19 \pm 5\%$ and $12 \pm 5\%$ to $24 \pm 10\%$ larger, respectively than those determined without considering heterogeneous N_2O_5 uptake. Accounting for additional N_2O_5 removal as described above does not change the conclusion that reactions of NO_3 with VOCs and reactions of N_2O_5 appeared to be comparable sinks for NO_3 .

The relative importance of gas-phase versus heterogeneous N_2O_5 loss as determined in the present work depends strongly on the rate coefficient for reaction of N_2O_5 with water vapor ($k_{(\text{H}_2\text{O}(\text{g})+\text{N}_2\text{O}_5)}$). The results of *Brown et al.* [2006a] suggest a value of $k_{(\text{H}_2\text{O}(\text{g})+\text{N}_2\text{O}_5)}$ that is lower than the current recommended value [*Atkinson et al.*, 2004] by a factor (denoted as f hereinafter) >2.6 . Our data also appear to be consistent with a reduced value of $k_{(\text{H}_2\text{O}(\text{g})+\text{N}_2\text{O}_5)}$. For example, on the night of July 11, using the average value of S_a ($162 \pm 67 \mu\text{m}^2 \text{cm}^{-3}$) from measurements aboard R/V *Brown* (the ship was on average 33 ± 7 km southeast of AI on this night), the derived values of $k'_{\text{N}_2\text{O}_5}$ ($= k'_{\text{indirect}} + k'_{\text{het}}$), and constraining the value of k'_{het} such that the average value of $\gamma \leq 0.037$ (the mean + 1σ value of *Hallquist et al.* [2000]) for the night of July 11, we obtained a reduction of $k_{(\text{H}_2\text{O}(\text{g})+\text{N}_2\text{O}_5)}$ by $f \leq 2.9$. The calculated value of f increases with S_a and would be underestimated if larger surface area densities were experienced at AI than aboard R/V *Brown*. However, f would be overestimated if γ was in fact smaller.

Reducing $k_{(\text{H}_2\text{O}(\text{g})+\text{N}_2\text{O}_5)}$ by $f = 2.9$ decreased the average value of $k'_{\text{indirect}}/k'_{\text{hom}}$ by $\sim 50\%$ to 0.25 ± 0.20 (Section I.3.1) and increased the derived upper limit of ρ_{het} to 3.1.

The average value of $k'_{\text{het}}/k'_{\text{hom}}$ increased from 0.14 ± 0.08 to 0.36 ± 0.20 , while the average contributions of aerosol N_2O_5 uptake to NO_3 and NO_x removal increased from minima of $\sim 10\%$ ($\rho_{\text{het}} = 0.2$) to as large as $40 \pm 19\%$ and $50 \pm 18\%$, respectively ($\rho_{\text{het}} = 3.1$; $f = 2.9$). The N_2O_5 loss efficiency was thus significantly repartitioned between gas-phase and heterogeneous chemistry. Presented in Table 3 is a comparison of the average values of $L(\text{NO}_x)$ and $P(\text{HNO}_3)$ resulting from VOC- and N_2O_5 -mediated NO_3 removal, including the gas-phase values given in Section I.3.1. The dependence of the N_2O_5 -mediated rates on $k_{(\text{H}_2\text{O}(\text{g})+\text{N}_2\text{O}_5)}$ is also shown.

When the N_2O_5 -mediated NO_3 loss efficiency is attributed entirely to heterogeneous hydrolysis the maximum derived average value of γ is 0.065 ± 0.014 , which seems unrealistically large based on the discussion above. This result suggests that it is inappropriate to assume N_2O_5 hydrolysis is an exclusively heterogeneous process.

The average contributions of N_2O_5 chemistry to nighttime NO_3 and NO_x removal were 51 to 54 ($\pm 25\%$) and $63 \pm 24\%$ to $66 \pm 23\%$ respectively, corresponding with the derived range of ρ_{het} . These values are independent of the precise value of $k_{(\text{H}_2\text{O}(\text{g})+\text{N}_2\text{O}_5)}$ following our methodology. A similar partitioning between direct and indirect NO_3 removal mechanisms in this region during July and August, 2002 was reported by *Aldener et al.* [2006]. The average relative contributions of gas-phase and heterogeneous mechanisms to nighttime NO_x removal are summarized for the limiting values of ρ_{het} and f in Figure 9.

I.3.5. Daytime versus Nighttime NO_x Removal

The average rate of daytime NO_x removal, determined using equation (7) for the daytime hours (05:30–20:30) between 05:30 on July 11 and 20:30 on July 28, was 0.43 ± 0.58 ppbv hr⁻¹. In comparison, the average rate of nighttime NO_x removal, determined using equation (6) for the nighttime hours (21:00–05:00) between July 8 and 28, ranged between 0.55 ± 0.54 ppbv hr⁻¹ and 0.62 ± 0.62 ppbv hr⁻¹. These rates correspond to the range of relative heterogeneous loss efficiencies that were derived in Section I.3.4 and are insensitive to repartitioning N₂O₅ removal between gas-phase and heterogeneous chemistry. Both NO₃ and OH mediated NO_x removal is expected to be relatively inefficient near sunrise and sunset, when the abundances of both oxidants reach their minima [e.g., *Warneke et al.*, 2004]. Hence, the average total NO_x removal during a 24 hr cycle was estimated by multiplying the average daytime and nighttime NO_x removal rates by the durations of the daytime and nighttime periods defined above. The resulting 24 hr-averaged NO_x removal was ~11 ppbv with nighttime NO_x removal contributing ~50% of the total, despite the nighttime hours representing only ~40% of the diel cycle. Accordingly, reduction of NO_x in polluted continental outflow is expected to be two fold greater than would be predicted based on daytime chemistry alone. This result provides additional evidence for the importance of nighttime NO₃ chemistry in this atmospheric environment.

Brown et al. [2004] inferred the relative importance of daytime and nighttime NO_x removal from the New England MBL during summertime by comparing daytime and nighttime HNO₃(g) production. They found that nighttime production on average

accounted for ~35% of the total production. The calculated average nighttime $\text{HNO}_3(\text{g})$ production rate was ~80% of the average daytime production rate. The rate of daytime $\text{HNO}_3(\text{g})$ production is roughly equivalent to the rate of daytime NO_x loss given by equation (7), while the rate of nighttime $\text{HNO}_3(\text{g})$ production was approximated using equation (6), where $k'_{\text{N}_2\text{O}_5}$ was used in place of k'_{indirect} and only VOCs that react with NO_3 via H-atom abstraction (DMS being most important (Section I.3.1.)) were considered:

$$P(\text{HNO}_3(\text{g}))_{\text{night}} \cong L_{\text{DMS}}(\text{NO}_3) + 2 \cdot L_{\text{N}_2\text{O}_5}(\text{NO}_3) \quad (12)$$

Equation (12) assumes that heterogeneous N_2O_5 uptake, as derived in Section I.3.4, primarily generates gas-phase HNO_3 . This should be valid for reaction of N_2O_5 with acidic sub- μm aerosol in this region [Brown *et al.*, 2004], however we have not determined the magnitude of N_2O_5 depositional loss to the ocean surface and thus the phase partitioning of the resultant HNO_3 is uncertain. The resulting estimated average rate of nighttime $\text{HNO}_3(\text{g})$ production ranged between $0.47 \pm 0.52 \text{ ppbv hr}^{-1}$ and $0.55 \pm 0.60 \text{ ppbv hr}^{-1}$, for $\rho_{\text{het}} = 0.2$ and 0.4 respectively (Table 3), corresponding with ~110–130% of the average daytime $\text{HNO}_3(\text{g})$ production rate. Thus, we conclude that average $P(\text{HNO}_3(\text{g}))_{\text{night}} \leq 1.3 \times \text{average } P(\text{HNO}_3(\text{g}))_{\text{day}}$. This range is in reasonable agreement with the findings of Brown *et al.* [2004], and further suggests that the variability in nighttime NO_3 chemistry in summer 2002 over this same region was largely reproduced in 2004. Such reproducibility in the atmospheric environment was also noted regarding properties of aerosol chemistry [Fischer *et al.*, 2006; Keene *et al.*, 2007]. Moreover, that our results suggest daytime and nighttime $\text{HNO}_3(\text{g})$ production rates were often

comparable may partially explain the occurrence of nocturnal peaks in $\text{HNO}_3(\text{g})$ mixing ratios measured at AI [Fischer *et al.*, 2006].

I.4. Summary

Measurements of trace gases important to the nighttime chemistry of NO_3 were measured at Appledore Island, ME during the 2004 ICARTT campaign. The suite of measurements including NO_3 , VOCs, O_3 and NO_2 were used in this study to determine the most important gas-phase nighttime loss mechanisms for NO_3 during the period July 8–28, 2004, and, together with backward trajectories, to understand the NO_3 chemistry that occurred during several individual nights. The importance of heterogeneous N_2O_5 chemistry for nocturnal NO_3 and NO_x removal was also investigated. The following conclusions were drawn from this work:

(1) This study confirmed the importance of biogenic VOCs as nighttime reactants with NO_3 in the NE MBL during the summertime. The average contribution of DMS, isoprene and monoterpenes to the loss efficiency of all measured VOCs was >75%. DMS appeared to be the dominant NO_3 reactant overall due to constant DMS emissions in this marine environment. On average DMS accounted for $51 \pm 34\%$ of the NO_3 loss efficiency of all measured VOCs. The inverse relationship between the NO_3 mixing ratio and the reactivity of biogenic compounds suggested that the abundance of biogenic compounds at AI was significantly modified by nighttime NO_3 chemistry.

(2) The chemistry of NO_3 was most active at AI under the influence of continental outflow when elevated levels of NO_x and VOCs were transported under southerly flow in

the MBL. Under these conditions, isoprene and the monoterpenes were typically the dominant NO_3 reactants at the beginning of the night. Conversely, reactions with NO_3 appeared to efficiently oxidize isoprene and the monoterpenes. Strong upwind NO_x emissions greatly enhanced the importance of N_2O_5 chemistry for NO_x removal, although, with significant upwind titration of O_3 , VOC oxidation and NO_x loss actually appeared to be suppressed by reduced NO_3 production.

(3) VOC- and N_2O_5 -mediated NO_3 removal appeared to be roughly equivalent. However, N_2O_5 removal is more efficient for NO_x removal than for NO_3 removal and the average contribution of N_2O_5 chemistry to total nighttime NO_x removal was 63–66%.

(4) Based on the recommended rate coefficient for reaction of N_2O_5 with $\text{H}_2\text{O}(\text{g})$ [Atkinson, *et al.*, 2004] heterogeneous N_2O_5 chemistry appeared to be of minor importance to nocturnal NO_3 chemistry with estimated minimum average contributions to nighttime NO_3 and NO_x removal of ~10%. The corresponding average derived probabilities γ for reaction of N_2O_5 with aerosols were ~0.003–0.019. This range agrees with previous work and properties of sub- μm aerosol at AI. Our results appeared to be consistent with those of Brown *et al.* [2006a], which suggest that gas-phase N_2O_5 reactivity is overestimated by the current recommended value of $k_{(\text{H}_2\text{O}(\text{g})+\text{N}_2\text{O}_5)}$. However, based on our analysis, it is equally probable that the recommended rate coefficient is correct. The estimated maximum average contributions of heterogeneous N_2O_5 chemistry to nighttime NO_3 and NO_x removal were ~40% and ~50% respectively, corresponding to a factor of 2.9 reduction in the recommended value of $k_{(\text{H}_2\text{O}(\text{g})+\text{N}_2\text{O}_5)}$. Larger reductions in $k_{(\text{H}_2\text{O}(\text{g})+\text{N}_2\text{O}_5)}$ yielded unrealistically large γ values, suggesting that a

component of gas-phase N_2O_5 hydrolysis was necessary to adequately describe the NO_3 measurements.

(5) The 24hr-averaged NO_x loss was ~ 11 ppbv with nighttime chemistry contributing $\sim 50\%$ despite the nighttime having been only $\sim 40\%$ of a diel cycle. It follows that true NO_x removal in this region during summertime should be roughly two times that estimated based on photochemistry alone.

(6) The maximum average rate of nighttime $\text{HNO}_3(\text{g})$ production was $\sim 130\%$ of the average daytime production rate. Thus, it is likely that nighttime NO_3 chemistry was an important mechanism for causing measured $\text{HNO}_3(\text{g})$ mixing ratios to exhibit secondary maxima after dark.

(7) The overall favorable agreement between the measured and calculated NO_3 mixing ratios for the nights of July 11, 16 and 25 suggests that the kinetic treatment presented here accurately reflects the general characteristics of nighttime NO_3 chemistry at AI during the ICARTT campaign and corroborates our understanding of the overall role of nocturnal NO_3 chemistry at this site.

(8) Finally, our results suggest that variability in the chemistry of the atmosphere in this region during summer 2002 was largely reproduced during the ICARTT campaign during summer 2004.

Under certain conditions, future measurements of NO_2 , O_3 and gas phase NO_3 reactants at this site could be used, in the absence of NO_3 measurements, to help infer the role of nocturnal NO_3 chemistry. More complete simultaneous measurements of aerosol properties would help constrain aerosol loss and reconcile possible discrepancies between laboratory and field measurements of $k_{(\text{H}_2\text{O}(\text{g})+\text{N}_2\text{O}_5)}$.

CHAPTER II.

AN INTERCOMPARISON OF GC-FID AND PTR-MS TOLUENE MEASUREMENTS

II.1. Introduction

Proton transfer reaction-mass spectrometry (PTR-MS) was recently developed for on-line monitoring of atmospheric volatile organic compounds (VOCs) [*Hansel et al.*, 1995; *Lindinger et al.*, 1998]. The method and its applications in atmospheric sciences were described in great detail in recent reviews [*de Gouw and Warneke*, 2007; *Blake et al.*, 2009]. The principal advantages of PTR-MS are its capability for sensitive, high frequency measurements in real time. A disadvantage is that the method does not distinguish between isomeric/isobaric compounds; furthermore, ion fragmentation, clustering and secondary ion-molecule reactions in the drift tube can interfere in the measurement of some compounds under certain conditions [*de Gouw and Warneke*, 2007]. Considerable effort has been made to characterize the performance of PTR-MS for quantification of atmospheric VOCs, demonstrating it to be a valuable analytical method for that purpose [*de Gouw et al.*, 2003a; *de Gouw et al.*, 2003b; *Warneke et al.*, 2001; *Warneke et al.*, 2003; *de Gouw and Warneke*, 2007]. Still, the compositional diversity of the atmosphere and widespread deployment of PTR-MS for trace gas monitoring requires continued validation work be carried out, and atmospheric environments remain for which PTR-MS validation studies are lacking [*de Gouw and*

Warneke, 2007]. In particular, validation work has not been carried out in forested environments where the VOC spectrum is expected to be dominated by biogenic compounds. The present work is aimed toward the validation of PTR-MS toluene measurements based on ambient trace gas measurements at a forested site in New England.

Toluene is a significant component of fossil fuel and biomass combustion emissions [*Andreae and Merlet, 2001; Schauer et al., 2002*]. It is also released to the atmosphere via fossil fuel and industrial solvents evaporation [*Singh and Zimmerman, 1992; White et al., 2009*]. Although biogenic toluene emissions have not been widely observed [*Helmig et al., 1998*], a recent report demonstrated that toluene may be directly emitted from some plant species [*White et al., 2009*], as was suggested by observations from two previous studies [*Heiden et al., 1999; Holzinger et al., 2000*]. Toluene is a ubiquitous component of atmospheric VOC loading, and atmospheric toluene measurements have been used to probe several important issues in atmospheric sciences including photochemical aging of pollutants [*Roberts et al., 1984; Parrish et al., 2007; Warneke et al., 2007*] and emissions inventory testing [*Warneke et al., 2007; Karl et al., 2009*]. Additionally, several studies demonstrated that toluene may contribute to secondary organic aerosol formation in certain environments [e.g., *Hurley et al., 2001*].

In the analysis of VOCs in ambient air by PTR-MS, toluene is quantified from its protonated molecular ion ($C_7H_9^+$) with a mass to charge ratio (m/z) of 93. Previous field studies conducted under conditions dominated by anthropogenic emissions generally showed good quantitative agreement between toluene measurements made both by PTR-MS and gas chromatography (GC) techniques [*Warneke et al., 2001; de Gouw et al.,*

2003a; *Warneke et al.*, 2003; *Kuster et al.*, 2004; *Rogers et al.*, 2006]. However, laboratory investigations pertinent to PTR-MS measurements of monoterpenes ($C_{10}H_{16}$), which have primarily biogenic sources [*Geron et al.*, 2000], demonstrated that samples of several common monoterpenes and their oxidation products may, under certain conditions, yield $m/z = 93$ ion fragments via reactions with H_3O^+ , O_2^+ and NO^+ in the PTR-MS drift tube [*Schoon et al.*, 2003; *Tani et al.*, 2003; *Warneke et al.*, 2003; *Schoon et al.*, 2004, *Tani et al.*, 2004; *Lee et al.*, 2006a, b; *Maleknia et al.*, 2007]. An analysis of toluene measurements made by PTR-MS and GC-MS in the New England coastal marine boundary layer, downwind of monoterpene source regions, found no evidence for interference of monoterpenes in the PTR-MS toluene measurements [*de Gouw et al.*, 2003a]. Stronger correlations between monoterpenes and the PTR-MS $m/z = 93$ signal were observed in a laboratory investigation of VOC emissions from Mediterranean holm oak [*Holzinger et al.*, 2000] and in a boreal forest environment [*Rinne et al.*, 2005], although their causes could not be identified unambiguously. It was shown that the $m/z = 93$ signal measured from holm oak could be attributed to *p*-cymene ($C_{10}H_{14}$), a biogenic VOC related to the monoterpenes [*Tani et al.*, 2003]. To date, no analysis of field data dedicated to quantification of potential interferences in PTR-MS toluene measurements related to sampling of monoterpenes has appeared in the literature.

The present investigation uses ambient measurements made at a forested site in New England under conditions of enhanced monoterpene loading to quantify potential interferences in PTR-MS toluene measurements associated with sampling of monoterpenes and their oxidation products. Details of the measurement site, the analytical systems used and the data analysis methods are given in Section II.2.

Measurements of monoterpenes by GC-flame ionization detection (FID) and toluene by GC-FID and PTR-MS are presented in Section II.3, together with a quantitative analysis of potential interferences in the PTR-MS toluene measurements. The major findings are summarized in Section II.4.

II.2. Methods

II.2.1. Experimental

Measurements reported in this work were made in Durham, NH at the University of New Hampshire AIRMAP atmospheric monitoring network site Thompson Farm (THF) [Talbot *et al.*, 2005] between July 24 and August 15, 2004, during the International Consortium for Atmospheric Research on Transport and Transformation (ICARTT) field campaign. The THF site (43.11 °N, 70.95 °W, 24 m elevation above sea level) is 24 km from the Gulf of Maine on an active corn farm, seasonally planted with alfalfa; it is surrounded by mixed hardwood/pine forest [Ollinger *et al.*, 1998; Justice *et al.*, 2002]. Ambient air was drawn at ~1500 standard liters per minute through a PFA Teflon-lined aluminum manifold from the top of a 15 m tower using a Gast R5-Series regenerative blower (Gast Manufacturing, Inc., Benton Harbor, MI). Sub-samples were directed to a suite of trace gas analyzers housed at the base of the tower.

This work focuses on toluene measurements made using a GC system and a PTR-MS [Lindinger *et al.*, 1998] and monoterpene measurements made using the GC system. Ancillary measurements included nitric oxide (NO) by chemiluminescence (model

42CTL, Thermo Environmental Instruments, Inc, Franklin, MA), ozone (O_3) by UV photometer (model 49C-PS, Thermo Environmental), nitrogen dioxide photolysis frequency ($J(NO_2)$) by filter radiometer (Metcon, Inc., Boulder, CO), and meteorological parameters, measured by a suite of Qualimetrics sensors (Qualimetrics, Inc., now All Weather, Inc., Sacramento, CA), including temperature by thermistor (model 5190C), pressure by capacitance manometer (model 7190), relative humidity (RH) by thin film capacitor (model 5190C), and wind speed by anemometer (model 2031). Selected operational parameters for each of the above measurement systems are given in Table 4. The GC system [Zhou *et al.*, 2005] and the operational parameters of the PTR-MS were described in previous publications [Talbot *et al.*, 2005; Ambrose *et al.*, 2007]. Specific details pertaining to the measurements in this work are described here.

The GC sample acquisition/injection system was a modified, liquid N_2 cooled, Entech sample concentrator (Entech Instruments, Inc., Simi Valley, CA). Samples (1200 cm^3) were drawn at $\sim 200\text{ cm}^3\text{ min}^{-1}$ via a downstream pump and mass flow controller (Unit Instruments, Inc., Yorba Linda, CA) through two $20\text{ cm} \times 0.3175\text{ cm}$ Silonite-coated stainless steel loops (Entech). The first loop was cooled to $-20\text{ }^\circ\text{C}$ for sample dehumidification; the second loop was packed with 60/80 mesh glass beads (Ohio Valley Specialty Company, Marietta, OH) and cooled to $-185\text{ }^\circ\text{C}$ for analyte enrichment. After sample trapping, the loops were flushed with 100 cm^3 of ultra high purity (UHP) He (Maine Oxy, Auburn, Maine) at $100\text{ cm}^3\text{ min}^{-1}$. The sample enrichment loop was resistively heated to $100\text{ }^\circ\text{C}$ in $\sim 10\text{ s}$ and the sample was injected in UHP He carrier (Maine Oxy), via an 8-port switching valve (SV) (Valco Instruments Company, Inc., Houston, TX), into a Shimadzu 17A GC (Shimadzu Corporation, Columbia, MD), where

the sample was split to four separate capillary columns. Nonmethane hydrocarbons (NMHCs) (C_6 – C_{11}) were separated on a 60 m \times 0.32 mm I.D., 1.0- μ m film thickness VF-5ms column (Varian, Inc., Walnut Creek, CA) and measured with an FID. Following injection, the sample dehumidification and enrichment loops were both heated and back-flushed with UHP He for 5 min at 100 °C to clean the loops in preparation for the next sample. The sample cycle time was \sim 42 min with a \sim 6 min acquisition time. A 1200 cm³ aliquot of one of two different whole air standards was analyzed every ninth sample for quantification of target compounds and to monitor system performance. In this work the average *n*-decane response factor (RF), $(14.2 \pm 0.9) \times 10^3$ ppbv⁻¹ (1σ ; $n = 40$), measured from assays of a whole air standard was used for quantification of monoterpenes in ambient samples.

$$RF_{\text{decane}} = \frac{A_{\text{decane}}}{MR_{\text{decane}}} \quad (1)$$

In equation (1) A_{decane} is the decane chromatographic peak area determined from analysis of the whole air standard containing a known decane mixing ratio, MR_{decane} . Although several of the measured monoterpenes were contained in one of the whole air standards their mixing ratios were observed to decrease over time. The monoterpenes are highly reactive and were previously shown to exhibit loss in VOC standards [Sive, 1998]. Calibration experiments with the THF GC system demonstrated that the RF for monoterpenes and other C_{10} hydrocarbons were in close agreement. In fact, one of the principal advantages of the FID is that it generally yields uniform efficiency (on a per carbon basis) for quantification of hydrocarbons [Schofield, 2008]. Therefore, we used decane, for which the standard mixing ratio was stable, to quantify the FID C_{10} RF.

The PTR-MS (Ionicon Analytik GmbH, Innsbruck, Austria) was operated with a drift tube pressure of 2 mbar and a potential of 600 V applied over the length of the drift tube. A series of 30 masses was monitored continuously; six masses were monitored for diagnostic purposes while the remaining 24 masses corresponded to the VOCs of interest. The dwell time for each of the 24 masses was 20 s, yielding a total measurement cycle of ~8 min. The system was zeroed every 2.5 hrs for 4 cycles by diverting the flow of ambient air through a heated catalytic converter (0.5% Pd on alumina at 450 °C) to oxidize the VOCs and determine system background signals. Calibrations for the PTR-MS system were conducted using three different high-pressure cylinders containing synthetic blends of selected NMHCs and oxygenated VOCs (OVOCs) at the ppbv level (Apel-Reimer Environmental, Inc., Broomfield, CO). Each of the cylinders used in the calibrations had an absolute accuracy of $<\pm 5\%$ for all gases. Using methods similar to those described previously [Apel *et al.*, 1998, 2003a], standards were diluted to atmospheric mixing ratios (ppbv to pptv levels) with catalytic converter-prepared zero air adjusted to maintain the humidity of the sampled air. Calibrations were conducted periodically to monitor PTR-MS performance and quantify the mixing ratios of target gases. Mixing ratios for each gas were calculated by using the normalized counts per second which were obtained by subtracting out the non-zero background signal for each compound.

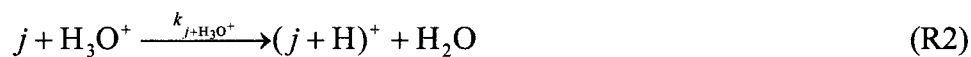
II.2.2. Calculations

The PTR-MS and GC-FID measurements were merged to the GC system time stamp. Only samples for which the GC-FID sample trapping interval and the PTR-MS sample cycle overlapped were included. The merged data were used to estimate the potential contribution of monoterpene fragmentation in the PTR-MS drift tube to the PTR-MS signal at $m/z = 93$ (nominally toluene).

The reaction of toluene (Tol) with H_3O^+ in the PTR-MS drift tube to produce the protonated molecular ion, $(\text{Tol} + \text{H})^+$, at $m/z = 93$ ($m93$) is described by reaction (R1),



where $k_{\text{Tol}+\text{H}_3\text{O}^+}$ is the rate constant for the reaction. Similarly, the reaction of compound j with H_3O^+ can be written as in reaction (R2).



For some atmospheric VOCs, including monoterpenes, the protonated molecular ion formed via reaction (R2) will fragment to lower m/z product ions under certain PTR-MS operating conditions. The production of $m/z = 93$ fragment ions from reaction of compound j with H_3O^+ can be written as in equation (R3),



where $\phi(93)_j$ is the $m93$ yield resulting from ionization of compound j . Therefore, the total rate of change of the concentration of $m/z = 93$ ions in the PTR-MS drift tube directly resulting from reaction of H_3O^+ with toluene and fragmentation of other compounds j is given by equation (2).

$$\frac{d[m93]}{dt} = k_{\text{Tol}+\text{H}_3\text{O}^+} \cdot [\text{Tol}] \cdot [\text{H}_3\text{O}^+] + [\text{H}_3\text{O}^+] \cdot \sum_j k_{j+\text{H}_3\text{O}^+} \cdot \phi(93)_j \cdot [j] \quad (2)$$

The rate constant for reaction of compound j with H_3O^+ and the concentration of j can be expressed as fractions of the corresponding rate constant for toluene and the toluene concentration, respectively.

$$k_{j+\text{H}_3\text{O}^+} = f_{k_j} \cdot k_{\text{Tol}+\text{H}_3\text{O}^+} \quad (3a)$$

$$[j] = f_j \cdot [\text{Tol}] \quad (3b)$$

Combining equations (3a) and (3b) with equation (2) gives equation (4).

$$\begin{aligned} \frac{d[m93]}{dt} &= k_{\text{Tol}+\text{H}_3\text{O}^+} \cdot [\text{Tol}] \cdot [\text{H}_3\text{O}^+] \cdot \left\{ 1 + \sum_j \phi(93)_j \cdot f_{k_j} \cdot f_j \right\} \\ &= k_{\text{Tol}+\text{H}_3\text{O}^+} \cdot [\text{Tol}] \cdot [\text{H}_3\text{O}^+] \cdot \{1 + F\} \end{aligned} \quad (4)$$

Integration of equation (4) over the time interval required for ions to traverse the drift tube, Δt , gives equation (5).

$$[m93] = k_{\text{Tol}+\text{H}_3\text{O}^+} \cdot [\text{Tol}] \cdot [\text{H}_3\text{O}^+] \cdot \{1 + F\} \cdot \Delta t \quad (5)$$

If there are no other compounds present which fragment to $m/z = 93$, all the values of $\phi(93)$ are zero, $F = 0$, and equation (5) reduces to the standard expression for integrated signal in PTR-MS [Lindinger *et al.*, 1998]. The toluene volume mixing ratio, $\text{VMR}(m93)$ (hereinafter referred to simply as the toluene mixing ratio), is quantified based on the ratio of the ion current (counts per second, cps) at $m/z = 93$, I_{m93} , to the normalized ion current (ncps) for H_3O^+ as shown in equation (6),

$$\text{VMR}(m93) = \frac{I_{m93} - I_{m93b}}{\left(\frac{I_{\text{H}_3\text{O}^+}}{10^6} \right) \cdot C_{\text{Tol}}} \quad (6)$$

where I_{m93b} is the background $m/z = 93$ ion current and C_{Tol} denotes the calibration factor (sensitivity) for toluene, typically expressed in units of ncps ppbv⁻¹. In this work the calibration factor was determined from assays of standard gas cylinders as described in Section II.2.1. Alternatively, the calibration factor can be determined from the instrument operating parameters, measured ion transmission efficiencies, Tr , and published values of $k_{\text{Tol}+\text{H}_3\text{O}^+}$ and H_3O^+ ion mobility, μ , as described previously [de Gouw and Warneke, 2007]. The ion transmission efficiency is related to the ion concentration and measured current as shown for the example of the $m/z = 93$ ion in equation (7),

$$I_{m93} - I_{m93b} = Tr_{m93} \cdot [m93] \quad (7)$$

Combining equation (6) with equation (7) gives equation (8).

$$\text{VMR}(m93) = \frac{Tr_{m93} \cdot [m93]}{\left(\frac{I_{\text{H}_3\text{O}^+}}{10^6}\right) \cdot C_{\text{Tol}}} \quad (8)$$

In ambient air samples with contributions to $[m93]$ from j as described above the true toluene mixing ratio, $\text{VMR}(m93)_t$, and the apparent measured toluene mixing ratio, $\text{VMR}(m93)_m$, can be defined as shown in equation (9), which follows from equations (5) and (8).

$$\text{VMR}(m93)_t = \text{VMR}(m93)_m \cdot \frac{1}{\{1 + F\}} \quad (9)$$

As expected, equation (9) shows that the value of $\text{VMR}(m93)_t$ will always be smaller than that of $\text{VMR}(m93)_m$ in the presence of monoterpenes that fragment to ion products at $m/z = 93$ (i.e., $F > 0$). Similar to equation (9) corrections can be made for (1) production of ion products at $m/z = 93$ from reactions of monoterpenes with O_2^+ and NO^+ in the PTR-MS drift tube and (2) fragmentation of monoterpenes oxidation products. It should

be noted that O_2^+ and NO^+ ionize by charge transfer rather than by proton transfer as for H_3O^+ . To account for reactions of O_2^+ and NO^+ with j , additional terms that represent abundances of O_2^+ and NO^+ relative to H_3O^+ in the PTR-MS drift tube are included in F . Values of F are obtained primarily from knowledge of monoterpenes present together with published data for parameters such as proton and charge transfer rate constants.

II.3. Results and Discussion

II.3.1. Monoterpene Distributions

Here we present GC-FID measurements of monoterpenes at THF during summer 2004. In the discussion that follows monoterpenes include $C_{10}H_{16}$ hydrocarbons as well as *p*-cymene ($C_{10}H_{14}$), which is a related biogenic hydrocarbon [Geron *et al.*, 2000]. The monoterpene composition of plant species in the northeastern United States was previously shown to consist mostly of α -pinene, Δ^3 -carene, β -pinene, *d*-limonene, sabinene, β -phellandrene, *p*-cymene, β -myrcene, ocimene, and terpinolene, whereas α - and β -pinene, camphene, Δ^3 -carene, β -myrcene, *d*-limonene, sabinene, *p*-cymene, and β -phellandrene were estimated to compose >95% of summertime monoterpenes emissions from forestland encompassing the THF site (Table 5) [Geron *et al.*, 2000]. At THF we identified and regularly measured α - and β -pinene, camphene, Δ^3 -carene, and *d*-limonene in ambient samples. All major chromatographic features observed in ambient chromatograms in the monoterpenes' retention time window were identified from whole air and synthetic standards.

Retention times (RTs) for additional monoterpenes not identified from qualitative and quantitative standards were estimated based on the observed correlation between measured RTs and published boiling point (b.p.) values for C₉–C₁₁ hydrocarbons in the primary working standard that eluted from the VF-5ms column between nonane (C₉H₂₀; b.p. = 150.82 °C) and undecane (C₁₁H₂₄; b.p. = 195.9 °C) (Figure 10, Table 6). The elution order of the normal alkanes did not follow the same trend as the aromatics and monoterpenes and so the *n*-alkanes were excluded from the regression analysis. Peak identifications for *o*-xylene and C₉–C₁₁ hydrocarbons in the primary working standard are shown in Figure 11. Table 6 lists b.p. values together with (1) measured average RTs for C₉–C₁₁ hydrocarbons identified in Figure 11 and (2) RTs predicted based on the regression analysis shown in Figure 10 for several additional monoterpenes. For comparison, the regression analysis shown in Figure 10 predicted RTs for camphene and Δ³-carene of 11.5 ± 0.3 min and 12.6 ± 0.2 min (Table 6), whereas the values measured from a multi-component synthetic standard were ~11.6 min and ~12.8 min, respectively. The agreement between predicted and measured RTs indicated that the RT versus b.p. relationship determined for C₉–C₁₁ hydrocarbons in the primary working standard was a good predictor of RTs for monoterpenes when measured values were not available.

Figure 12 shows an example chromatogram from the night of August 2, when significantly elevated monoterpene mixing ratios were measured. The unidentified peak at ~13.3 min, labeled “UnID”, was within the estimated retention time windows for ocimene and *p*-cymene (Table 6), which were not identified from qualitative and quantitative standards. The area of the unidentified peak was strongly correlated with those of the other major monoterpenes, as illustrated in Figure 13; however, it typically

represented a minor fraction of the total monoterpene mixing ratio. Other minor features that could be attributed to β -phellandrene, α -terpinene, γ -terpinene, and terpinolene were also observed while the monoterpene mixing ratio was elevated; however, the corresponding mixing ratios, estimated using the *n*-decane RF, were typically below the instrumental limit of detection (LOD) for the monoterpenes (0.010 ppbv). Due to their apparent low abundance monoterpenes other than those measured (Table 5) were not considered in the following analysis.

A time series of the monoterpene mixing ratios measured between 22:00 on July 24 and 06:00 on August 15 is presented in Figure 14. Measurements of $J(\text{NO}_2)$, expressed as 10 min average values normalized to the summertime (June to August) maximum, $7.9 \times 10^{-3} \text{ s}^{-1}$, reflect relative solar irradiance intensity and delineate daytime and nighttime periods. Sunrise, sunset times ranged from ~05:27, 20:13 on July 24 to ~05:50, 19:46 on August 15, as determined using the NOAA Sunrise/Sunset Calculator (www.ssr.noaa.gov/highlights/sunrise/sunrise.html; accessed on May 22, 2009). The highest monoterpene mixing ratios were measured during the nighttime hours under calm conditions (wind speed $<0.5 \text{ m s}^{-1}$) and with more humidity, which may have contributed to the nocturnal emissions [Geron *et al.*, 2000]. Previous work demonstrated that the nocturnal boundary layer in the region encompassing the THF site can lead to nighttime surface enhancements in trace gases with local emissions sources [Talbot *et al.*, 2005; White *et al.*, 2008], which likely contributed significantly to the nighttime monoterpene maxima. The observed daytime minima in the monoterpene mixing ratios were likely driven by increased ventilation of the boundary layer as well as greater oxidation by

hydroxyl radical (OH) and O₃ during the daytime despite higher monoterpene emissions during the day owing to warmer temperatures [Guenther *et al.*, 1993].

Table 5 compares estimated summertime monoterpene fluxes [Geron *et al.*, 2000] for forestland encompassing the THF site and average relative ambient monoterpene distributions for summer 2004 based on data shown in Figure 14. The flux estimates were derived from regional tree species distributions, monoterpene composition and emissions at 30 °C [Geron *et al.*, 2000]. The flux uncertainty was within a factor of 2 to 3, given uncertainties in monoterpene composition, emissions and tree species distributions [Geron *et al.*, 2000]. The estimated flux distribution and measured mixing ratio distributions were in partial quantitative agreement for the dominant monoterpenes, except a greater abundance of camphene than β -pinene was measured, and β -myrcene was not measured. The measured daytime and nighttime mixing ratio distributions were in close agreement, as observed previously at a rural site in Colorado [Roberts *et al.*, 1985].

Based on data collected between 1990 and 1999, land cover in Strafford County, in which the THF site is situated, consisted mostly of mixed forestland (~57% of forestland) and deciduous tree species (~30% of forestland) [Justice *et al.*, 2002], for which monoterpene composition and emissions data were relatively scarce when the regional monoterpenes flux estimates shown in Table 5 were compiled [Geron *et al.*, 2000]. Thus, it is conceivable that local patterns of tree species distribution and monoterpene emissions contributed to the differences between the emissions and mixing ratio distributions in Table 5. The monoterpenes react rapidly with OH, O₃ and the nitrate radical (NO₃) [Atkinson, 1994; Atkinson and Arey, 2003], and monoterpene

oxidation between emission and sampling likely contributed to the measured monoterpene distribution at THF. The lifetime of β -myrcene with respect to reaction with O₃ is much shorter than for the monoterpenes measured at THF [Atkinson and Arey, 2003], which might partially explain why β -myrcene was not measured in ambient air at THF, despite the relatively high β -myrcene emissions flux predicted for the THF region [Geron *et al.*, 2000].

II.3.2. GC-FID/PTR-MS Toluene Field Intercomparison

Several laboratory and field intercomparisons among PTR-MS and GC-based toluene measurements were conducted previously, with most studies demonstrating good quantitative agreement between PTR-MS and the more established chromatography-based measurement techniques. These include comparison of PTR-MS with (1) GC-FID (offline) at a suburban site in the Netherlands during March, 2000 [Warneke *et al.*, 2001]; (2) GC-MS, with ion trap and quadrupole MS, at a suburban site in Houston, TX during August and September, 2000 [Kuster *et al.*, 2004]; (3) GC-MS aboard a research ship in the New England coastal marine boundary layer (CMBL) during July and August, 2002 [de Gouw *et al.*, 2003a]; (4) GC-FID at a suburban site in Tokyo, Japan during November, 2002 [Kato *et al.*, 2004]; (5) GC-FID (offline) at a laboratory biomass combustion facility [Christian *et al.*, 2004]; (6) GC-FID (offline) in the Mexico City metropolitan area during April and May, 2003 [Rogers *et al.*, 2006]; (7) GC-FID (offline) aboard a research aircraft over New England and eastern Canada during July, 2004 [de

Gouw et al., 2006]; and (8) GC-MS and GC-FID (offline) aboard a research aircraft in the vicinity of Mexico City during March, 2006 [*Karl et al.*, 2009].

Analyses coupling GC with PTR-MS (GC-PTR-MS) were also employed to determine the specificity of PTR-MS for measuring atmospheric toluene. In air samples collected at urban sites (Utrecht, The Netherlands and Boulder, CO) during March, 2001 and January, 2002 and a remote site in the Austrian Alps during March, 2001 only toluene contributed to the PTR-MS $m/z = 93$ signal [*de Gouw et al.*, 2003b; *Warneke et al.*, 2003]. Laboratory GC-PTR-MS measurements showed α - and β -pinene to yield minor quantities of $m/z = 93$ ion fragments [*Warneke et al.*, 2003]. To accommodate the laboratory results *de Gouw et al.* [2003a] fit PTR-MS $m/z = 93$ signal to a linear combination of toluene and either α - or β -pinene measured by GC-MS using data collected in the New England CMBL during summertime. However, they did not obtain significant contributions from α - and β -pinene to PTR-MS $m/z = 93$ signal under conditions of elevated monoterpene mixing ratios.

Here we compare toluene measurements by GC-FID and PTR-MS from the AIRMAP THF monitoring site during the summer of 2004. Figure 15 shows time series of toluene mixing ratios measured by GC-FID and PTR-MS from 22:00 on July 24 to 06:00 on August 15. Overall the two systems tracked each other well from values at or near the GC-FID and PTR-MS LODs to maxima of 0.42 ± 0.02 ppbv (GC-FID) and 0.52 ± 0.03 ppbv (PTR-MS).

The GC-FID and PTR-MS data sets yielded 351 merged samples in which toluene was above the LOD for the PTR-MS (0.015 ppbv) and GC-FID (0.005 ppbv), with median toluene mixing ratios of 0.085 ± 0.006 ppbv (GC-FID) and 0.085 ± 0.017 ppbv

(PTR-MS). For 60% of the merged samples the toluene mixing ratios measured with the two systems agreed quantitatively within the combined 1σ measurement precisions. Figure 16 shows a linear correlation plot for the merged data. The parameters of simple least squares regression and orthogonal least squares regression (determined using JMPTM statistical software) are given in Table 7 (Treatments A and A', respectively). Orthogonal least squares accounts for errors in both independent and dependent variables [Tan and Iglewicz, 1999] and was applied in a previous intercomparison among ambient PTR-MS and GC-MS toluene measurements [de Gouw *et al.*, 2003a]. As shown in Table 7 the results of both regression analyses agree quantitatively in terms of the regression parameters and the coefficients of determination. In the following discussion the results of different treatments of the PTR-MS toluene data are analyzed in terms of simple least squares regression parameters.

II.3.3. Sources of Interference from Monoterpene Fragmentation

The C₁₀H₁₆ monoterpenes are typically detected by PTR-MS as the protonated molecular ion ($m/z = 137$) and a dominant fragment ion with $m/z = 81$. As discussed in greater detail below $m/z = 93$ ions may also be generated from monoterpene fragmentation in the PTR-MS drift tube. The $m/z = 93, 81$ and 137 signals were observed by PTR-MS in a laboratory study of VOC emissions from Mediterranean holm oak [Holzinger *et al.*, 2000], consistent with (1) a biogenic toluene source, as was observed from sunflower and Scots pine by GC-MS [Heiden *et al.*, 1999] and alfalfa by GC-FID [White *et al.*, 2009], and (2) monoterpene fragmentation in the PTR-MS drift tube [Tani

et al., 2003]. In a factor analysis applied to PTR-MS measurements of VOCs in a boreal forest during July, 2004 the $m/z = 93$, 81 and 137 signals loaded strongly on the same factor [Rinne *et al.*, 2005]; however, the implications were not discussed.

Here we discuss several possible sources of interferences in PTR-MS analysis of toluene related to simultaneous sampling and analysis of monoterpenes. During the period from July 24 to August 15, 2004 toluene and monoterpenes were quantified by GC-FID from a total of 600 ambient samples at THF. The ratio of the sum of the monoterpene mixing ratio to the GC-FID toluene mixing ratio, hereinafter denoted by Δ_{Mon} , ranged from <0.25 to 31 ± 2 , with a median value of 2.4. For the merged data set ($n = 349$) the median value of Δ_{Mon} was 2.6 ± 0.2 . By comparison maximum Δ_{Mon} values of >5 were reported from measurements made in the Gulf of Maine during summer of 2002 [de Gouw *et al.*, 2003a]. Thus, it appears we observed relatively large enhancements in monoterpenes relative to toluene at the THF site during summer 2004 and our data provide a unique test of the specificity of PTR-MS for measurement of toluene in an atmospheric environment strongly influenced by biogenic monoterpene emissions.

It is expected that the generation of ion products at $m/z = 93$ by monoterpene fragmentation in the PTR-MS drift tube would result in (1) a positive bias in the PTR-MS toluene measurements as compared with the GC-FID measurements, and (2) a positive correlation between Δ_{Mon} and the magnitude of the PTR-MS bias. An overall positive bias of $\sim 13\%$ was observed in the PTR-MS measurements as indicated by the slope of the least squares regression fit to the merged data in Figure 16 (Table 7, treatment A). Although the observed bias is consistent with an additional source of $m/z = 93$ ions in the

PTR-MS instrument it could have been introduced in the calibrations or resulted from errors in the blank signal quantification and subtraction. Figure 17 compares time series of the PTR-MS error (percent difference with respect to the GC toluene measurements), hereinafter denoted as $\epsilon_{\text{PTR-MS}}$, and Δ_{Mon} . Maxima in the values of $\epsilon_{\text{PTR-MS}}$ and Δ_{Mon} generally occurred during nighttime but did not appear to be well correlated, suggesting qualitatively that interference in the PTR-MS toluene measurements from monoterpene fragmentation was unimportant at THF. Quantitative estimates of potential interferences in the PTR-MS toluene measurements are presented below.

II.3.3.1. Reactions with H_3O^+ .

Ion products were detected at $m/z = 93$ in laboratory PTR-MS analyses of six monoterpenes, α -pinene [Warneke *et al.*, 2003; Maleknia *et al.*, 2007], β -pinene [Warneke *et al.*, 2003], d -limonene [Maleknia *et al.*, 2007], γ -terpinene [Maleknia *et al.*, 2007], α -terpinene [Lee *et al.*, 2006b], and p -cymene [Tani *et al.*, 2003, 2004; Maleknia *et al.*, 2007], and in the analysis of α -pinene and β -myrcene by selected ion flow tube mass spectrometry (SIFT-MS) using H_3O^+ as reagent ion [Schoon *et al.*, 2003]. Table 8 compares yields of $m/z = 93$ fragment ions, $\phi(93)$, reported in the literature. When more than one set of operating parameters was employed, as in several of the above studies [Tani *et al.*, 2003, 2004; Maleknia *et al.*, 2007], fragmentation data chosen for comparison in Table 8 correspond with operating parameters most similar to those used at THF. When data were not available regarding the fraction of NO^+ and O_2^+ in the PTR-MS drift tube, the reported values of $\phi(93)$ were attributed entirely to H_3O^+ reactions;

however, contributions from reactions of the parent monoterpenes with NO^+ and O_2^+ should not be ruled out (see below). It is also important to note that fragmentation patterns are partly controlled by PTR-MS operating conditions, which differed between studies; therefore, the yields reported in Table 8 may differ significantly from the actual yields obtained at THF. Table 9 gives the instrumental operating parameters, when available, corresponding with the fragmentation yields reported in Table 8 as well as the parameters employed at THF during summer 2004. Also given in Table 9 are mean H_3O^+ kinetic energies, KE_{ion} , calculated from the tabulated operating parameters using equation (10) [McFarland *et al.*, 1973],

$$\text{KE}_{\text{ion}} = \frac{1}{2} \cdot m \cdot v_d^2 + \frac{1}{2} \cdot M_b \cdot v_d^2 + \frac{3}{2} \cdot k_B \cdot T \quad (10)$$

where m and M_b are the H_3O^+ and buffer gas molecular weights, respectively, v_d is the H_3O^+ drift velocity, T is the drift tube temperature, and k_B is the Boltzmann constant. The drift velocity was calculated using equation (11) [de Gouw and Warneke, 2007],

$$v_d = \frac{\mu_0 \cdot N_0 \cdot E}{N} \quad (11)$$

where μ_0 is the reduced H_3O^+ mobility in the buffer gas, N_0 is the gas number density at standard temperature and pressure, E is the electric field strength, and N is the gas number density under the experimental conditions. The values of KE_{ion} in Table 9 allow H_3O^+ -neutral collision energies to be compared between studies. Increasing KE_{ion} generally results in greater product ion fragmentation in the PTR-MS drift tube [c.f., Tani *et al.*, 2003].

Although most previous studies reported values of $\phi(93) \leq 1\%$ from PTR-MS analysis and reaction with H_3O^+ of the monoterpenes measured at THF, two showed

$\phi(93) > 1\%$ from PTR-MS analysis of α -pinene [Warneke *et al.*, 2003; Maleknia *et al.*, 2007], while one study reported $\phi(93) > 1\%$ from PTR-MS analysis of β -pinene [Warneke *et al.*, 2003]. Impurities in liquid monoterpene standards employed in previous laboratory PTR-MS studies were measured at $m/z = 93$ [Tani *et al.*, 2003], and it is possible that uncharacterized impurities contributed to the maximum $\phi(93)$ value of 12% shown in Table 8. However, it is less likely that interference from impurities contributed to the high $\phi(93)$ values of 7% measured for α - and β -pinene in a GC-PTR-MS analysis of synthetic gas standards [Warneke *et al.*, 2003]. Therefore, we considered values of $\phi(93)$ significantly greater than 1% in quantifying possible interferences from α - and β -pinene fragmentation in the PTR-MS drift tube.

Corrections to the PTR-MS toluene mixing ratios were calculated for reactions of H_3O^+ with the measured monoterpenes as shown in Section II.2.2 using values of Δ_{Mon} from the GC-FID measurements; proton transfer reaction rate constants measured previously for toluene [Španěl and Smith, 1998], α - and β -pinene [Tani *et al.*, 2003]; and integer values of $\phi(93)$ within the range of those reported previously (Table 8). To simplify the analysis we only considered corrections for which the value of $\phi(93)$ for α -pinene was \geq that for β -pinene, consistent with previous observations (Table 8). Table 7 presents quantitative data comparing the GC-FID and PTR-MS toluene measurements for several fragmentation corrections (treatments B to F) applied to the PTR-MS measurements. We defined fragmentation corrections that improved quantitative agreement between the GC-FID and PTR-MS measurements as those which (1) reduced the deviation of the simple least squares regression slope from unity and (2) increased the percentage of data for which both instruments agreed within combined measurement

precisions. The minimum fragmentation correction used a value of $\phi(93) = 1\%$ for α -pinene (treatment B). The best quantitative agreement between the two data sets was achieved with $\phi(93) = 2\%$ for α -pinene and 1% for β -pinene (treatment C). For treatment C the median, 75th and 95th percentile corrections were 3%, 8% and 19%, respectively; most of the corrections were within the PTR-MS measurement precision and were therefore insignificant. Values of $\phi(93) > 5\%$ for α -pinene (e.g., treatment D) resulted in poorer quantitative agreement than for the uncorrected measurements. Thus, our data appear to be most consistent with small values of $\phi(93)$ for the measured monoterpenes and only a minor interference in the PTR-MS toluene measurements from reactions of monoterpenes with H_3O^+ in the PTR-MS drift tube.

II.3.3.2. Reactions with O_2^+ and NO^+ .

The O_2^+ and NO^+ ions are formed in low yield in the PTR-MS ion source drift region [Hansel *et al.*, 1995; de Gouw and Warneke, 2007], and their reactions with monoterpenes were shown to generate products that may interfere with the PTR-MS signal at $m/z = 93$. Reactions of O_2^+ with α - and β -pinene, *d*-limonene, Δ^3 -carene, β -myrcene, and camphene in the flow tube of a SIFT-MS instrument produced fragment ion products with $\phi_{93} > 10\%$ in all cases (Table 8) [Schoon *et al.*, 2003]. Similarly, reactions of NO^+ with β -myrcene yielded fragment ion products with $\phi(93) = 22\%$ [Schoon *et al.*, 2003]. Lower yields (<5%) of $m/z = 93$ products were measured for reactions of NO^+ with α - and β -pinene, *d*-limonene, Δ^3 -carene, and camphene [Schoon *et al.*, 2003]. It is important to note that the absence of a strong electric field along the SIFT-MS flow tube

results in substantially lower H_3O^+ -neutral collision energies in SIFT-MS than in PTR-MS, as illustrated by values of KE_{ion} given in Table 9. Furthermore, the stabilities of reaction intermediates are affected by the buffer gas, which differs between SIFT-MS and PTR-MS. Table 8 compares values of $\phi(81)$ measured for several monoterpenes by SIFT-MS, using H_3O^+ as reagent ion, and PTR-MS, illustrating that the extent of monoterpene fragmentation (1) was greater at higher ratios of electric field strength to gas number density, E/N , in PTR-MS analyses and (2) was significantly greater, by a factor of $1.8 \pm 0.7(1\sigma)$, in PTR-MS (with $E/N = 120\text{--}150$ Td) than in SIFT-MS analyses. Accordingly, fragmentation yields from reactions of monoterpenes with O_2^+ and NO^+ at THF likely were significantly higher than those observed by SIFT-MS.

Corrections to the PTR-MS toluene mixing ratios were calculated for reactions of O_2^+ with the measured monoterpenes in the PTR-MS drift tube (Table 7, treatment E). The calculations used rate constants and fragmentation patterns measured by SIFT-MS (Table 8) [Schoon *et al.*, 2003]. At THF the PTR-MS signal at $m/z = 32$, which we attributed to O_2^+ , was typically <1% of the H_3O^+ signal during summer 2004, and the median correction to the PTR-MS toluene mixing ratios was <1%, while the 95th percentile correction was 6%. The quantitative agreement with the GC-FID measurements was slightly improved as compared with the uncorrected PTR-MS measurements (Table 7); however, the corrections were entirely within the PTR-MS measurement precision and therefore were insignificant. Increasing the values of $\phi(93)$ (Table 8) by a factor of 2 for O_2^+ reactions with the measured monoterpenes, yielding $\phi(93) = 100\%$ for α - and β -pinene, did not significantly influence the results for treatment E. Applying corrections for H_3O^+ and O_2^+ reactions together (treatment F) did

not significantly affect agreement with the GC-FID measurements compared to when corrections were applied only for H_3O^+ reactions. Our calculations suggest that reactions of monoterpenes with O_2^+ in the PTR-MS drift tube likely resulted in a minor additional source of $m/z = 93$ fragment ions which did not interfere significantly with the measured toluene mixing ratios.

The PTR-MS signal at $m/z = 31$, with contributions from $^{15}\text{N}^{16}\text{O}^+$ and likely also the protonated molecular ion of formaldehyde (H_3CO^+) [de Gouw and Warneke, 2007], was typically $<0.001\%$ of the H_3O^+ signal. The corresponding $^{14}\text{N}^{16}\text{O}^+$ signal at $m/z = 30$ (unmeasured) was calculated to be $<0.3\%$. Thus, considering that values of $\phi(93)$ for NO^+ reactions are generally lower than those for O_2^+ (Table 8), reactions of monoterpenes with NO^+ in the PTR-MS drift tube likely did not significantly affect the measured $m/z = 93$ ion current.

II.3.4. Sources of Interference from Monoterpene Oxidation Products

Table 10 gives yields of $m/z = 93$ fragment ions from ozonolysis and photooxidation products of several monoterpenes. Reported formation yields for the oxidation products are also tabulated. Reactions of H_3O^+ with oxidation products of α -pinene and Δ^3 -carene were shown by SIFT-MS to give fragment ions at $m/z = 93$ [Schoon *et al.*, 2004]. Products from ozonolysis of β -myrcene and terpinolene were detected by PTR-MS at $m/z = 93$ in a recent laboratory chamber study [Lee *et al.*, 2006a]. In an investigation of monoterpene photochemistry by the same group [Lee *et al.*, 2006b] photooxidation of β -myrcene, Δ^3 -carene, γ -terpinene and terpinolene gave products

detected by PTR-MS at $m/z = 93$ with >5% molar yield, whereas photooxidation of β -pinene gave products detected at $m/z = 93$ with <5% molar yield. Ocimene undergoes similar ozonolysis and photooxidation chemistry as β -myrcene [Reissell *et al.*, 2002], and therefore could potentially also yield an additional indirect source of $m/z = 93$ fragment ions in PTR-MS analysis of monoterpenes during periods of active oxidation chemistry. In the following discussion we consider production of $m/z = 93$ fragment ions from reactions of identified oxidation products of the monoterpenes measured at THF: pinonaldehyde, α -pinene oxide and caronaldehyde.

II.3.4.1. Ozonolysis Products.

We used O_3 measurements, together with published kinetic data for O_3 -monoterpene reactions and product formation yields (Table 10) to estimate production rates of pinonaldehyde and α -pinene oxide from α -pinene ozonolysis, and caronaldehyde from Δ^3 -carene ozonolysis at THF. Unless otherwise indicated kinetic and product yield data from the most recent recommendations of the IUPAC Subcommittee for Gas Kinetic Data Evaluation [Atkinson *et al.*, 2006, 2009] and from previous critical reviews [Atkinson, 1994; Atkinson, 1997] were used. Local conditions of pressure and temperature were used in all kinetic calculations; temperature dependencies have not been quantified for oxidation reactions of the majority of the monoterpenes. The calculated pinonaldehyde production rates, based on a yield of $16 \pm 3\%$ (Table 10), ranged from <0.001 to 0.023 ± 0.015 ppbv hr⁻¹, with uncertainty governed mostly by contribution from the rate constant [Atkinson *et al.*, 2009]. The measured α -pinene

mixing ratios were linearly interpolated between consecutive GC-FID samples to estimate pinonaldehyde production rates at 5 min time resolution. Pinonaldehyde mixing ratios were estimated by summing the 5 min production rates over 1 hour intervals, and ranged from <0.001 to 0.023 ± 0.004 ppbv. Corrections to the PTR-MS toluene measurements for reactions of H_3O^+ with pinonaldehyde were calculated as described above for reactions of H_3O^+ and O_2^+ with the parent monoterpenes. A value of $\phi(93) = 0.02$ (Table 10) and the measured proton transfer rate coefficient for pinonaldehyde [Schoon *et al.*, 2004] resulted in negligible, 95th percentile $<1\%$, corrections to the PTR-MS toluene mixing ratios. The pinonaldehyde mixing ratio estimates bear considerable uncertainty since atmospheric loss processes and transport were not taken into account. To partially account for the possibility of a higher value of $\phi(93)$ and greater pinonaldehyde accumulation in the sampled air, calculations were performed with the SIFT-MS value of $\phi(93)$ increased by a factor of 2. With $\phi(93) = 0.04$ the 95th percentile correction remained $<1\%$. Calculated production rates for α -pinene oxide and caronaldehyde were considerably lower than for pinonaldehyde, <0.003 and <0.001 ppbv hr^{-1} respectively, therefore it is likely that sampling of α -pinene oxide and caronaldehyde from O_3 -initiated oxidation of α -pinene and Δ^3 -carene did not significantly interfere in the PTR-MS toluene measurement.

II.3.4.2. Photooxidation Products.

Because no measurements of OH have been made at THF to date the quantitative contribution of OH to monoterpene oxidation at THF is highly uncertain. We used a

simple approximation of OH concentrations, together with published kinetic data [Atkinson, 1989; Atkinson, 1994; Atkinson *et al.*, 2006, 2009] and formation yields for monoterpene photooxidation products (Table 10) to estimate production rates of pinonaldehyde and caronaldehyde from reactions of OH with α -pinene and Δ^3 -carene, respectively. Considering only daytime OH chemistry the time rate of change of the pinonaldehyde mixing ratio was approximated by equation (12a).

$$\frac{d[\text{Pinon.}]}{dt} = P_{\text{Pinon}} - k'_{\text{OH} + \text{Pinon}} \cdot [\text{Pinon}] \quad (12a)$$

$$P_{\text{Pinon.}} = k_{\text{OH} + \alpha\text{-Pin}} \cdot f_{\text{Pinon}} \cdot [\alpha\text{-Pin}] \cdot [\text{OH}] \quad (12b)$$

$$k'_{\text{OH} + \text{Pinon}} = k_{\text{OH} + \text{Pinon}} \cdot [\text{OH}] \quad (12c)$$

Here P_{Pinon} is the pinonaldehyde production rate, f_{Pinon} denotes the formation yield of pinonaldehyde from reactions of OH with α -pinene, and the bracketed terms represent concentrations where α -Pin and Pinon stand for α -pinene and pinonaldehyde, respectively. Pinonaldehyde mixing ratios were estimated by integrating equation (12a) stepwise over twelve consecutive 5 min intervals (1 hr), with the initial condition that $[\text{Pinon}] = 0$. For each 5 min interval, the terms P_{Pinon} and $k'_{\text{OH} + \text{Pinon}}$ were calculated from the interpolated (5 min intervals) α -pinene mixing ratios and a constant OH concentration of 2×10^6 molecules cm^{-3} . The starting value of $[\text{Pinon}]$ was taken from integration over the preceding interval. Caronaldehyde mixing ratios were estimated analogous to the pinonaldehyde estimates. Integration of equation (12a) and the method used for estimating pinonaldehyde mixing ratios from α -pinene ozonolysis are equivalent when the second term on the right side of equation (12a) is excluded, which is appropriate for the slow O_3 -carbonyl reactions [c.f., Hakola *et al.*, 1994]. A similar method as outlined

above was previously applied to estimate nighttime nitrate radical mixing ratios at the AIRMAP atmospheric monitoring station on Appledore Island, Maine [Ambrose *et al.*, 2007]. The approach is less appropriate here because the pinonaldehyde lifetime may be long enough for transport to partially govern its atmospheric mixing ratios. As for the pinonaldehyde levels estimated from α -pinene ozonolysis, the mixing ratios estimated from OH oxidation bear large uncertainties. The calculated pinonaldehyde production rates ranged from <0.001 to 0.11 ± 0.09 ppbv hr⁻¹ based on an upper limit pinonaldehyde yield of $87 \pm 20\%$ (Table 10). The 1 hr integrated pinonaldehyde mixing ratios ranged from <0.001 to 0.10 ± 0.02 ppbv, with maximum values occurring during the early morning hours, 06:00 to 07:30. A value of $\phi(93) = 0.02$ (Table 10) and the measured proton transfer rate coefficient for pinonaldehyde [Schoon *et al.*, 2004] resulted in negligible, 95th percentile $<1\%$, corrections to the PTR-MS toluene mixing ratios during the daytime hours. Measured OH concentrations were shown previously to be strongly correlated with solar ultraviolet radiation (UV) [Ehhalt and Rohrer, 2000; Rohrer and Berresheim, 2006]. An approximation of OH that is consistent with the observed correlations between the OH concentration and solar UV would give lower OH concentrations and reduced oxidation rates at dawn, resulting in smaller corrections than for the case of a uniform OH concentration. Calculated production rates for caronaldehyde were slightly lower than for pinonaldehyde, <0.09 ppbv hr⁻¹, while the SIFT-MS value of $\phi(93)$ [Schoon *et al.*, 2004] is only a factor of 1.5 higher for caronaldehyde (Table 10). Thus, it is likely that sampling of caronaldehyde from the oxidation of Δ^3 -carene by OH did not significantly interfere in the PTR-MS toluene analysis.

In addition to daytime photochemistry, reactions of O₃ with alkenes were shown previously to generate OH in the dark [Atkinson, 1994]. Yields of OH determined previously from ozonolysis of the monoterpenes measured at THF were typically large and ranged from ≤0.18 for camphene to 1.06 (±50%) for Δ³-carene [Atkinson, 1997]. Based on measured nighttime monoterpene and O₃ mixing ratios and published kinetic data [Atkinson, 1994; Atkinson *et al.*, 2009] and OH yields [Atkinson, 1997] the median nighttime OH production rate at THF was calculated to be ~0.03 ppbv hr⁻¹ and dominated by α-pinene ozonolysis. For comparison, daytime OH production rates were calculated for the reaction sequence (R4) + (R5) using measurements of atmospheric pressure, RH, and *J*(NO₂) and published kinetic data for reactions of singlet oxygen, O¹D, with N₂, O₂, and H₂O [Atkinson *et al.*, 2004].



Values of *J*(O¹D) were estimated from the *J*(NO₂) measurements using equation (13), which was derived from observations during summertime at a research site in northern Germany [Ehhalt and Rohrer, 2000].

$$J(\text{O}^1\text{D}) = \left(\frac{J(\text{NO}_2)}{1.6} \right)^2 \quad (13)$$

The median daytime OH production rate from reactions (R4) and (R5) was calculated to be ~0.1 ppbv hr⁻¹, and may represent <25% of the total daytime OH production [Rohrer and Berresheim, 2006]. Thus, it is expected that OH made a small but perhaps non-negligible contribution to nighttime monoterpenes oxidation at THF. Published mechanisms for the oxidation of α-pinene by OH require values of

$\text{VMR}(\text{NO})/\text{VMR}(\text{Mon}) \geq 1$ for maximal yield of pinonaldehyde [Pinho *et al.*, 2007]. Pinonaldehyde yields significantly lower than the values given in Table 10 were observed previously from photooxidation of α -pinene in the absence of NO [Hatakeyama *et al.*, 1991]. Nighttime NO levels at THF were typically below the 0.06 ppbv instrumental LOD, 95th percentile <0.15 ppbv, and values of $\text{VMR}(\text{NO})/\text{VMR}(\text{Mon})$ were typically <0.01, 95th percentile <0.21. Thus, nighttime OH-initiated production of pinonaldehyde and caronaldehyde (by analogy) was expected to be significantly lower than daytime production despite higher monoterpene mixing ratios during nighttime. In conclusion the above analysis suggests that products of OH-initiate monoterpene oxidation did not interfere with the PTR-MS toluene measurement at THF.

II.3.5. Additional Contributions to PTR-MS Signal at $m/z = 93$

For completeness it should be noted that, in addition to toluene and fragment ions produced from monoterpenes and their oxidation products, chloroacetone was also shown to yield an $m/z = 93$ ion ($\text{C}_3\text{H}_6\text{ClO}^+$) when measured via PTR-MS [Warneke *et al.*, 2003]. Also, several laboratory studies have attributed PTR-MS measurements of $m/z = 93$ ions to proton-bound ethanol dimers ($\text{C}_4\text{H}_{13}\text{O}_2^+$; $(\text{EtOH})_2 + \text{H}^+$) [Steeghs *et al.*, 2004; Maleknia *et al.*, 2007].

II.3.5.1. Chloroacetone.

A potential source of chloroacetone in the atmosphere is chlorine atom-initiated oxidation of methacrolein (MACR) [*Canosa-Mas et al.*, 2001; *Orlando et al.*, 2003], which could be important in certain coastal regions. The THF site was shown previously to be influenced during summertime by marine air masses that penetrate inland from the Gulf of Maine [*Zhou et al.*, 2005, 2008]. Likewise, the export of terrestrial air masses offshore was observed from trace gas measurements at the AIRMAP atmospheric monitoring site on Appledore Island [*Ambrose et al.*, 2007; *White et al.*, 2008]. It is feasible that under certain conditions the confluence of marine and terrestrial air masses upwind of THF facilitated oxidation of MACR by Cl atom and subsequent transport of the resulting oxidation products over THF. We measured the sum of MACR and methyl vinyl ketone (both at $m/z = 71$) by PTR-MS at THF and estimates of summertime Cl atom concentrations during 2004 for the Gulf of Maine were reported previously [*Pszenny et al.*, 2007]. However, it is beyond the scope of this work to estimate chloroacetone mixing ratios at THF. Chloroacetone is not commonly measured in the atmosphere, and its mixing ratios are expected to be low [*Warneke et al.*, 2003]. It is probable that interference in the PTR-MS toluene measurements from chloroacetone was minimal at THF.

II.3.5.2. Proton-bound Ethanol Dimer ((EtOH)₂ + H)⁺.

Recent PTR-MS measurements of pure ethanol vapor showed ((EtOH)₂ + H)⁺ to be the dominant ion product [Maleknia *et al.*, 2007]. However, in a study of root secreted VOCs the abundance of ((EtOH)₂ + H)⁺ was reported as a few percent of protonated ethanol ($m/z = 47$; (EtOH + H)⁺) [Steeghs *et al.*, 2004], and no $m/z = 93$ signal was attributed to EtOH in a GC-PTR-MS study [Warneke *et al.*, 2003]. Experimental and computational studies demonstrated that clustering of EtOH molecules occurs in the equilibrium vapor over liquid samples, and that cluster size distribution depends on the degree of saturation of the vapor phase [Shi *et al.*, 2002; Liu *et al.*, 2007]. It seems likely that sampling of pure, saturated ethanol vapor contributed significantly to the abundance of ((EtOH)₂ + H)⁺ that was observed previously by PTR-MS [Maleknia *et al.*, 2007]. The relative abundance of ((EtOH)₂ + H)⁺ in the PTR-MS analysis of ambient air is expected to be at or below the levels (few percent of total product ions) reported in the study of root emissions [Steeghs *et al.*, 2004]. We found the $m/z = 47$ signal to be unreliable for measurement of EtOH in ambient air due to low sensitivity and significant interferences. Interference in the PTR-MS $m/z = 93$ signal from ((EtOH)₂ + H)⁺ cannot be fully evaluated from our data, but it is not likely to be significant.

II.4. Summary

In the analysis of atmospheric VOCs by PTR-MS, toluene is quantified as its protonated molecular ion at $m/z = 93$. Previous laboratory PTR-MS and SIFT-MS

studies suggested additional sources of $m/z = 93$ ions associated with sampling and analysis of several monoterpenes, including fragmentation of the parent monoterpenes and their carbonyl oxidation products in the PTR-MS drift tube [Schoon *et al.*, 2003; Tani *et al.*, 2003; Warneke *et al.*, 2003; Schoon *et al.*, 2004, Tani *et al.*, 2004; Lee *et al.*, 2006a, b; Maleknia *et al.*, 2007]. To date, studies dedicated to evaluating the importance of these additional $m/z = 93$ sources in ambient air have not appeared in the literature; in general, PTR-MS validation studies have not been carried out in forested environments where the largest quantities of monoterpenes and their oxidation products are expected to be encountered.

We conducted a quantitative comparison between GC-FID and PTR-MS toluene measurements made at the AIRMAP THF atmospheric monitoring station during the summer of 2004. Concurrent measurements of monoterpenes, including α - and β -pinene, camphene, Δ^3 -carene, and *d*-limonene, by GC-FID demonstrated that the monoterpene abundance regularly greatly exceeded that of toluene during the nighttime hours under calm conditions. The data presented a unique test of PTR-MS specificity for toluene measurement in an atmospheric environment heavily influenced by biogenic monoterpene emissions.

The GC-FID and PTR-MS toluene measurements ranged between <0.015 to ~ 0.5 ppbv and were generally in good quantitative agreement as observed in previous intercomparison studies. An overall $\sim 13\%$ positive bias was observed for the PTR-MS measurements, but did not correlate strongly with coincident monoterpene enhancements, as would be expected if monoterpene fragmentation contributed significantly to the PTR-

MS signal at $m/z = 93$. The bias could have been introduced in the calibrations or in quantifying the PTR-MS background.

Potential sources of $m/z = 93$ fragment ions associated with sampling and analysis of monoterpenes by PTR-MS were quantified and included reactions of the measured monoterpenes and some of their atmospheric oxidation products with H_3O^+ , O_2^+ and NO^+ in the PTR-MS drift tube. Their significance was evaluated in terms of corresponding calculated corrections to the PTR-MS toluene mixing ratios. Yields of $m/z = 93$ fragment ions, $\phi(93)$, and kinetic parameters for the associated ion-molecule reactions were taken from the PTR-MS and SIFT-MS literature. Kinetic parameters for reactions of the monoterpenes and their primary carbonyl oxidation products with O_3 and hydroxyl radical, together with measured O_3 mixing ratios and an assumed constant OH concentration were used to estimate mixing ratios for the carbonyls. Our data were most consistent with $\phi(93)$ values of a few percent for reactions of H_3O^+ with α - and β -pinene, which resulted in mostly insignificant corrections to the PTR-MS toluene measurements. Negligibly small corrections to the PTR-MS measurements were also calculated for reactions of the measured monoterpenes with O_2^+ and NO^+ . Likewise, levels of the monoterpene oxidation products pinonaldehyde, α -pinene oxide and caronaldehyde were estimated to be too low to significantly interfere with the PTR-MS toluene measurement. Overall, the calculated fragmentation corrections increased by <10% the number of PTR-MS toluene measurements that agreed quantitatively with the GC-FID measurements.

Our results suggest that with our PTR-MS operating conditions, under the atmospheric conditions encountered at THF, interferences in PTR-MS toluene measurement associated with monoterpene sampling is not significant. This work

extends the range of atmospheric conditions under which the specificity of the PTR-MS technique for atmospheric VOC measurement has been validated. The data interpretation methods presented here should be more generally applicable for verifying the extent of analyte fragmentation in PTR-MS analysis of ambient air samples.

CHAPTER III.

DEVELOPEMENT OF A GAS CHROMATOGRAPHIC SYSTEM FOR MEASUREMENT OF HYDROGEN CYANIDE IN THE LOWER ATMOSPHERE

III.1. Introduction

Biomass burning is generally thought to be the major source of hydrogen cyanide (HCN) in the atmosphere [Li *et al.*, 2000, 2003; Shim *et al.*, 2007]. Pyrolysis of N-containing functionalities in the fuel is the primary mechanism proposed for HCN release from biomass combustion [Glarborg *et al.*, 2003; Johnson and Kang, 1971]. Hydrogen cyanide has been measured from field biomass fires [Hurst *et al.*, 1994; Goode *et al.*, 2000; Yokelson *et al.*, 2007], and from laboratory biomass combustion systems [Lobert *et al.*, 1991; Holzinger *et al.*, 1999; Christian *et al.*, 2004; Becidan *et al.*, 2007]. Elevated free tropospheric HCN columns were measured from the International Scientific Station of the Jungfraujoch (ISSJ) in the Swiss Alps by solar infrared spectroscopy (IR) during 1998, coinciding with a period of intense biomass burning in the tropics [Rinsland *et al.*, 2000].

Low HCN mixing ratios were observed in urban plumes off the United States West Coast, suggesting that automobile emissions make a small contribution to the total global HCN budget [Singh *et al.*, 2003], consistent with previous conclusions [Lobert *et al.*, 1991]. It is well known that HCN is an important intermediate in nitric oxide (NO) formation in non-N containing fuels [Dagaut *et al.*, 2008]. Variability in the correlation

between column abundances of HCN and carbon monoxide (CO), a general combustion tracer, measured at ISSJ suggested that fossil fuel combustion sources of HCN could be significant [Rinsland *et al.*, 2000]. Two recent studies reported direct measurement of HCN in automobile exhaust [Karlsson, 2004; Baum *et al.*, 2007]. Positive, though highly variable, correlations between HCN and CO were observed in vehicle exhaust plumes at a suburban site in Massachusetts during October, 2007 [Knighton *et al.*, 2009].

The significance of biogenic emissions to the global HCN budget has long been questioned [Cicerone and Zellner, 1983; Mahieu *et al.*, 1997; Rinsland *et al.*, 2000; Singh *et al.*, 2003; Li *et al.*, 2003; Shim *et al.*, 2007]. Many plant species are known to produce cyanogenic glycosides, which may through enzymatic mechanisms produce HCN [Vetter, 2000]. A large number of plant species have been shown to be potential HCN emitters [Aikman *et al.*, 1996]. It has been shown for several plant species that cyanogenic glycosides and the enzymes responsible for HCN production are separately compartmentalized within the plant tissue, which presumably prevents large scale HCN release [Poulton and Li, 1994]. Recently, Custer *et al.* [2000] observed HCN emissions from wounded clover using negative ion-chemical ionization mass spectrometry (NI-CIMS) with HO^- as reagent ion.

The atmospheric chemistry of HCN was described in detail previously [Cicerone and Zellner, 1983], with some modifications discussed recently by Kleinböhl *et al.* [2006]. Reaction with hydroxyl radical (OH) in the troposphere was shown to be the primary gas-phase loss mechanism for HCN in the atmosphere, imposing a lifetime of a few years. Reaction with singlet oxygen (O^1D) was estimated to become important in the lower stratosphere. Uptake to the ocean was recently shown to potentially be the

dominant atmospheric sink for HCN [Li *et al.*, 2000]. Estimates of the HCN lifetime with respect to ocean uptake range from 2 to 5.3 months [Li *et al.*, 2001, 2003; Singh *et al.*, 2003]. Details of the ocean sink mechanism are lacking at this time.

Although HCN does not appear to play a significant role in atmospheric chemistry, it may represent an important N-source in remote oceanic environments [Li *et al.*, 2000]. Additionally, it may be a useful tracer for biomass burning emissions [Yokelson *et al.*, 2007]. Finally, biogenic production of HCN and carbonyl compounds, which do play an important role in atmospheric chemistry [e.g., Singh *et al.*, 1995], are known to be associated [Vetter, 2000]. Considerable uncertainties remain regarding contributions to the HCN source budget on regional and global scales. Measurements in the lower atmosphere may provide the best means for reducing such uncertainties, but are lacking at this time.

Most previous atmospheric HCN measurements were made using solar IR spectroscopy [e.g., Rinsland *et al.*, 2007]. In-situ measurements were first made in the stratosphere by negative ion-chemical ionization mass spectrometry (NI-CIMS) [e.g., Schneider *et al.*, 1997]. Later, in-situ measurements in the troposphere were made by (1) matrix-isolation Fourier transform IR (FTIR) spectroscopy performed offline on grab samples of biomass burning plumes [Hurst *et al.*, 1994], (2) long-path FTIR spectroscopy within biomass burning plumes [Goode *et al.*, 2000; Yokelson *et al.*, 2007], (3) a GC system, using a reduction gas detector [Singh *et al.*, 2003], (4) NI-CIMS using CF_3O^- as reagent ion [Crouse *et al.*, 2006; Yokelson *et al.*, 2007], and (5) proton transfer reaction-mass spectrometry (PTR-MS) [Knighton *et al.*, 2009]. In-situ measurements of background HCN levels by IR spectroscopy have not been reported. Instruments based

on NI-CIMS typically exhibit reduced sensitivity at elevated H₂O vapor pressures [Crouse *et al.*, 2006]; therefore their use has been inhibited in much of the lower atmosphere. The low proton affinity of HCN [Holzinger *et al.*, 1999] and potential interference from ethene [Knighton *et al.*, 2009] have complicated measurement of HCN in the atmosphere by PTR-MS, though these issues may be overcome through calibration. Only one report of in-situ surface measurements has appeared in the literature [Knighton *et al.*, 2009].

In order to improve our understanding of the role of HCN in the atmosphere a GC instrument, incorporating a flame thermionic detector (FTD), was developed and deployed for atmospheric measurement of HCN at the AIRMAP atmospheric monitoring station THF2 during a weeklong period in April, 2009. A detailed description of the instrument and tests performed during its development is given in Section III.2. Results obtained during the initial testing phases as well as ambient measurements are presented in Section III.3. Conclusions and suggestions for further study are given in Section III.4.

III.2. Experimental

III.2.1. Measurement Site Location

The GC-FTD instrument was deployed for ambient measurements between April 2 and 9, 2009 at the University of New Hampshire's AIRMAP atmospheric monitoring station at Thompson Farm (THF2; 43.1078 °N, 70.9517 °W, 40 m elevation above sea level (a.s.l)), located within a stand of mixed hardwood/pine forest ~320 m from the

original Thompson Farm monitoring station (THF). Construction of THF2 began during the 2007–2008 winter and the station was brought on-line for atmospheric monitoring during the summer of 2008. At THF2 a 24 m observation tower extends above the surrounding forest canopy. Ambient air was drawn at ~ 1500 STP 1 min^{-1} (standard temperature of 273 K and pressure of 1 atm, respectively) through a PFA Teflon-lined aluminum manifold from the top of the tower using a Gast R7-Series regenerative blower (Gast Manufacturing, Inc., Benton Harbor, MI). Sub-samples were directed to a suite of trace gas analyzers, including the GC-FTD instrument, housed at the base of the tower. The temperature in the instrument room was maintained at ~ 22 °C between April 2 and 9 when an analysis of ambient air was performed.

III.2.2. Configuration of the GC-FTD Instrument

Figure 18 shows a schematic of the GC-FTD instrument. The HCN calibration standard was a permeation tube source (VICI Metronics, Inc., Poughkeepsie, NY) contained in a glass chamber, which was temperature-regulated using an OMEGA CN76000 Series temperature controller (OMEGA Engineering, Inc., Stamford, CT). Standard samples of HCN were prepared in ultra high purity (UHP) N_2 (Maine Oxy, Auburn, Maine) using an MKS type 1479A mass flow controller (MKS Instruments, Inc., Andover, MA) coupled with an MKS type 247D digital readout. The flow controller accuracy was checked with a Gilibrator System flow calibrator (Gillian Instrument Co., now Sensidyne, Clearwater, FL). The standard samples were further diluted in zero air to ambient levels (~ 0.01 to 1 ppbv) using a commercial zero air generator (Apel Riemer Environmental, Inc.,

Broomfield, CO). Sample volumes of 250 STP cm³ were concentrated at -110 °C in a 20 cm × 0.3175 cm i.d. Silonite-coated loop (Entech Instruments, Inc., Simi Valley, CA) packed with 1 mm diameter glass beads (Ohio Valley Specialty Co., Marietta, OH) and contained in an MMR model CC2202 Cryofocus System (MMR Technologies, Mountain View, CA; see *Sive et al.* [2005] for further details). Prior to their capture samples were dried at -30 °C in a second 20 cm × 0.3175 cm i.d. Silonite-coated loop (Entech Instruments, Inc., Simi Valley, CA) contained in the Cryofocus System. Sample injections were performed in UHP He onto a 25 m × 0.32 mm i.d., 5 µm film thickness CP PoraBOND Q column (Varian, Inc., Palo Alto, CA) using a VICI 8-port switching valve (SV) (Valco Instruments Company, Inc., Houston, TX). According to the manufacturer's specifications the CP PoraBOND Q column is a bonded porous polymer PLOT column exhibiting low bleed and high stability under exposure to water. A similar type of stationary phase, in combination with an FTD, was previously employed for separation of cyanides from the headspace of blood samples [*Seto et al.*, 1993]. The sample dehumidification and capture loops, Cryofocus System and 8-port SV were incorporated in a custom built, fully automated sample acquisition system that was described in detail in a previous publication [*Sive et al.*, 2005]. For measurement of HCN, an additional 4-port SV (VICI) was incorporated into the sample acquisition system to permit isolation of the sample capture loop between sample trapping and injection (Figure 18). The column and a Shimadzu FTD (Shimadzu Corporation, Columbia, MD) were housed in a temperature programmed Shimadzu model 2014c GC. The GC oven temperature program was 40 °C for 7.5 min, 15 °C min⁻¹ to 150 °C, 150 °C for 4 min. The FTD was operated at 200 °C and a constant voltage of 80% relative to

maximum. The carrier flow rate at the initial column temperature was 21.6 ± 0.2 (1σ) STP $\text{cm}^3 \text{min}^{-1}$ as measured with a Hewlett Packard soap bubble flow meter. The makeup gas was UHP He at a nominal flow rate of $\sim 10 \text{ cm}^3 \text{min}^{-1}$, while UHP H_2 and purified ambient air from an Aadco 737-series Pure Air Generator (Aadco, Cleves, OH) were also supplied to the FTD at nominal flow rates of $\sim 1 \text{ cm}^3 \text{min}^{-1}$ and $\sim 100 \text{ cm}^3 \text{min}^{-1}$, respectively [Shimadzu Corporation, 2004]. Activated charcoal/molecular sieve traps, prepared in-house and purchased from Ohio Valley, were used with all cylinders for further purification. Additionally, a VICI HP2 helium purifier was used for the He carrier gas. Gas transfer lines were constructed of Silcosteel (Restek, Bellefonte, PA) and PFA 450 Teflon (E & S Technologies, Inc., Chelmsford, MA) of varying i.d.

The operational protocol of the instrument was as follows (refer to Figure 18): stage 1, cool: T1 and T2 cooled in preparation for sample acquisition; stage 2, flush: inlet lines flushed with ambient air or standard to condition prior to trapping; stage 3, trap: sample dehumidified in T1 and trapped in T2; stage 4, flush: inlet lines flushed with UHP He to purge residual sample constituents; stage 5, trap: UHP He trapped to displace O_2 and O_3 from the loop; stage 6, desorb: T2 isolated and heated to vaporize trapped HCN; stage 7, inject: sample injected in UHP He; stage 8, bake: T1 and T2 heated and flushed with UHP He in preparation for the next sample. Table 11 indicates the positions of the valves in Figure 18 during each sample cycle stage.

III.2.3. Instrument Development

Several configurations that differed from the description in Section II.2.2 were tested during development of the HCN instrument and are illustrated in Figures 19 and 20. They included (1) a 60 m × 0.32 mm i.d., 1 μm film thickness Carbowax 20M column (Ohio Valley), (2) a VICI model D-2 pulsed discharge helium ionization detector (PDHID) [Wentworth *et al.*, 1994; Forsyth, 2004], (3) a Shimadzu flame ionization detector (FID), and (4) a separate VICI 6-port SV and gas transfer manifold for manual sample injection. Additional MKS mass flow controllers were of type 1179A and 1479A. Carbowax 20M was first selected as chromatographic stationary phase because a similar polyethylene glycol (PEG) stationary phase was used earlier in a GC instrument for measurement of HCN on an aircraft platform over the western Pacific [Singh *et al.*, 2003]. We tested an FID for measurement of HCN because the FID is used routinely for measurement of atmospheric hydrocarbons in our laboratory and others [Apel *et al.*, 2003b], and to the best of our knowledge the sensitivity of the FID to HCN was not reported previously. Our motivation for testing a PDHID was that ~10-fold higher sensitivity to <C₉ organics was observed previously for the PDHID compared with the FID [Wentworth *et al.*, 1994].

III.2.3.1. PDHID Experiments.

Experiments conducted with the PDHID used only the Carbowax 20M column. Standard samples were prepared primarily in UHP He, although UHP N₂ and zero air

matrices were also analyzed. Sample injections were performed using a VICI 6-port SV with 0.2159 cm i.d. Silcosteel loops of varying length (yielding volumes of 5, 10 and 15 cm³) at room temperature (Figure 19a, b) or the glass bead packed Silonite-coated loop in the Cryofocus System (Figures 19c, 20). The column and detector were housed in a Shimadzu model 17A GC. The PDHID was operated primarily at 40 °C, although several testes at 100 °C were performed. The discharge gas was UHP He, further purified with a VICI HP2 He purifier and supplied to the detector at 11 ± 2 to 127 ± 6 cm³ min⁻¹, as determined by calibration with the soap bubble flow meter. For several experiments a 4-port SV and water bubbler with deionized water were used for humidification of standard samples (Figure 19). To test the system performance with a matrix similar to ambient air the standard dilution components were configured as shown in Figure 19d, which enabled standards to be prepared in UHP N₂ and further diluted in zero air. The zero air generator was supplied with laboratory air. To overcome interference from N₂ in the HCN analysis a 4-port SV and UHP He cylinder were incorporated as shown in Figures 19 (c, d) and 20 so that the sample enrichment loop could be purged of N₂ prior to injection of samples prepared in N₂ and N₂/zero air matrices. The configurations in Figures 19a and 20 allowed for reduced consumption of the UHP N₂ diluent when preparing standard samples.

III.2.3.2. FID Experiments.

Experiments with the FID used the VICI 6-port SV, 5 cm³ Silcosteel loop, Carbowax 20M column and Shimadzu 17A GC (Figure 19a). The sample diluent gas

was UHP He. The FID was operated at 250 °C and was supplied with UHP H₂ and ultra zero air (Maine Oxy) at nominal flow rates of ~70 and ~550 cm³ min⁻¹, respectively [Shimadzu Corporation, 1995].

III.2.3.3. Preparation of an Acetonitrile Qualitative Standard.

Headspace vapor from a ~3 ml glass vial containing ~1 ml of HPLC grade CH₃CN (EMD Chemicals, Inc., Gibbstown, NJ) was drawn with a syringe through a Parafilm cover (American National Can™, Greenwich, CT) and diluted in ambient air at the inlet of an evacuated ($P \approx 1.5 \times 10^{-2}$ Torr) 1 l electropolished stainless steel canister. The canister was previously flushed with ambient air. After filling with dilute CH₃CN vapor the canister was pressurized with ambient air to 20 ± 10 psig with a metal bellows pump. The ambient temperature was estimated to be in the range -10 to 10°C, over which the CH₃CN vapor pressure was calculated to range between 14 and 42 Torr based on literature data [Lide, 2008]. Assuming >90% transfer of the headspace gas the HCN mixing ratio in the pressurized canister was calculated to be ~2 to 4 ppmv. For analysis the CH₃CN canister was connected to the sample inlet of the SSV (Figure 18b) with a tee fitting; the canister was temporarily opened during trapping of an ambient sample to introduce a small volume of standard into the sample stream.

III.3. Results and Discussion

III.3.1. Sample Dehumidification and Enrichment

A range of temperatures for sample dehumidification and enrichment were tested using the instrument configurations shown in Figure 19b and 19c, respectively. The experiments were designed to determine (1) the minimum dehumidification loop (T1) temperature at which HCN loss was negligible and (2) the maximum sample enrichment loop (T2) temperature that yielded 100% HCN trapping efficiency. For the Cryofocus System used the T1 temperature range was limited to values ≥ -30 °C.

To quantify potential HCN loss in T1 the system response to standard samples was measured for T1 temperatures between -30 °C and 30 °C. Standard samples were prepared at 46 ± 5 ppbv in UHP He; the mass of HCN injected was 0.8 ± 0.1 ng. Compared to the system response for $T(T1) = 30$ °C the relative response for $T(T1) = -30$ °C was 1.00 ± 0.01 (1σ ; $n = 2$), indicating that HCN was passed through the sample dehumidification loop with 100% efficiency at the minimum achievable T1 temperature. Thus it was concluded that a T1 temperature of -30 °C was optimal for sample dehumidification.

The instrument configuration shown in figure 19b was modified such that RH and temperature of the effluent from T1 could be sampled with a Testo model 605-H1 Mini Thermohygrometer (Testo, Inc., Flanders, NJ). Dry (RH <5%) and humidified UHP He were mixed to an average measured final humidity of 57 ± 4 % (1σ ; $n = 9$) at 22.6 ± 0.7 °C (room temperature). The measured humidity compared favorably with a value of $63 \pm$

7 % calculated based on the gas flow rates, temperature, pressure, and H₂O saturation vapor pressure ($p^\circ(\text{H}_2\text{O})$) data from the literature [Lide, 2008]. A linear regression fit to a plot of $\ln(p^\circ(\text{H}_2\text{O}))$ versus T^{-1} for temperatures in the range 5 °C to 25 °C yielded $m = \Delta H_{\text{vap}}(\text{H}_2\text{O}) \cdot R^{-1} = 5348 \pm 8 \text{ K}$ and $b = 21.11 \pm 0.03$, where $\Delta H_{\text{vap}}(\text{H}_2\text{O})$ is the enthalpy of vaporization for H₂O. The uncertainty in the calculated RH represents contributions from the flow rates (<5%), temperature (0.5 °C), pressure (assumed to be ~1 to 2 psi), and the fit to the literature $p^\circ(\text{H}_2\text{O})$ data. A portion of the humidified He was flowed through T1 at ~200 STP cm³ min⁻¹ and the effluent humidity was measured as a function of the T1 temperature in the range -30 °C to 30 °C. The H₂O trapping efficiency, ε , was calculated as the relative difference between the calculated (calc) and measured (meas) effluent RH.

$$\varepsilon = \frac{\text{RH}_{\text{calc}} - \text{RH}_{\text{meas}}}{\text{RH}_{\text{calc}}} \cdot 100 \quad (1)$$

Figure 21 shows a plot of the measured H₂O trapping efficiency as a function of T1 temperature. The corresponding measured RH and calculated H₂O partial pressures ($p(\text{H}_2\text{O})$) are indicated. With $T(\text{T1}) \leq -20$ °C the measured values of ε were >90%, while RH and $p(\text{H}_2\text{O})$ were reduced to <5% and <1 Torr, respectively. For analyses with the Cryofocus System the mass of H₂O in each sample was estimated from the measured or calculated input RH and the trapping efficiency data of Figure 21.

Figure 22 shows a plot of the relative PDHID response to standard HCN samples for T2 temperatures ranging between -150 °C and -90 °C. A relative response of unity represents 100% trapping efficiency. The HCN mixing ratio in the standard samples was 46 ± 9 ppbv, while the sample flow rate and volume were 198 ± 7 STP cm³ min⁻¹ and 50 ± 2 STP cm³, respectively, corresponding with injections of 2.8 ± 0.2 ng of HCN. Standard samples were prepared in UHP He. Error bars in Figure 22 represent

uncertainties in the permeation tube emission rate ($\pm 5 \text{ ng min}^{-1}$), the dilution system flow rates ($< 5\%$) and the sample trapping time ($\sim 0.5 \text{ s}$). The trapping efficiency was determined to be 100% within the measurement uncertainties for T2 temperatures ≤ -110 °C. Therefore, -110 °C was taken to be the optimal T2 temperature for HCN analysis.

III.3.2. Results with PHDID and FID

III.3.2.1. Response Comparison between PDHID and FID.

The response of the PDHID to HCN was compared with that of the FID for $5.00 \pm 0.05 \text{ cm}^3$ samples of $9.7 \pm 0.7 \text{ ppbv}$ HCN in dry He using direct loop injection (Figure 19a). The mass of HCN analyzed was $0.059 \pm 0.006 \text{ ng}$. The PDHID response ($2.1 \pm 0.3 \times 10^4 \text{ AU ng}^{-1}$; AU, peak area unit) was 14 ± 3 times higher than that of the FID ($1.5 \pm 0.3 \times 10^3 \text{ AU ng}^{-1}$) with comparable precision of $\pm 6\%$ and $\pm 17\%$ (1σ , $n = 7$) for the PDHID and FID, respectively. The method detection limit (MDL) [Lavagnini and Magno, 2006] with respect to HCN was estimated to be $0.015 \pm 0.002 \text{ ng}$ and $0.032 \pm 0.006 \text{ ng}$ for the FID and PDHID, respectively, using equation (2).

$$\text{MDL} = 3.14 \cdot \sigma \quad (2)$$

Here, σ is the standard deviation in the analytical response to standard samples ($n = 7$) containing analyte quantities 2 to 5 times larger than the expected MDL [Lavagnini and Magno, 2006]. In this work the ratio of HCN mass injected to estimated MDL ($m_{\text{inj}}/\text{MDL}$) was 3.9 ± 0.6 and 1.8 ± 0.4 for the PDHID and FID, respectively. Table 12 gives, as a function of HCN mixing ratio, sample volumes required to yield a detectable

HCN signal, based on the estimated MDLs. Corresponding sample acquisition times for a nominal flow rate of $200 \text{ STP cm}^3 \text{ min}^{-1}$ are also given. A study using an atmospheric chemical transport model suggested minimum annual average HCN mixing ratios in the range of 0.010 to 0.100 ppbv in the marine boundary layer [Li *et al.*, 2000]. A median HCN mixing ratio of 0.130 ppbv was reported from air-borne measurements made at altitudes $<2 \text{ km}$ in relatively unpolluted air masses over the Northwestern Pacific [Singh *et al.*, 2003]. The THF site is 24 km from the Gulf of Maine and is frequently influenced by marine air masses [Zhou *et al.*, 2005, 2008]. It is therefore feasible that HCN mixing ratios near the minima measured and predicted for the marine boundary layer could be encountered at THF. Boundary layer dynamics were shown previously to strongly influence trace gas mixing ratios at the THF site, with some compounds (e.g., ozone (O_3) and methanol (CH_3OH)) depleted at the surface during nighttime beneath a low altitude boundary layer inversion [Talbot *et al.*, 2005; Mao *et al.*, 2006]. The behavior of HCN under similar conditions is unknown and the possibility of depletion events cannot be ruled out. Therefore, an analytical system capable of quantifying HCN at mixing ratios as low as 0.010 ppbv is desirable. The data in Table 12 demonstrate that the response of the FID and PDHID should be adequate to quantify HCN mixing ratios of $\geq 0.100 \text{ ppbv}$. The sample volumes necessary to quantify HCN with either detector are expected to be impractically large for HCN mixing ratios $< 0.010 \text{ ppbv}$, although the PDHID may be capable of measuring HCN down to 0.010 ppbv.

III.3.2.2. Response of the PDHID to Permanent Gases.

The PDHID is a universal detector and responds to atmospheric permanent gases (e.g., O₂, N₂), H₂O and common inorganic pollutants including carbon monoxide (CO) and carbon dioxide (CO₂) [Wentworth *et al.*, 1992; Forsyth, 2004]. To determine potential interferences from several common atmospheric inorganic and organic gases, analyses were performed for samples of (1) UHP N₂ diluted with UHP He, (2) humidified UHP He (Figure 19c), (3) a synthetic blend of methane (CH₄), acetylene (C₂H₂), ethane (C₂H₆), CO, and CO₂ in N₂, and (4) catalytic-converter prepared zero air (Figure 19d). Retention times for N₂ and H₂O were determined from (1) and (2), respectively, while those for the remaining gases tested could not be individually assigned.

Figure 23 shows chromatograms for blank UHP He samples and a standard sample prepared in UHP N₂/zero air. For the standard sample, the sample enrichment loop (T2) was purged with ~70 STP cm³ UHP He following sample trapping. Traces of N₂ and H₂O were present in all samples analyzed. An N₂ peak is clearly observable in the blank and standard chromatograms in Figure 23, while an H₂O peak is also observable in the latter. The HCN peak was well resolved from N₂, H₂O, the light hydrocarbons analyzed in (3), and other inorganic atmospheric gases present in the zero air matrix. However, it should be noted that the HCN peak was obscured by a broad N₂ tail when T2 was not purged with He between sample capture and injection. Additionally, the PDHID background signal appeared to increase significantly with the amount of water trapped in T2. The measured RH value for the zero air was 15 ± 3% (equivalent to the laboratory air) at the time the standard chromatogram shown in Figure

23 was recorded. Although the observed background signal enhancement was fairly reproducible it was accompanied by an undesirable increase in the baseline slope with the GC temperature program, which would be expected to reduce measurement precision in ambient air samples. The background signal enhancement appeared to increase with detector temperature.

III.3.2.3. Blank Measurement with PDHID.

Method blanks were periodically analyzed during all phases of the instrument development. Blank samples were typically prepared with the HCN permeation tube removed from the permeation oven. Non-zero HCN levels were usually detected in the blanks and were calculated to range from <1% to ~25% of the standard mixing ratio. Several experiments were performed to characterize the blank response and are described below. Their results were used to quantify contributions of the standard dilution system components to blank HCN levels observed.

The standard dilution system shown in Figure 19a was reconfigured to isolate its components as illustrated in Figure 24. The HCN chromatographic peak area (A_{HCN}) was measured for blank samples prepared with each configuration. The measured peak areas, diluent flow rates (f), sample loop volume (V) and response (R) were used to calculate HCN emission rates (e°) for the isolated components (equation (3)), where it was assumed that surface desorption of HCN was the primary source of HCN in the blank samples. Blank responses were typically higher after (1) the system was left stagnant

overnight and (2) analysis of high concentration standards, consistent with an HCN desorption model.

$$e^{\circ} = \frac{A_{\text{HCN}}}{V \cdot R} \cdot f \quad (3)$$

The calculated value of e° for the permeation oven was $2.6 \pm 0.3 \text{ ng min}^{-1}$, which was ~2% of that for the permeation tube standard. Values of e° for the remaining components were calculated to be factors of ~20 to 50 lower than for the oven. The overall contribution to HCN in the blanks was attributed mostly to a single flow controller which had earlier been exposed to relatively high HCN mixing ratios. To assess the validity of the blank source apportionment the calculated emission rates were used to predict blank responses for the configuration shown in Figure 19a. For the day on which the emission rates were estimated, the measured HCN chromatographic peak area, $522 \pm 23 \text{ AU}$ (1σ ; $n = 2$), appeared to agree well with the calculated value $597 \pm 167 \text{ AU}$, which supported the validity of the assumed desorption model and the measured blank source apportionment. The calculated blank HCN concentration decreased significantly over the course of several days following the emission rate determination, suggesting decreasing emission rates for the standard dilution system components. Blank responses predicted using emission rates reduced in proportion to the calculated blank HCN concentration reduction are compared with the measured responses in Figure 25. The initial blank responses (i.e., 522, 597 AU) are also plotted. As shown in Figure 25, the measured and predicted blank responses were in good agreement and therefore appeared to be described fairly well according to the assumed desorption model and the measured blank source apportionment.

The emission rate estimates and equation (3) suggested that the relative blank response could be reduced by (1) reducing the HCN concentration in the standard dilution system and (2) increasing the flow rates through the permeation oven and downstream components. The HCN concentration could be reduced independent of diluent flow rate by reducing the total internal pressure of the standard dilution system. Although the result in (2) was confirmed experimentally, practical limitations were imposed by the HCN standard permeation rate and the desire to maintain reasonable diluent gas economy. Thus, nonzero blank HCN levels had to be tolerated. For future work it is recommended that a standard with at least a 10-fold lower permeation rate and/or an N₂ generator for the diluent gas supply be used.

III.3.2.4. Long Term Stability of PDHID Response.

Here the stability of the GC-PDHID instrument over the entire period of laboratory testing is assessed. Figure 26 shows a plot of the PDHID response to HCN (expressed as chromatographic peak area units (AU) per pg of HCN injected) as a function of the number of sample injections performed. The data in Figure 26 are labeled by diluent gas and sample loop configuration. In addition to different diluent gases and loop configurations, a range of discharge gas flow rates ($\sim 11 \pm 2$ to 127 ± 6 cm³ min⁻¹) were used. It is clear from Figure 26 that the PDHID response decreased significantly over the course of testing, and the decreasing trend appeared to dominate over any variations resulting from changes to the sample matrix, instrument configuration and operating parameters.

Significant response drift with time does not appear to be a common feature of the PDHID detector. However, it is feasible that contamination of the discharge electrodes would result in loss of response. The discharge electrodes may become contaminated under operating conditions where any of the following parameters exceed an empirical threshold value: (1) column flow rate; (2) column bleed [*Valco Instruments Co. Inc.*, 1998]; (3) organic analyte concentration [*Wentworth et al.*, 1994]. Finally, exhaustion of the discharge gas purifier, which was not tested, would have resulted in higher levels of impurities in the discharge gas, which would have facilitated contamination of the discharge electrodes. In the detector and carrier gas inlet configuration of the VICI PDHID used in this work, the discharge electrodes are purged by the discharge gas, which minimizes exposure of the discharge electrodes to impurities in the column effluent. A minimum discharge flow rate of $30 \text{ cm}^3 \text{ min}^{-1}$ is specified by the manufacturer [*Valco Instruments Co. Inc.*, 1998].

Preliminary tests with the PDHID demonstrated that higher response was achieved at lower discharge flow rates, and for most of the time during which the PDHID was operated the discharge flow rate was 18 ± 2 to $25 \pm 3 \text{ ml min}^{-1}$. Comparable carrier gas flow rates were estimated based on the measured N_2 retention time and the estimated volume of the components between the sample loop and the detector. Therefore, the gas flow rates to the PDHID may have been inadequate to safeguard against contamination of the discharge electrodes.

It was previously reported that degradation of Carbowax 20M stationary phases is accelerated by traces of H_2O and O_2 [*Barry*, 2004], suggesting that such phases should not be suitable for chromatographic analysis of ambient air. It is possible that

degradation of the Carbowax 20M stationary phase following injections of samples containing air and water vapor resulted in increased column bleed, which would have facilitated contamination of the detector. It should be noted that the vast majority of samples analyzed over the time period represented in Figure 26 were prepared using relatively dry cylinder gas.

In this work the HCN mass analyzed was on the order of a few ng or less, which appears to be well within an acceptable range for organic analytes based on previous work [*Wentworth et al.*, 1994].

The PDHID baseline noise was observed to increase with temperature; therefore, a low operating temperature of 40 °C was selected. After several months of operation at 40 °C the detector temperature was temporarily increased to 100 °C. Subsequently, the background signal increased significantly, probably as a result of re-volatilization of compounds that condensed during operation at 40 °C. The background level recovered when the detector temperature was reset to 40 °C; therefore, baking the detector did not appear to affect response.

III.3.3. Results with FTD

III.3.3.1. Dependence of Response on Detector Bead Voltage.

Figure 27 shows a plot of the FTD response to HCN measured as a function of the detector voltage. Measurements were performed using the instrument configuration shown in Figure 20. The HCN mass analyzed was 1.2 ± 0.1 ng. The GC temperature

program was as given in Figure 22. As shown in Figure 27 near zero response to HCN was observed below a threshold voltage of ~70%. The response appeared to maximize at voltages between 85% and 90%, and declined at higher voltages.

III.3.3.2. Response Comparison and MDL.

The FTD response and MDL with respect to HCN were determined based on an analysis of standard samples of 0.068 ± 0.008 ng HCN (0.22 ± 0.03 ppbv) prepared in UHP N₂. Components for sample acquisition and standard dilution were configured as shown in Figures 18b and 20, respectively. The FTD response was $1.07 \pm 0.08 \times 10^6$ AU ng⁻¹ and therefore higher than that of the PDHID by a factor of ~50. It should be noted that FTD detectors are known to exhibit loss of response with operation time [*Colón and Baird, 2004*], the rate of decrease for the Shimadzu FTD being proportional to the detector bead voltage [*Shimadzu Corporation, 2004*]. The response given above was ~50% below the maximum response measured with a newly conditioned detector bead. The FTD MDL for HCN was determined to be 0.012 ± 0.001 ng, with a measurement precision of $\pm 4\%$ (1σ , $n = 7$). This MDL value corresponds with an HCN VMR of ~0.04 ppbv at a trapping volume of 250 cm³. The FTD MDL is compared with those for the PDHID and FID (Section III.3.2.1) in terms of sampling requirements in Table 12. Despite the FTD response to HCN being much larger the MDL for this detector did not appear to be significantly lower than that of the PDHID. However, the value of m_{inj}/MDL at which the FTD MDL was determined (5.6 ± 0.8) was significantly higher than for the PDHID MDL determination. It may be appropriate to scale down the FTD

MDL based on the difference in m_{inj}/MDL . The modest improvement in detection was accompanied by a major improvement in selectivity (see below).

III.3.3.3. Carrier Gas Flow Rate.

The carrier gas flow rate through the PoraBOND Q column was measured as a function of carrier pressure, in the range 30 to 130 psig, and column temperature, in the range 40 to 110 °C, (Figure 28) using the Hewlet Packard flow meter. The flow meter temperature was measured with a Fluke IR thermometer (model 63, Everett, WA); the surface probed was an area of the body that was covered with flat black adhesive tape. Measured flow rates were normalized to 0 °C, but were not corrected for water vapor partial pressure. The decrease in carrier flow rate (at constant pressure) with increasing temperature (Figure 28) results from increased viscosity of the carrier gas [Bartram, 2004], and possibly also flow restriction via swelling of the column stationary phase.

III.3.3.4. Influence of Injection Parameters on HCN Chromatographic Analysis.

Figure 29 compares several standard chromatograms recorded as a function of injection temperature (T_{inj}), which was varied by adjusting the time delay between the start of sample desorption and injection. The HCN mixing ratio was 1.0 ± 0.1 ppbv, while the HCN mass injected was 0.30 ± 0.04 ng. With T_{inj} below the HCN boiling temperature ($T_b(\text{HCN}) = 26$ °C [Lide, 2008]) the HCN peak was broad and irregular, while significant improvement in peak shape was observed with T_{inj} well above $T_b(\text{HCN})$.

As T_{inj} was increased above the HCN melting temperature ($T_m(\text{HCN}) = -13\text{ }^{\circ}\text{C}$ [Lide, 2008]) the chromatographic peak area decreased significantly, consistent with a loss of sample from the injection volume. The apparent loss of sample may be attributed to pressure driven flow induced by increasing temperature in the sample enrichment loop during desorption. The measured peak areas suggest sample loss was $28 \pm 4\%$ for T_{inj} in the range 56 to 85 $^{\circ}\text{C}$. A 4-port SV was incorporated in the instrument to isolate the sample enrichment loop and prevent sample outflow during desorption (Figure 18). Figure 29 shows a chromatogram recorded with the sample enrichment loop isolated during desorption and $T_{inj} = 83\text{ }^{\circ}\text{C}$ (sample 016). For samples injected at high temperature (in the range of 56 to 85 $^{\circ}\text{C}$) and T2 isolated during desorption the average peak area was $15 \pm 8\%$ lower than for samples injected at low temperature ($T_{inj} = -70\text{ }^{\circ}\text{C}$), indicating the isolation valve significantly improved sample transfer to the column. More measurements would be required to reduce uncertainties in the above response comparisons.

III.3.3.5. Ambient Air Analysis with GC-FTD Instrument.

With the instrument configured as shown in Figure 18, ambient air was analyzed continuously between April 2 and 9, 2009. Standards prepared in UHP N_2 and zero air were periodically analyzed for calibration. Additionally, the background HCN level in the zero air was monitored. Background HCN in the standard dilution system was shown to be governed by the zero air generator, likely as a result of incomplete catalytic conversion of HCN. The HCN mixing ratio in the standard samples was set in the range

from 0.13 ± 0.01 to 0.50 ± 0.05 ppbv. Figure 30 shows the measured response to 0.50 ± 0.05 ppbv HCN as a function of operation time. The linear trend in response was roughly $-0.3\% \text{ hour}^{-1}$ and resulted from exhaustion of the detector bead. Although such loss of sensitivity is undesirable, it appears to be well characterized, and thus accounted for, by calibration. Figure 31 shows the measurements from Figure 30 following de-trending. The measurement precision (1σ) was $\sim 5\%$. Figure 32 shows a calibration curve constructed from all the de-trended standard and blank responses. Figure 33 shows a time series of the ambient HCN VMR measurements, derived from the de-trended raw responses using the calibration curve in Figure 32. The range of the ambient HCN mixing ratios was ~ 0.07 to 0.31 ppbv, which appeared to agree well with previous tropospheric measurements [e.g., *Singh et al.*, 2003; *Rinsland et al.*, 2007]. The measurement uncertainty was estimated to be ~ 0.015 to 0.030 ppbv based on the calibration curve shown in Figure 32. Results from the first field deployment of the GC-FTD system suggest that the instrument has the capability to measure HCN in the PBL with high sensitivity, selectivity and precision. Future use of this instrument should yield valuable information regarding the temporal variability and budget of HCN in the lower atmosphere.

III.3.3.6. Qualitative Identification of Acetonitrile (CH_3CN) in Ambient Air Samples.

Only a single chromatographic peak, in addition to that for HCN, was observed in ambient chromatograms recorded during April, 2009. Figure 34 compares ambient

chromatograms recorded before and after spiking the sample inlet with CH₃CN qualitative standard. The peak at ~12 min retention time is clearly identified as CH₃CN.

III.4. Summary

A GC-FTD instrument was developed for measurement of HCN in the lower atmosphere and was deployed for testing at the AIRMAP atmospheric monitoring station THF2 for a 1 week period during April, 2009. The FTD was chosen for its superior response and selectivity for HCN compared with the FID and PDHID detectors. A low bleed, robust porous polymer PLOT column was chosen for analyte separation. Quantitative calibration of the HCN measurements was performed by dynamic dilution of a certified permeation tube standard in UHP N₂ and catalytic converter-prepared zero air. Only two compounds were observed in ambient air samples analyzed in April, 2009. These were identified as HCN and CH₃CN based on the retention times of pure standard samples. During continuous operation, the FTD showed a linearly decreasing response of $-0.3\% \text{ hour}^{-1}$. The overall precision was $\sim 5\%$. The range of the ambient HCN mixing ratios was ~ 0.07 to 0.31 ppbv with an overall uncertainty of ~ 0.015 to 0.030 ppbv as determined from a linear calibration curve. The instrument MDL was estimated to be ~ 0.04 ppbv for the 250 cm^3 sample volume used. Overall the instrument performed well, however malfunction of the Cryofocus System that was used prevented collection of a longer observation record. For long term measurements, the FTD bead would require periodic reconditioning. It is possible that further refinements in operating parameters can reduce the frequency of such maintenance. With proper calibration this system could

potentially yield CH₃CN measurements. The use of an N₂ generator for standard dilution and/or a permeation tube with a lower emission rate (e.g., <10 ng min⁻¹) would be desirable for future work in order to reduce background HCN levels in the standard dilution system and improve diluent gas economy.

TABLES

1. Measurement details for atmospheric observations at AI during the ICARTT campaign.

Variables measured	Analytical scheme ^a	Sampling interval ^f	Sample cycle period, τ	Integration time	LOD	Accuracy
<i>Chemical variables</i>						
C ₂ -C ₁₀ NMHCs	GC-FID ^b	7/2–8/13	1 hr	5 min ^g	0.002–0.003 ppbv	±10%
OVOCs	GC-MS ^b					
C ₈ -C ₁₀ aromatics	PTR-MS	7/1–8/13	10 min	20 s	0.010 ppbv	±15%
DMS						
OVOCs						
NO ₃	DOAS ^c	7/8–8/11	5 min	5 min	3.4 pptv	±1.7 pptv
HCHO			15 min	15 min	0.6 ppbv	±0.3 ppbv
NO ₂			15 min	15 min	0.30 ppbv	±0.15 ppbv
CO	IR absorbance (2200 cm ⁻¹) ^d		1 min	1 min	10 ppbv	±5 ppbv
NO	Chemiluminescence ^d		1 min	1 min	0.075 ppbv	±0.020 ppbv
O ₃	UV absorbance (254 nm) ^d		1 min	1 min	1 ppbv	±1 ppbv
<i>Meteorological variables^e</i>						
Ambient P	Barometer		1 hr	2 min	800 mbar	±1 mbar
Ambient T	Thermistor		1 hr	2 min	–40 to 50 °C	±1 °C
Dew T	RH probe		1 hr	2 min	–35 to 30 °C	±1 °C
Wind direction	Anemometer		10 min	2 min	0–360 ° from N	±10 °
Wind speed					0–62 m s ⁻¹	±1 m s ⁻¹

^aThe following sources should be consulted for detailed descriptions of these systems:

^b*Sive et al.* [2005]; *Zhou et al.* [2005].

^c*Alicke et al.* [2002]; *Pikelnaya et al.* [2007].

^d*Mao and Talbot* [2004].

^e*National Data Buoy Center* [2004].

^fIntervals are indicated only for systems that were not operational during the entire campaign (4 July – 15 August).

^gValue denotes the time interval over which canister samples were collected.

2. Rate data applicable to nighttime gas-phase NO₃ chemistry and pertaining to the chemical variables monitored at AI during the ICARTT campaign.^a

NO ₃ sink / Reaction	<i>A</i> (cm ³ molecule ⁻¹ s ⁻¹)	<i>B</i> (K)	<i>k</i> ^{b,c} (cm ³ molecule ⁻¹ s ⁻¹)
<i>Alkanes</i>			
Ethane			1 × 10 ⁻¹⁷
Propane ^d			7 × 10 ⁻¹⁷
<i>i</i> -Butane ^e	3.05 × 10 ⁻¹²	3060 ± 99	1.06 × 10 ⁻¹⁶ (±40%)
<i>n</i> -Butane ^f	2.8 × 10 ⁻¹²	3280 ± 400	4.6 × 10 ⁻¹⁷ (±58%)
Cyclopentane ^g			1.7 × 10 ⁻¹⁷
<i>i</i> -Pentane ^h	2.99 × 10 ⁻¹²	2927 ± 173	1.62 × 10 ⁻¹⁶ (±35%)
<i>n</i> -Pentane ^h			8.7 × 10 ⁻¹⁷
2,2-Dimethylbutane ^g			2.7 × 10 ⁻¹⁷
Methylcyclopentane ^g			3.2 × 10 ⁻¹⁶
Cyclohexane ^h			1.4 × 10 ⁻¹⁶
2-Methylpentane ^h			1.8 × 10 ⁻¹⁶
3-Methylpentane ^h			2.2 × 10 ⁻¹⁶
<i>n</i> -Hexane ^h			1.1 × 10 ⁻¹⁶
<i>n</i> -Heptane ^h			1.5 × 10 ⁻¹⁶
2,3-Dimethylpentane ^g			3.3 × 10 ⁻¹⁶
2,4-Dimethylpentane ^h			1.5 × 10 ⁻¹⁶
<i>n</i> -Octane ^h			1.9 × 10 ⁻¹⁶
2,2,4-Trimethylpentane ^h			9 × 10 ⁻¹⁷
2,3,4-Trimethylpentane ^g			4.4 × 10 ⁻¹⁶
<i>n</i> -Nonane ^h			2.3 × 10 ⁻¹⁶ (±40%)
<i>n</i> -Decane ^h			2.8 × 10 ⁻¹⁶
<i>Alkenes and Alkynes</i>			
Ethene ^f	3.3 × 10 ⁻¹²	2880 ± 500	2.1 × 10 ⁻¹⁶ (±58%)
Ethyne ^f			1 × 10 ⁻¹⁶
Propene ^f	4.6 × 10 ⁻¹³	1155 ± 300	9.5 × 10 ⁻¹⁵ (±58%)
1-Butene ^h	3.14 × 10 ⁻¹³	938 ± 106	1.35 × 10 ⁻¹⁴ (±30%)
<i>c</i> -2-Butene ^h			3.50 × 10 ⁻¹³
<i>i</i> -Butene ^h			3.32 × 10 ⁻¹³
<i>t</i> -2-Butene ^{h,i}	1.22 × 10 ⁻¹⁸	-382 ± 28	3.90 × 10 ⁻¹³
2-Methyl-2-butene ^h			9.37 × 10 ⁻¹²
1-Pentene ^j			1.20 × 10 ⁻¹⁴
<i>c</i> -2-Pentene ^j			6.55 × 10 ⁻¹³
<i>t</i> -2-Pentene ^j			3.78 × 10 ⁻¹³
<i>Biogenics</i>			
<i>a</i> -Pinene ^h	1.19 × 10 ⁻¹²	-490 ± 97	6.16 × 10 ⁻¹² (±30%)
<i>b</i> -Pinene ^h			2.51 × 10 ⁻¹² (±40%)
Camphene ^h			6.6 × 10 ⁻¹³ (±35%)
<i>d</i> -Limonene ^h			1.22 × 10 ⁻¹¹ (±35%)
DMS ^k	1.9 × 10 ⁻¹³	-520 ± 200	1.1 × 10 ⁻¹² (±41%)
Isoprene ^h	3.03 × 10 ⁻¹²	446 ± 60	6.78 × 10 ⁻¹³

2. Rate data applicable to nighttime gas-phase NO₃ chemistry and pertaining to the chemical variables monitored at AI during the ICARTT campaign – continued.^a

NO ₃ sink / Reaction	<i>A</i> (cm ³ molecule ⁻¹ s ⁻¹)	<i>B</i> (K)	<i>k</i> ^{b,c} (cm ³ molecule ⁻¹ s ⁻¹)
<i>Aromatics</i>			
Toluene			6.8 × 10 ⁻¹⁷
Ethylbenzene			5.7 × 10 ⁻¹⁶
<i>m</i> + <i>p</i> -Xylene ^l			3.43 × 10 ⁻¹⁶ (±74%)
<i>o</i> -Xylene			3.77 × 10 ⁻¹⁶
<i>i</i> -Propylbenzene ^m			1.4 × 10 ⁻¹⁶
<i>n</i> -Propylbenzene ^m			1.4 × 10 ⁻¹⁶
2-Ethyltoluene ^m			7.1 × 10 ⁻¹⁶
3-Ethyltoluene ^m			4.5 × 10 ⁻¹⁶
4-Ethyltoluene ^m			8.6 × 10 ⁻¹⁷
1,2,3-Trimethylbenzene ⁿ			1.86 × 10 ⁻¹⁵
1,2,4-Trimethylbenzene ⁿ			1.81 × 10 ⁻¹⁵
1,3,5-Trimethylbenzene			8.00 × 10 ⁻¹⁶
<i>OVOCs</i>			
Acetaldehyde ^f	1.4 × 10 ⁻¹²	1860 ± 500	2.7 × 10 ⁻¹⁵ (±58%)
Acetone ^f			3 × 10 ⁻¹⁷
Formaldehyde ^f			5.8 × 10 ⁻¹⁶
Methanol	9.4 × 10 ⁻¹²	2650 ± 700	1.30 × 10 ⁻¹⁶ (±220%)
<i>Additional</i>			
R1 ^k	1.4 × 10 ⁻¹³	2470 ± 150	3.5 × 10 ⁻¹⁷ (±15%)
R3 ^k	1.8 × 10 ⁻¹¹	-110 ± 100	2.6 × 10 ⁻¹¹ (±26%)
R4 ^o	<i>K</i> _{eq} = (2.8 ± 0.6) × 10 ⁻¹¹ (cm ³ molecule ⁻¹)		
R6a + R6b			^{k,p} (9.7 ± 7.6) × 10 ⁻²²
R7 ^k			1.19 × 10 ⁻¹¹

^aFrom *Atkinson* [1991] unless otherwise indicated.

^bCalculated at 298 K; given by: $k = A \cdot \exp^{-(B/T)}$.

^cUncertain by a factor of 2 unless otherwise indicated.

^dFrom *Atkinson et al.* [1997].

^eFrom *Atkinson* [1994].

^fFrom *Atkinson et al.* [1999].

^gDerived from bond-additivity relationships of *Atkinson* [1991].

^hFrom *Atkinson* [1997].

ⁱGiven by: $k = A \cdot T^2 \cdot \exp^{-(B/T)}$.

^jFrom *Pfrang et al.* [2005].

^kFrom *Atkinson et al.* [2004].

^lAverage of values from *m*- and *p*-xylene from *Atkinson* [1991].

^mFrom *Jenkin et al.* [2003].

ⁿCalculated at 294 K.

^oCalculated from parameters given by *Atkinson et al.* [2004].

^pTotal rate coefficient with respect to (R6a) and (R6b) calculated at 290 K with [H₂O(g)] = (4.0 ± 0.4) × 10¹⁷ molecules cm⁻³.

3. Comparison between rates of NO_x loss and HNO₃ production from NO₃ and N₂O₅ mechanisms for selected times during the ICARTT campaign.

Date	$L_j(\text{NO}_x)^{\text{a,b}}$						$P_{\text{VOCs}}(\text{HNO}_3)^{\text{a}}$
	$j = \text{VOCs}$	$j = \text{indirect}$		$j = \text{het}$			
		$f = 0^{\text{c}}$	$f = 2.9$	$\rho_{\text{het}} = 0.2^{\text{d}}$	$\rho_{\text{het}} = 0.4$	$\rho_{\text{het}} = 3.1$	
July 8–28 ^e	0.12	0.36	0.12	0.07	0.14	0.38	0.04
July 12 01:00	0.08	0.50	0.17	0.10	0.20	0.53	0.03
July 12 05:00	0.13	1.07	0.37	0.21	0.43	1.13	0.02
July 16–17 ^f	0.19	0.85	0.29	0.17	0.34	0.89	0.06
July 17 ^g	0.10	0.11	0.04	0.02	0.04	0.12	0.01
July 26 03:00	0.65	0.18	0.06	0.04	0.07	0.19	0.01

^aUnits are ppbv hr⁻¹.

^bNO_x loss rate via sink j ; For N₂O₅ mechanisms, $L(\text{NO}_x) = P(\text{HNO}_3)$.

^c $L_{\text{indirect}}(\text{NO}_x)$ was calculated for $k_{(\text{H}_2\text{O}(\text{g})+\text{N}_2\text{O}_5)}$ reduced by factor f (see Section I.3.4 for details).

^d $L_{\text{het}}(\text{NO}_x)$ is expressed as a function of the ratio, ρ_{het} , of $k_{\text{het}}^{\text{I}}$ to $k_{\text{indirect}}^{\text{I}}$ (see Section I.3.4 for details); $\rho_{\text{het}} = 0.2, 0.4$ correspond with $f = 0$; $\rho_{\text{het}} = 3.1$ corresponds with $f = 2.9$; total rates are obtained by summing all j components.

^eAverage values for nighttime hours (21:00–05:00).

^fAverage values for the period from 22:00 on July 16 to 03:00 on July 17.

^gAverage values for the period from 04:00 to 05:00.

4. Operational and quality parameters for analytical systems operated at THF during summer 2004 and from which measurements were used in this work.

Variables measured	Analytical Scheme	Sample cycle period	Integration time	LOD or range	Precision	Accuracy
<i>Chemical variables</i>						
Toluene	GC-FID	~40 min	~6 min	0.005 ppbv	±5%	±5% ^a
Monoterpenes ^b				0.010 ppbv	±5%	±5% ^a
Toluene	PTR-MS	8 min	20 s	0.015 ppbv	±5% ^c	±15% ^d
O ₃	UV absorbance ^e	1 min	1 min	1 ppbv	±1%	
NO	O ₃ chemiluminescence	1 min	1 min	0.060 ppbv	<±17%	
<i>Meteorological variables</i>						
Pressure	Manometer	1 min	1 min	500–1100 mbar	±0.03 mbar	±0.08 mbar
Temperature	Thermistor	1 min	1 min	–40 to 60 °C	±0.1 °C	±0.2 °C
Relative Humidity	Thin film capacitor	1 min	1 min	0–100%	±0.3%	±2 to ±3%
Wind speed	Anemometer	1 min	1 min	0–75 m s ^{–1} ^f		±1% or ±0.07 m s ^{–1}
<i>Other</i>						
<i>J</i> (NO ₂)	Filter radiometer	1 min	1 min	1 × 10 ^{–6} s ^{–1}		

^aFor standard mixing ratio.

^bQuality parameters derived from analysis of *n*-decane standard.

^cFor calibration factor (C_{Tol}) determination; measurement precision was estimated from counting statistics as described previously [Hayward *et al.*, 2002; de Gouw *et al.*, 2003a] and was ≥10%.

^dBased on least squares linear regression against GC-FID toluene measurements.

^e254 nm.

^fThreshold = 0.45 m s^{–1}.

5. Comparison between monoterpene emission fluxes calculated by *Geron et al.* [2000] for forestland encompassing the THF site and relative monoterpene abundances from mixing ratios measured by GC-FID at THF between July 24 and August 15, 2004.

Monoterpene	E° ($\mu\text{g C m}^{-2} \text{ h}^{-1}$) ^a	THF (%) ^b	
		Daytime ^c	Nighttime ^d
α -pinene	39.1 (24.6)	36 \pm 10	40 \pm 12
β -pinene	23.9 (15.0)	22 \pm 8	25 \pm 7
camphene	21.4 (13.5)	30 \pm 11	25 \pm 12
Δ^3 -carene	19.1 (12.0)	7 \pm 4	7 \pm 2
β -myrcene	16.4 (10.3)	NM ^e	NM
<i>d</i> -limonene	16.0 (10.1)	4 \pm 3	3 \pm 2
sabinene	8.2 (5.2)	NM	NM
<i>p</i> -cymene	6.2 (3.9)	NM	NM
β -phellandrene	4.8 (3.0)	NM	NM
thujene	1.9 (1.2)	NM	NM
α -terpinene	1.5 (0.9)	NM	NM
terpinolene	0.3 (0.2)	NM	NM
γ -terpinene	0.16 (0.1)	NM	NM
ocimene	0.1 (0.1)	NM	NM

^a E° , emission flux [*Geron et al.*, 2000]; percentage of total shown in parentheses.

^bMeasured average $\pm 1\sigma$ relative ambient mixing ratio distribution.

^c $n = 369$.

^d $n = 244$.

^eNM, not measured.

6. Measured retention times for C₉–C₁₁ hydrocarbons in the THF GC system primary working standard that eluted between nonane and undecane on the VF-5ms column together with predicted retention times for several additional monoterpenes.

Compound	b.p. (°C) ^a	RT (min) ^b
<i>n</i> -nonane	150.82	10.18 ± 0.04
<i>i</i> -propylbenzene	152.41	10.89 ± 0.05
α -pinene	156.2	11.14 ± 0.04
<i>n</i> -propylbenzene	159.24	11.54 ± 0.05
camphene	158 to 161	11.5 ± 0.3 ^c
3-ethyltoluene	161.3	11.68 ± 0.05
4-ethyltoluene	162	11.76 ± 0.05
1,3,5-TMB	164.74	11.85 ± 0.05
2-ethyltoluene	165.2	12.09 ± 0.05
β -pinene	166	12.17 ± 0.05
<i>n</i> -decane	174.15	12.27 ± 0.05
β -myrcene	167	12.2 ± 0.2 ^c
1,2,4-TMB	169.38	12.43 ± 0.05
Δ^3 -carene	171	12.6 ± 0.2 ^c
β -phellandrene	171.5	12.6 ± 0.1
1,2,3-TMB	176.12	13.08 ± 0.05
α -terpinene	174	12.9 ± 0.2 ^c
ocimene	177	13.1 ± 0.2 ^d
<i>p</i> -cymene	177.1	13.2 ± 0.1 ^c
<i>d</i> -limonene	178	13.18 ± 0.05
1,3-DEB	181.1	13.54 ± 0.05
1,4-DEB	183.7	13.75 ± 0.05
1,2-DEB	184	13.84 ± 0.06
γ -terpinene	183	13.7 ± 0.2 ^c
terpinolene	186	14.0 ± 0.2 ^c
undecane	195.9	14.42 ± 0.06

^a[Lide, 2008].

^bMeasured average $\pm 3\sigma$ except where noted otherwise.

^cDerived from linear regression between RT and b.p. for compounds in the primary working standard; errors represent 0.01 to 1 °C uncertainty in b.p. values and the 95% prediction interval on the RT values determined from regression analysis.

^d[Graedel, 1979].

7. Quantitative comparison between GC-FID and PTR-MS toluene measurements for different monoterpene fragmentation corrections applied to the PTR-MS data.

Treatment ^a	Regression Parameters			% Agreement ^c
	m^b	b^b	r^2	
A	1.13 ± 0.02	-0.008 ± 0.003	0.908	60.1
A'	1.16 ± 0.02	-0.011 ± 0.001	0.908	60.1
B	1.07 ± 0.02	-0.005 ± 0.002	0.910	62.8
C	1.00 ± 0.02	-0.003 ± 0.002	0.907	64.8
D	0.84 ± 0.02	0.004 ± 0.002	0.858	57.6
E	1.10 ± 0.02	-0.007 ± 0.002	0.911	61.0
F	0.97 ± 0.02	-0.002 ± 0.002	0.909	65.3

^aData treatment description: A, PTR-MS data uncorrected, correlation analyzed using simple least squares regression; A', same as A, but analyzed using orthogonal least squares regression with variance ratio, $\lambda = \sigma^2_{\text{PTR-MS}}/\sigma^2_{\text{GC-FID}} = 4.6 \pm 1.6$; B, PTR-MS data corrected assuming $\phi(93) = 1\%$ for reaction of H_3O^+ with α -pinene; C, same as B, but $\phi(93) = 2\%$ for α -pinene and 1% for β -pinene; D, same as B, but $\phi(93) = 7\%$ for α -pinene; E, PTR-MS data corrected for reactions of O_2^+ with measured monoterpenes using $\phi(93)$ from [Schoon *et al.*, 2003]; F, PTR-MS data corrected for reactions of H_3O^+ , as in treatment C, and O_2^+ , as in treatment E.

^bUncertainties are standard errors, except those for orthogonal least squares parameters which reflect 1σ range of λ .

^cPercentage of samples for which GC-FID and PTR-MS values agreed within combined 1σ measurement precisions.

8. Comparison of reported yields of $m/z = 93$ fragment ions associated with analysis of monoterpenes by PTR-MS and SIFT-MS.

Monoterpene	$\phi(93)$ (%) vs. Reagent			$\phi(81)$ (%) ^{a, c}
	H ₃ O ⁺ ^a	O ₂ ⁺ ^b	NO ⁺ ^b	
α -pinene	12 ^d	52 ^e	4 ^e	57 ^{d, f}
	7 ^g			45 ^{h, i}
	1 ^e			40 ^{j, k}
	<1 ^l			31 ^{g, m}
	<0.1 ^{j, k}			30 ^{e, b}
camphene	<1 ^{d, e}	13 ^e	<1 ^e	
β -pinene	7 ^g	56 ^e	3 ^e	70 ^{d, f}
	<1 ^{d, e, l}			40 ^{j, k}
	<0.1 ^{j, k}			33 ^{e, b}
β -myrcene	1 ^e	61 ^e	22 ^e	26 ^{e, b}
	<1 ^{d, e, l}	1 ^e		
Δ^3 -carene	<1 ^{d, e, l}	41 ^e	4 ^e	30 ^{j, k}
	<0.1 ^{j, k}			19 ^{e, b}
α -terpinene	<20 ⁿ			
	<1 ^l			
<i>p</i> -cymene	91 ^d			
	85 ^{h, i}			
<i>d</i> -limonene	1 ^d	26 ^e	<1 ^e	72 ^{d, f}
	<1 ^e			40 ^{j, k}
	<0.1 ^{j, k}			22 ^{e, b}
γ -terpinene	3 ^d			
	<1 ⁿ			
terpinolene	<1 ^{d, l}			

^aNO⁺ and O₂⁺ abundances were not specified and ion transmission efficiency corrections were not applied in the PTR-MS studies and may have contributed to the reported ion yields.

^bSIFT-MS; He carrier gas; yield corrected for ion transmission efficiency.

^cFrom reaction with H₃O⁺.

^d[Maleknia *et al.*, 2007].

^e[Schoon *et al.*, 2003].

^f $E/N = 140$ to 150 Td.

^g[Warneke *et al.*, 2003].

^h[Tani *et al.*, 2004].

ⁱ $E/N = 142$ Td.

^j[Tani *et al.*, 2003].

^k $E/N = 120$ Td; percentage of total ion signal including isotopic signal.

^l[Lee *et al.*, 2006a].

^m $E/N = 106$ Td.

ⁿ[Lee *et al.*, 2006b].

9. Comparison of PTR-MS operating parameters employed at THF during summer of 2004 and in selected studies reported in the literature.

P_{DT} (mbar)	T_{DT} (K)	E (V cm ⁻¹)	E/N (Td) ^a	KE_{ion} (kJ mole ⁻¹) ^b	Reference
1.8–2.1	303–333	60 ^c	120–150	23.5–39.8	[Maleknia <i>et al.</i> , 2007]
1.8–2.1	296 ^d	41.7–62.5	142	32.8	[Tani <i>et al.</i> , 2004]
2.005 ± 0.005	318	62.5	137	30.7	This work
ND	ND	ND	120	>23.3 ^c	[Tani <i>et al.</i> , 2003]
2.4	ND	ND	106	>18.4 ^e	[Warneke <i>et al.</i> , 2003]
1.47	298	0.08	0.22	3.7 ^f	[Schoon <i>et al.</i> , 2003] ^g
2.2	ND	ND	ND	ND	[Lee <i>et al.</i> , 2006a,b]

Abbreviations: DT, drift tube; ND, no data.

^a1Td (Townsend) = 10⁻¹⁷ V cm².

^bCalculated from published values of μ_0 in N₂ [Dalton *et al.*, 1976].

^cDrift tube length assumed to be 9.6 cm.

^dCalculated from P_{DT} and E/N .

^eAssumed T_{DT} > 21 °C.

^fEquivalent to thermal energy.

^gSIFT-MS; conditions correspond with flow tube.

10. Comparison of reported yields of $m/z = 93$ fragment ions associated with analysis of monoterpene oxidation products by PTR-MS and SIFT-MS.

Monoterpene	Oxidation Product	Yield (%) vs. Oxidant		
		OH	O ₃	$\phi(93)$ (%) ^a
α -pinene	pinonaldehyde	47–83 ^b	19–34 ^c	2 ^d
	α -pinene oxide	28–87 ^e	16 ± 3 ^e 5.4 ± 0.6 ^c 2 ^e	9 ^d
β -pinene	UnID ^f	<5 ^b		100 ^g
β -myrcene	4-vinyl-4-pentenal	32–41 ^b	49 ± 8 ^c	>70 ^{b, g, h} , >10 ^{c, g, h}
Δ^3 -carene	caronaldehyde	34 ± 8 ⁱ	≤8 ⁱ	3 ^d
	UnID	>5 ^b		100 ^g
ocimene ^{j, k}	4-methyl-3,5-hexadienal ^l	<2	<33	
<i>d</i> -limonene	UnID	<5 ^b		100 ^g
γ -terpinene	UnID	>5 ^b		100 ^g
terpinolene	4-methyl-3-cyclohexen-1-one	43 ± 7 ^b	53 ± 9 ^c	47 ^{b, g, h} , 9 ^{c, g, h}

^aFrom reaction with H₃O⁺ unless indicated otherwise.

^b[Lee *et al.*, 2006b].

^c[Lee *et al.*, 2006a].

^d[Schoon *et al.*, 2004].

^e[Atkinson *et al.*, 2006].

^fUnID, unidentified oxidation products.

^gNO⁺ and O₂⁺ abundances were not specified and may have contributed to reported fragmentation.

^hAssuming dehydration of the corresponding protonated oxidation product in the PTR-MS drift tube was the only source of the reported yield.

ⁱ[Hakola *et al.*, 1994].

^j*cis*-, *trans*- mixture.

^k[Reissell *et al.*, 2002].

^lProtonated molecular ion may dehydrate to a $m/z = 93$ fragment ion as observed for other 110 amu products [Lee *et al.*, 2006a, b].

11. Operational protocol of the GC-FTD instrument.

Valve ^a	Sample cycle stage, valve position							
	1. Cool ^b	2. Preflush ^c	3. Trap ^c	4. Preflush ^d	5. Trap ^d	6. Desorb ^b	7. Inject ^d	8. Bake
SSV	6, 7, 8	1, 3, 4, 5	1, 3, 4, 5	2	2	6, 7, 8	2	2
SV ^e	A	A	A	A	A	A	B	A
SV ^f	A	A	A	A	A	B	A	A
V1	closed	open	closed	open	closed	closed	closed	closed
V2	closed	closed	open	closed	open	closed	closed	closed
V3	closed	open	closed	open	closed	closed	closed	closed

^aAs labeled in Figure 18.

^bSSV is in a dead end position.

^cAmbient or standard sample.

^dHe.

^eEight-port SV.

^fFour-port SV.

12. Sample volumes (at standard temperature and pressure) required to yield HCN masses greater than the PDHID, FID and FTD MDL.

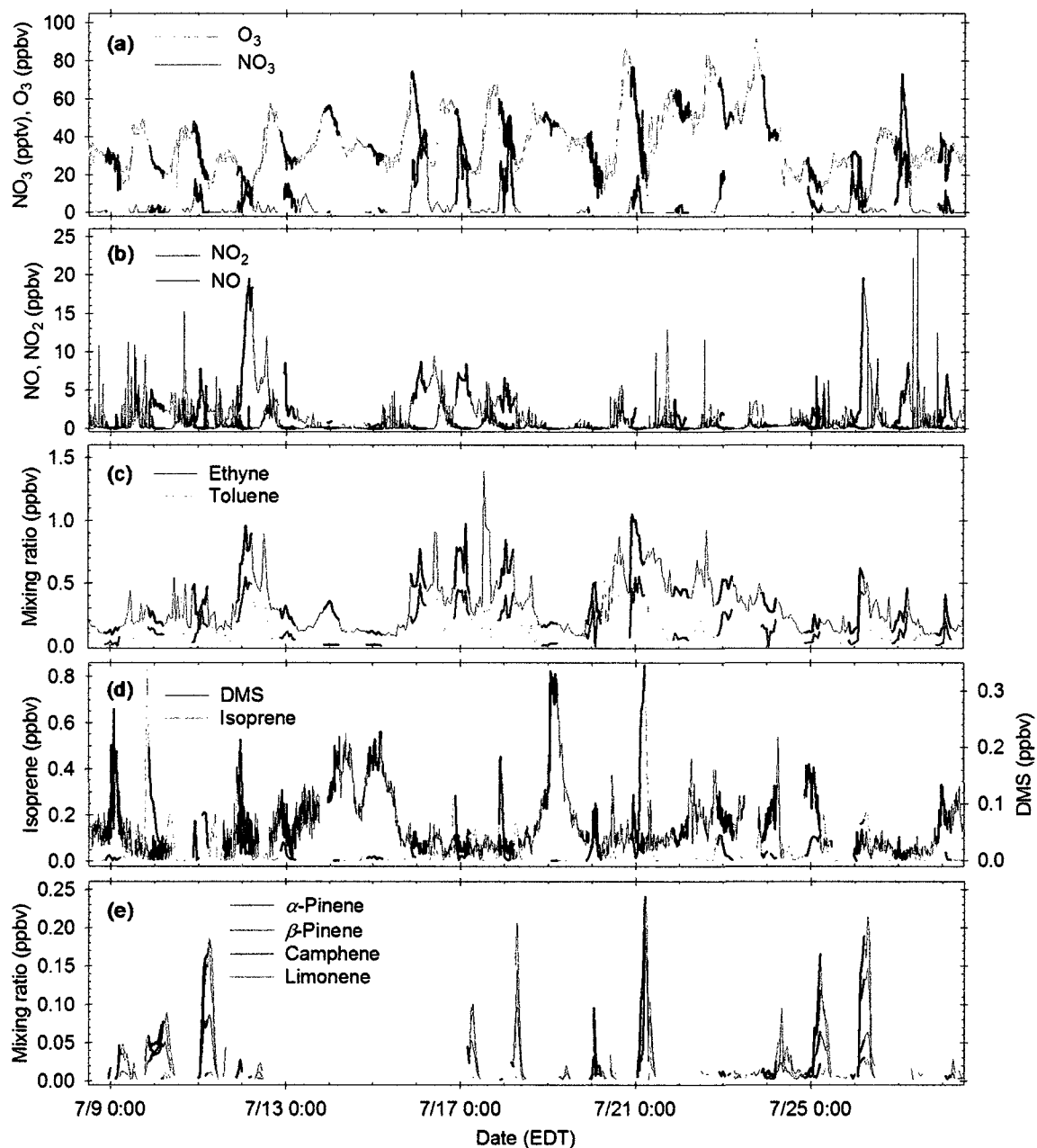
HCN (ppbv)	V_{PDHID} (liters) ^a	t_{PDHID} (min) ^b	V_{FID} (liters)	t_{FID} (min)	V_{FTD} (liters)	t_{FTD} (min)
0.100	0.12 ± 0.02	0.62 ± 0.08	0.26 ± 0.05	1.3 ± 0.2	0.101 ± 0.008	0.50 ± 0.04
0.010	1.2 ± 0.2	6.2 ± 0.8	2.6 ± 0.5	13 ± 2	1.01 ± 0.08	5.0 ± 0.4
0.001	12 ± 2	62 ± 8	26 ± 5	132 ± 23	10.1 ± 0.8	50 ± 4

PDHID, FID and FTD MDL = 0.015 ± 0.002 ng HCN, 0.032 ± 0.006 ng HCN, and 0.012 ± 0.001 ng HCN respectively.

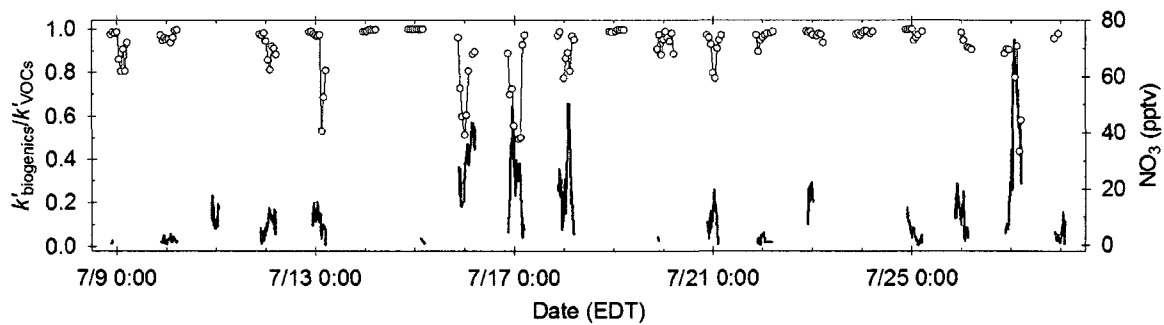
^aSample volume.

^bTrapping time at 0.2 l min^{-1} .

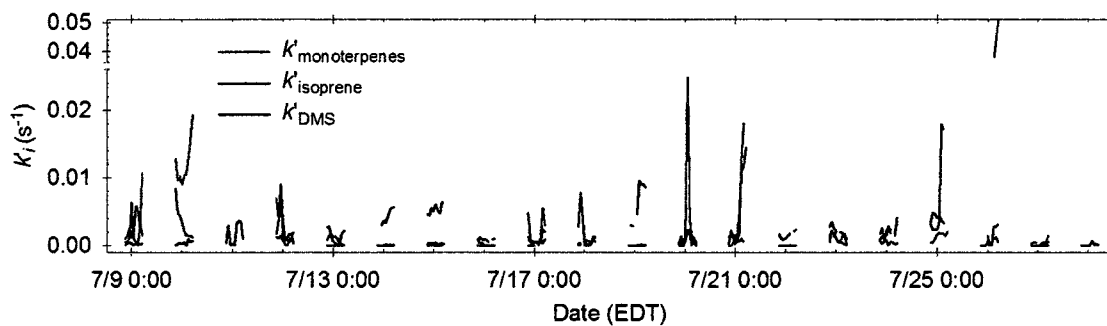
FIGURES



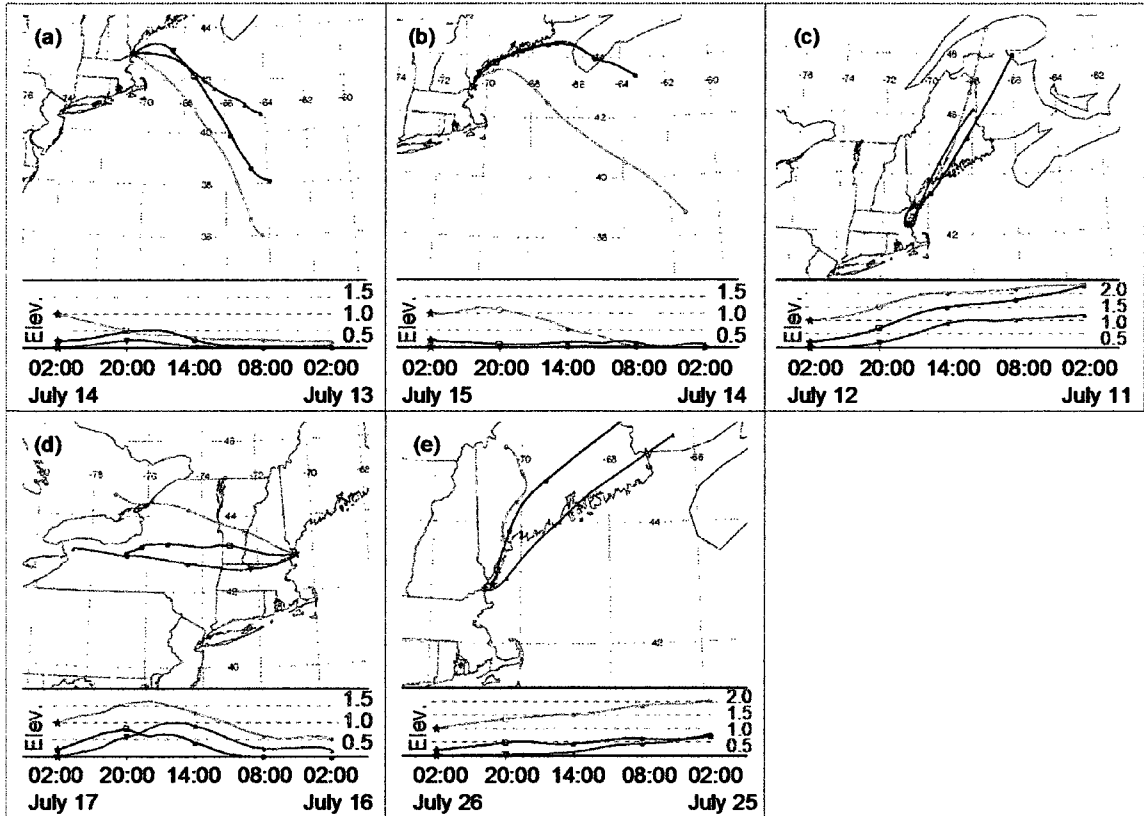
1. Time series of selected trace gases measured between noon on July 8 and noon on July 28. (a) NO_3 and O_3 ; (b) NO and NO_2 ; (c) ethyne and toluene; (d) isoprene and DMS; (e) monoterpenes. Segments of thickened lines indicate measurements made during the nighttime hours (21:00–05:00). Uncertainties are described in Table 1.



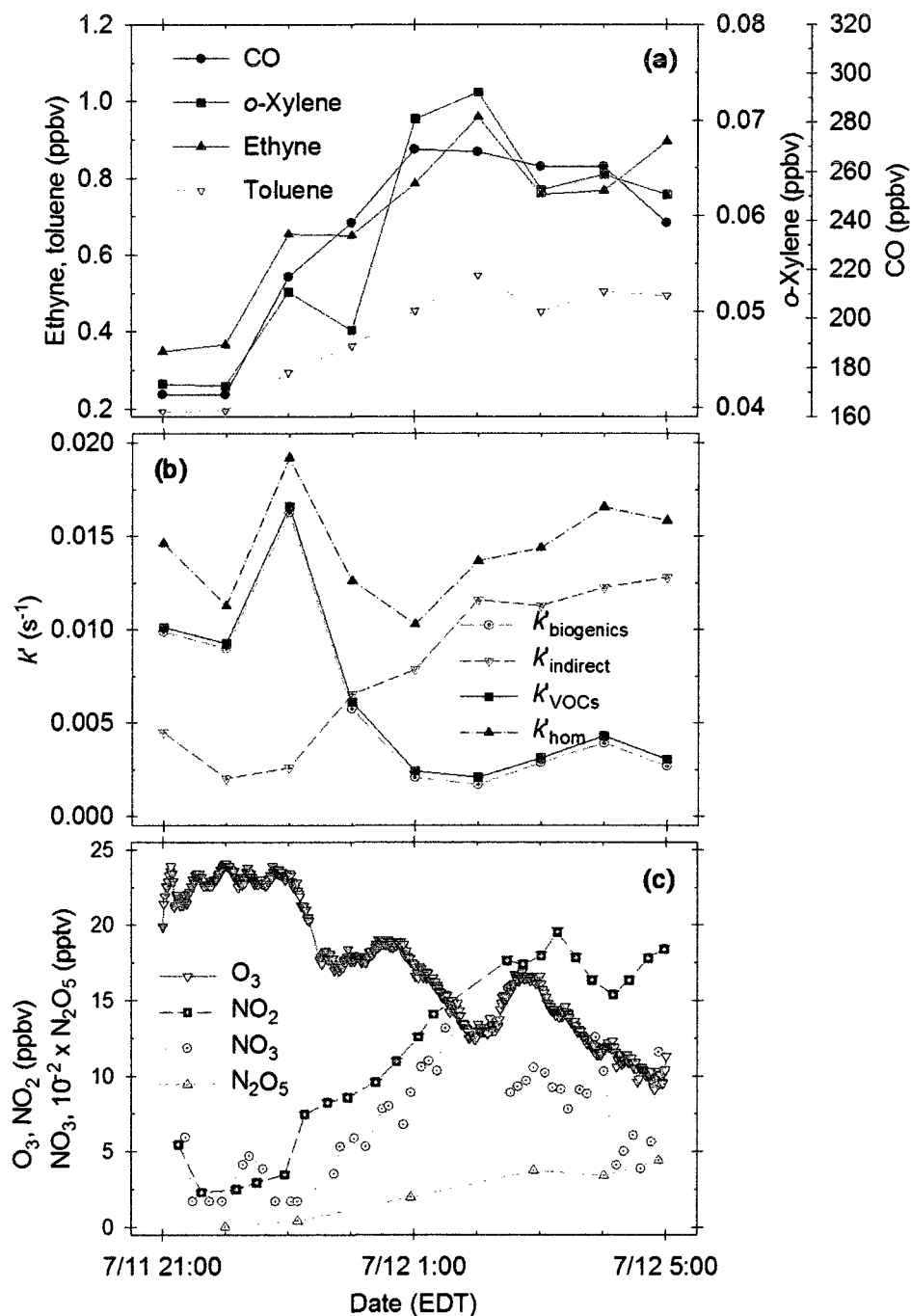
2. Relative biogenic reactivity calculated for the nighttime hours between 21:00 on July 8 and 05:00 on July 28. Open circles show the reactivity of the biogenic compounds relative to that of all the measured VOCs. The NO_3 mixing ratios (green trace) measured during the nighttime hours are reproduced for comparison. The average uncertainty in the calculated values of $k'_{\text{biogenics}}/k'_{\text{VOCs}}$ was 50%.



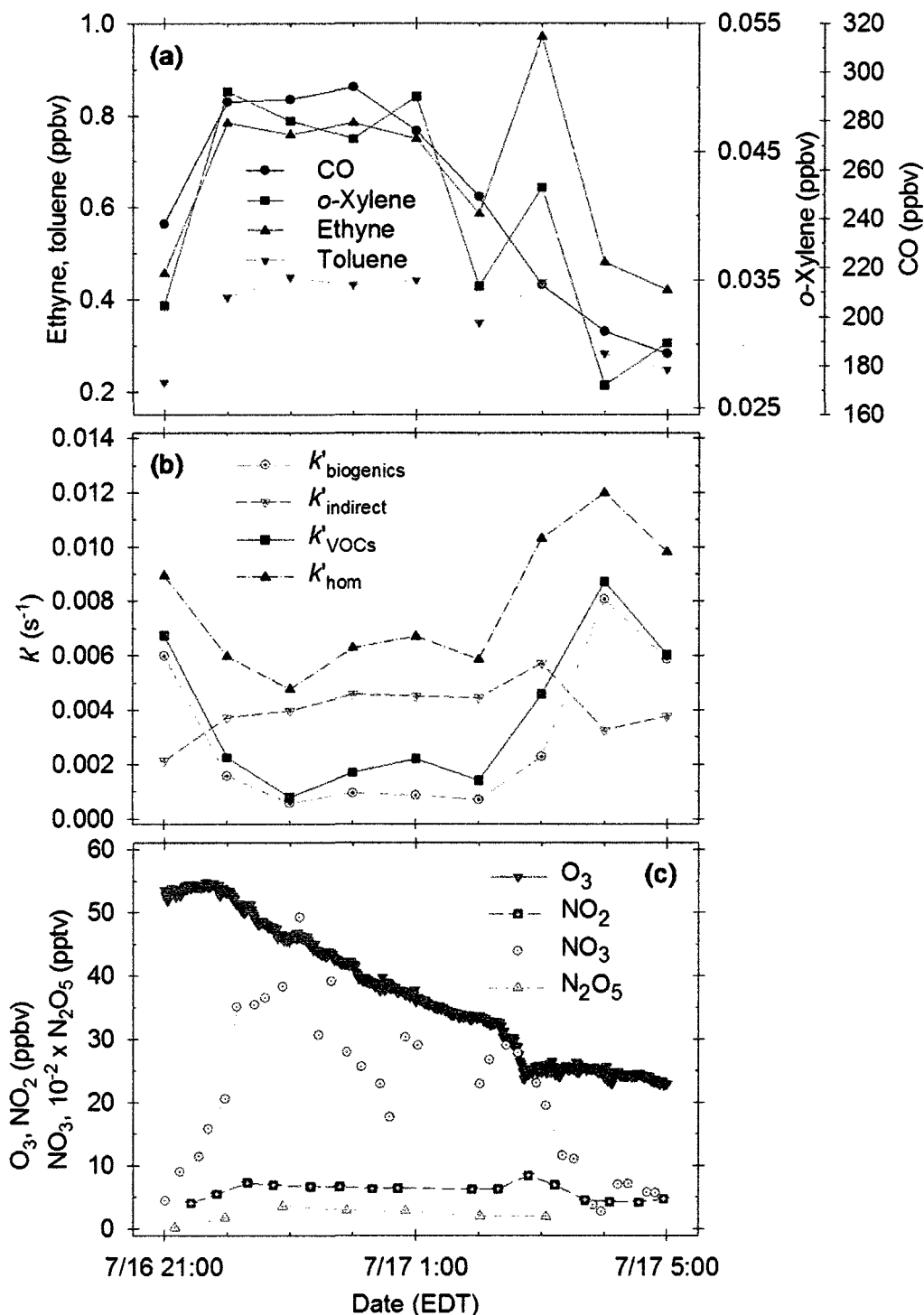
3. Absolute reactivity of DMS, monoterpenes and isoprene calculated for the nighttime hours between 21:00 on July 8 and 05:00 on July 28. Note the break in the ordinate between 0.026 and 0.036 s^{-1} . The average uncertainties in the values of k_i , where i = DMS, isoprene and monoterpenes were 60%, 60% and 30%, respectively.



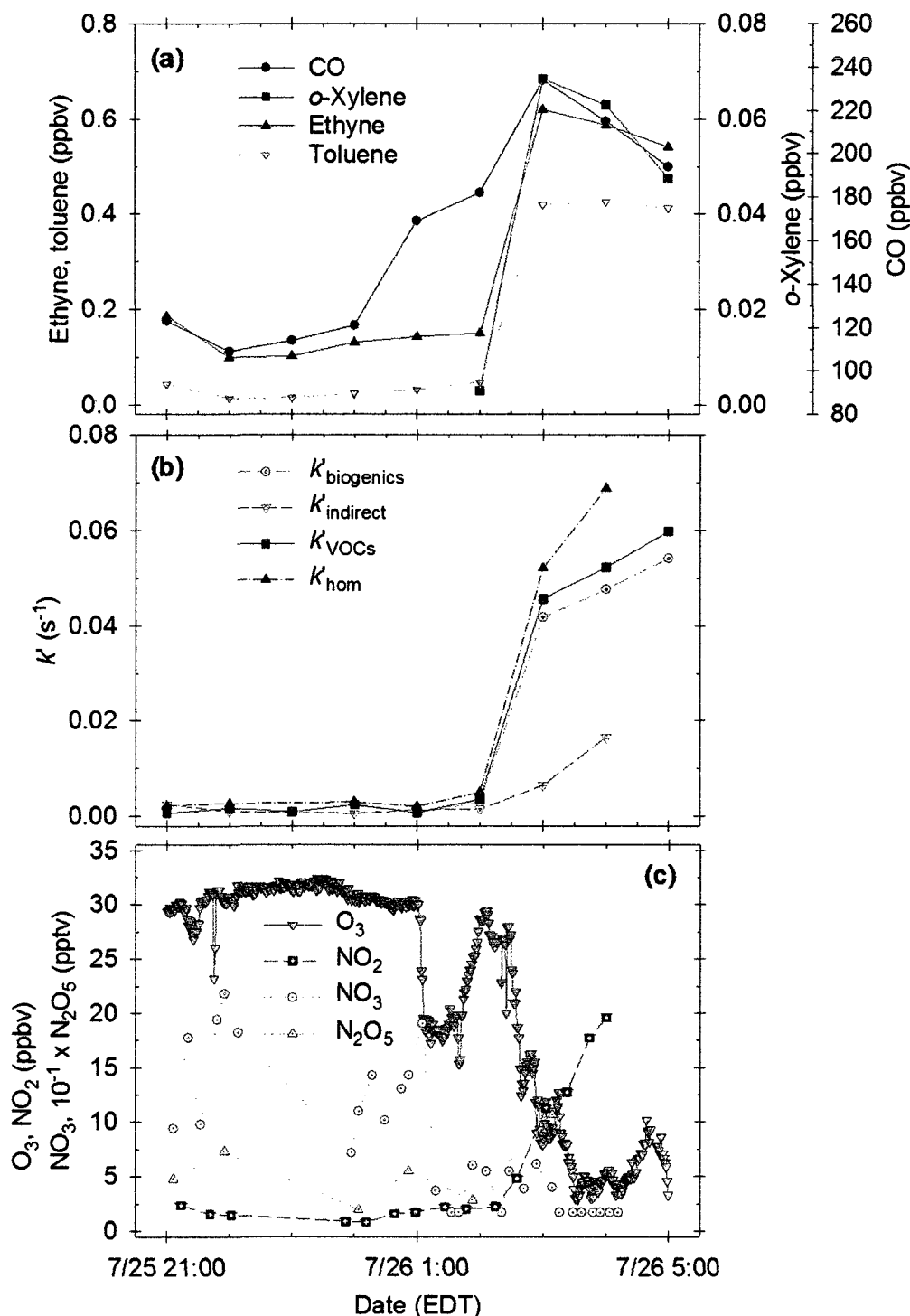
4. HYSPLIT trajectories for selected case study periods. (a) July 13; (b) July 14; (c) July 11; (d) July 16; (e) July 25. Units of elevation (Elev.) are in $m (\times 10^{-3})$ above ground level (a.g.l.). Red, blue and green trajectories end at AI (star) at 10, 200 and 1000 m a.g.l., respectively.



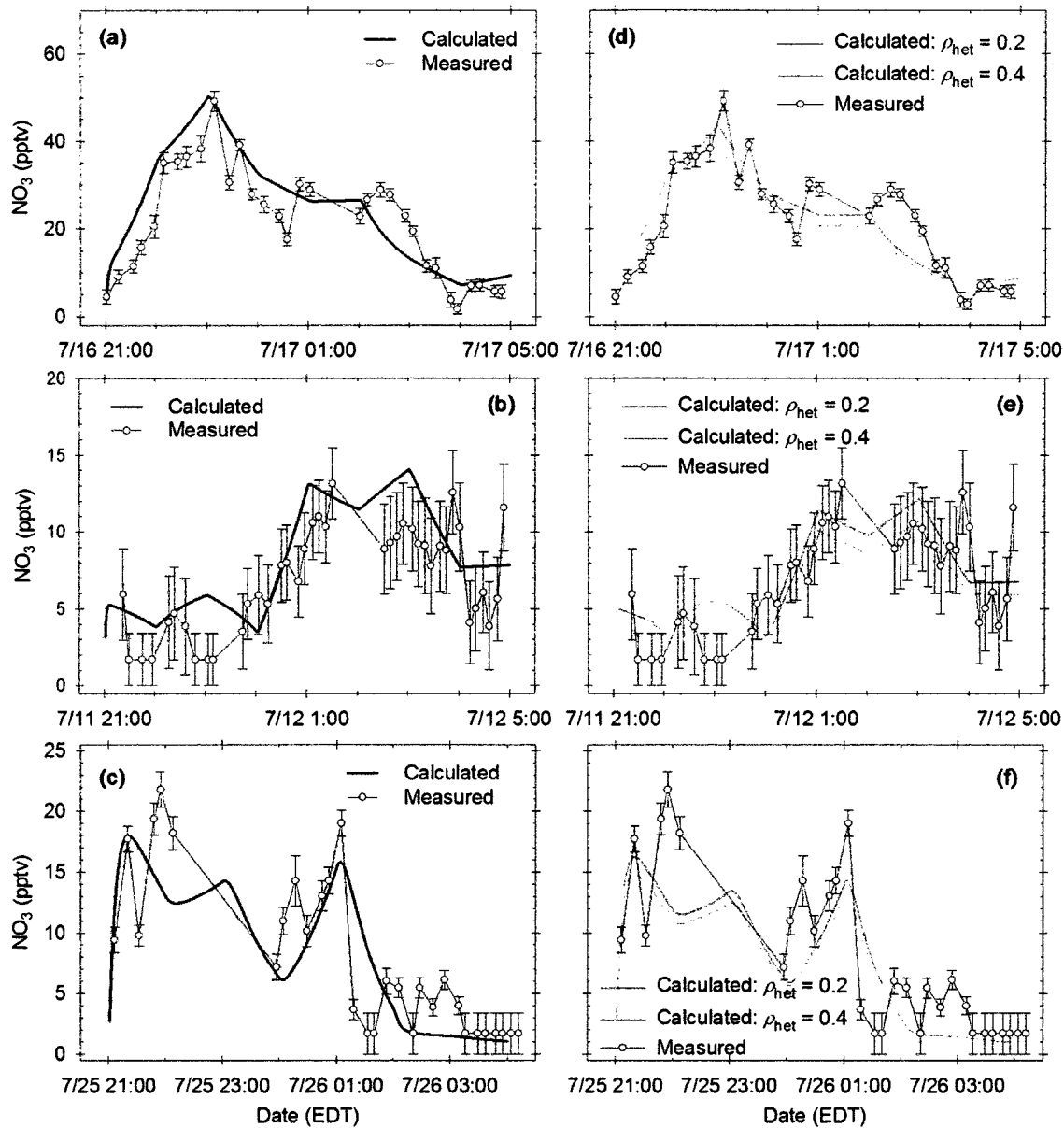
5. Atmospheric composition and chemistry on the night of July 11. (a) Measured mixing ratios of ethyne, toluene, *o*-xylene, and CO (averaged hourly). (b) Contributions to the total NO_3 loss efficiency; for the nighttime hours between 21:00 on July 8 and 05:00 on July 28, the average uncertainties in the values of k'_{indirect} , k'_{VOCs} , $k'_{\text{biogenics}}$, and k'_{hom} were 80%, 30%, 40%, and 40%, respectively. (c) Measured mixing ratios of NO_2 , NO_3 and O_3 and calculated mixing ratios of N_2O_5 ; the average uncertainty in the calculated mixing ratios of N_2O_5 was 60%; uncertainties in the measured NO_2 , NO_3 and O_3 mixing ratios are described in Table 1; NO_3 measurements below the LOD (Table 1) were set to $0.5 \times \text{LOD}$.



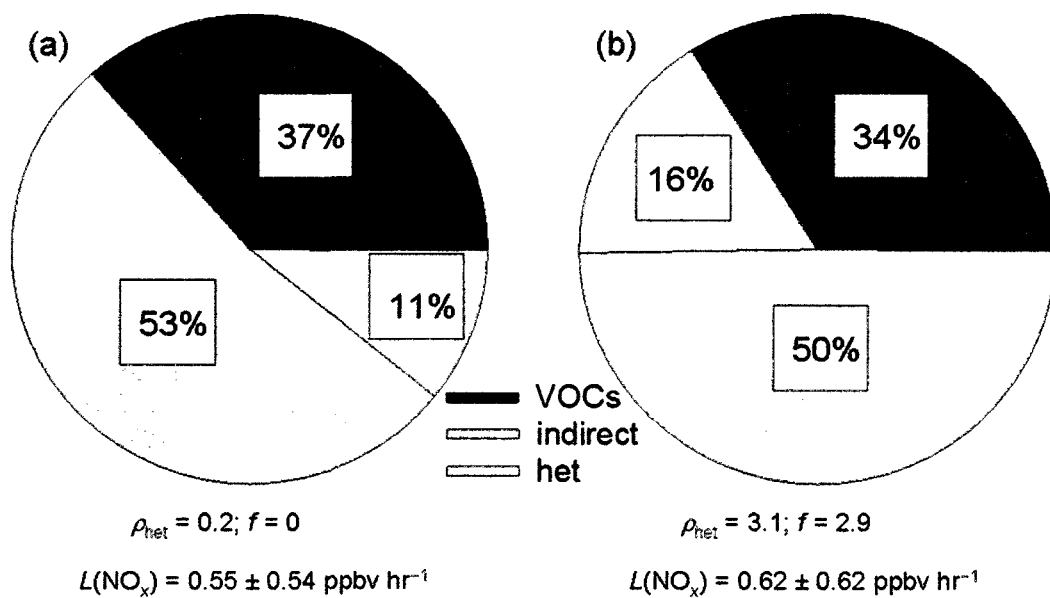
6. Atmospheric composition and chemistry on the night of July 16. (a) Measured mixing ratios of ethyne, toluene, *o*-xylene, and CO (averaged hourly). (b) Contributions to the total NO_3 loss efficiency on the night of July 16; uncertainties are the same as described in Figure 5b. (c) Measured mixing ratios of NO_2 , NO_3 and O_3 and calculated mixing ratios of N_2O_5 for the night of July 16; uncertainties are the same as described in Figure 5c.



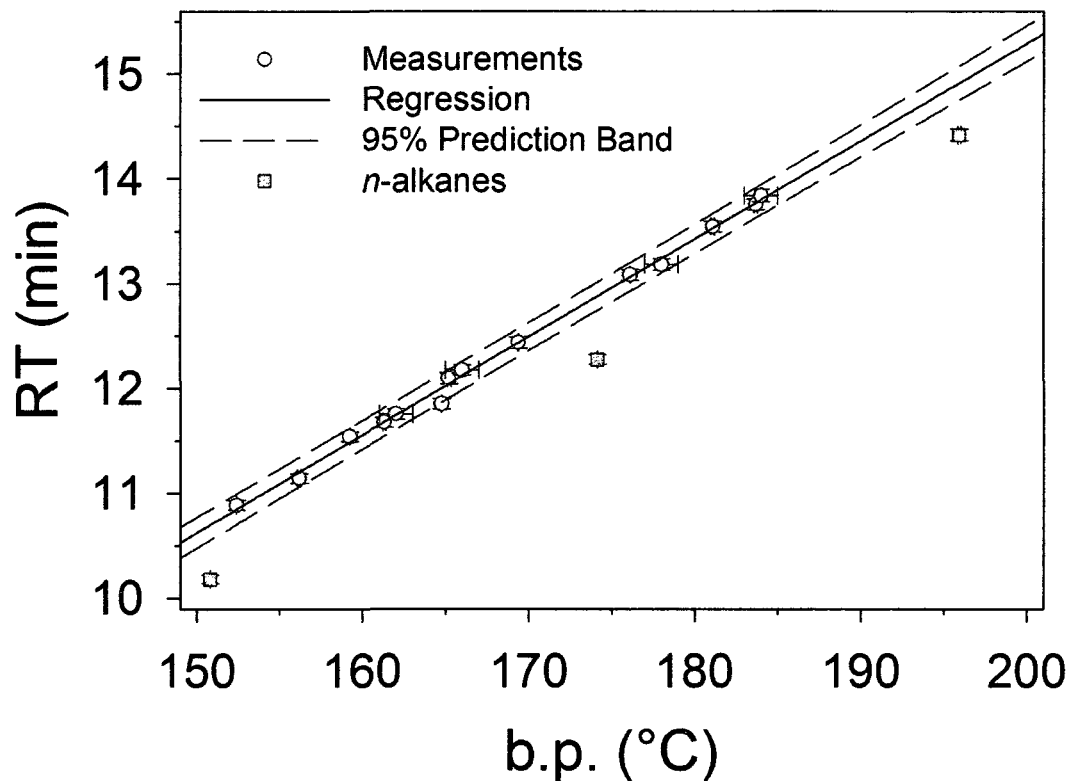
7. Atmospheric composition and chemistry on the night of July 25. (a) Measured mixing ratios of ethyne, toluene, *o*-xylene, and CO (averaged hourly). (b) Contributions to the total NO_3 loss efficiency on the night of July 25; uncertainties are the same as described in Figure 5b. (c) Measured mixing ratios of NO_2 , NO_3 and O_3 and calculated mixing ratios of N_2O_5 for the night of July 25. Uncertainties are the same as described in Figure 5c. NO_3 measurements below the LOD (Table 1) were treated as in Figure 5c.



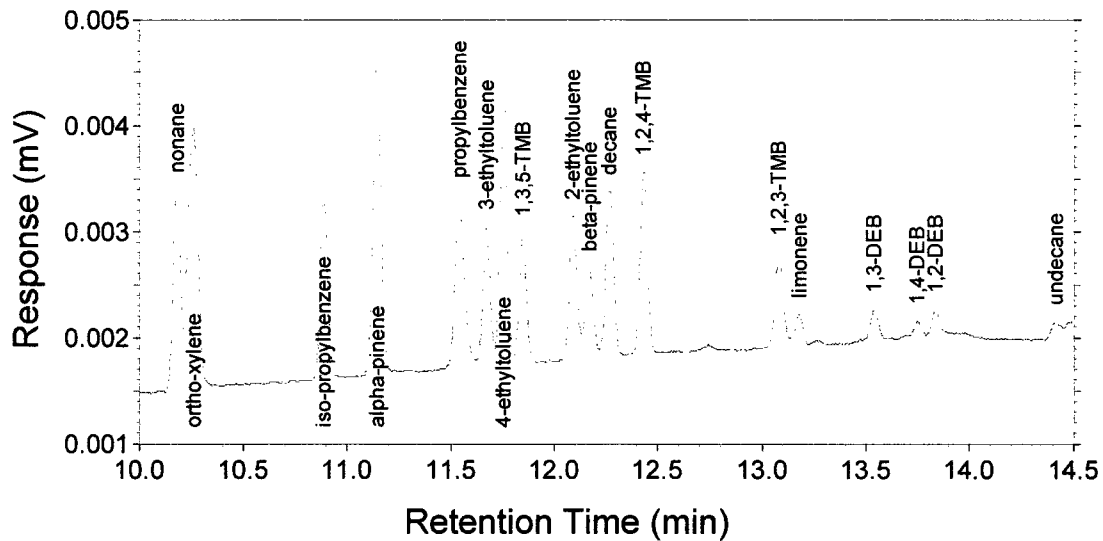
8. Measured versus calculated NO_3 mixing ratios. Calculations were performed using equation (10) for the nights of July 11 (a and d), July 16 (b and e) and July 25 (c and f). Calculated values in a–c include only gas phase loss processes for NO_3 and N_2O_5 whereas calculated values in d–f include limits for heterogeneous loss of N_2O_5 to aerosol and the ocean surface. Gray shaded regions in a–c represent uncertainty in the calculated values, the average being $\sim 30\%$ for July 11 and 16 and $\sim 20\%$ for July 25. Shaded regions in d, e and f define limits of the calculated values based on uncertainties shown in a, b and c, respectively. Measurements below the LOD (Table 1) were treated as in Figure 5c with uncertainties set to 100%.



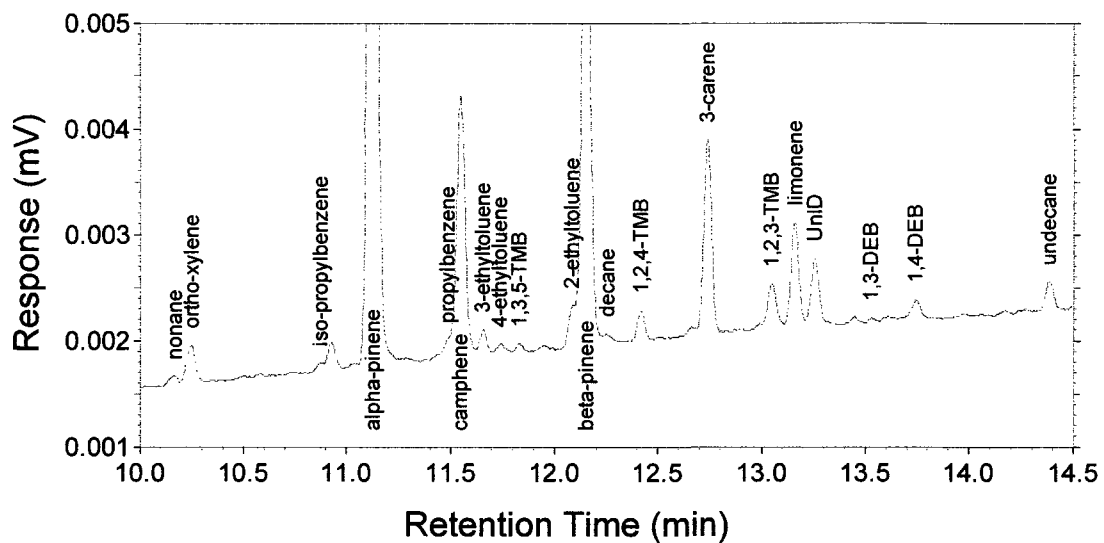
9. Average relative contributions of gas-phase and heterogeneous mechanisms to NO_x removal for the period July 8–28. (a) Minimum heterogeneous contribution; (b) maximum heterogeneous contribution (see text for details).



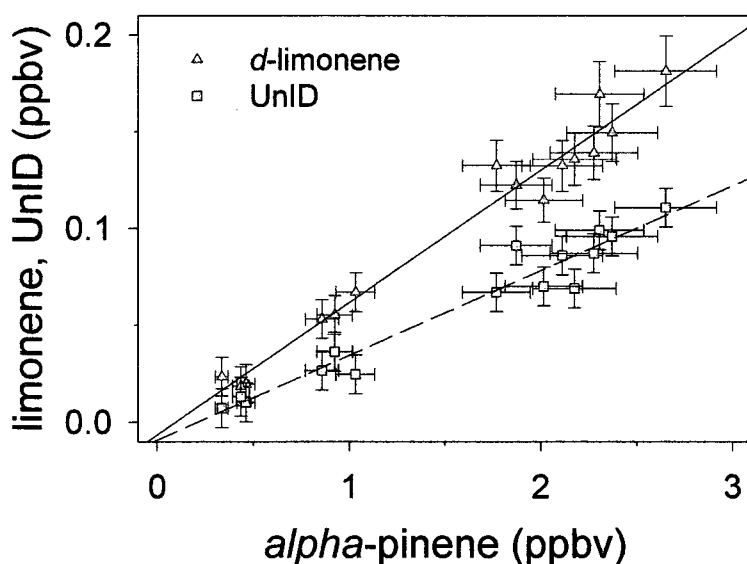
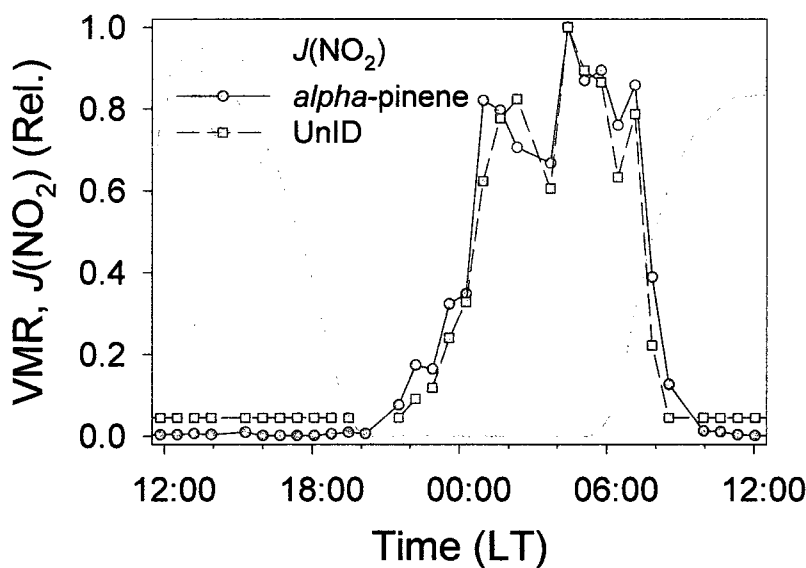
10. Linear correlation between elution order (retention time) and boiling point for C₉–C₁₁ compounds in the THF GC system primary working standard that eluted from the VF-5ms column between nonane and undecane. The regression line was derived by a simple least squares analysis which excluded data for the *n*-alkanes. Error bars are 0.04 to 0.06 min, representing 3 σ of the mean values determined from standard chromatograms, and 0.01 to 1 °C (taken to be 1 unit in the least significant digit of the literature b.p. values).



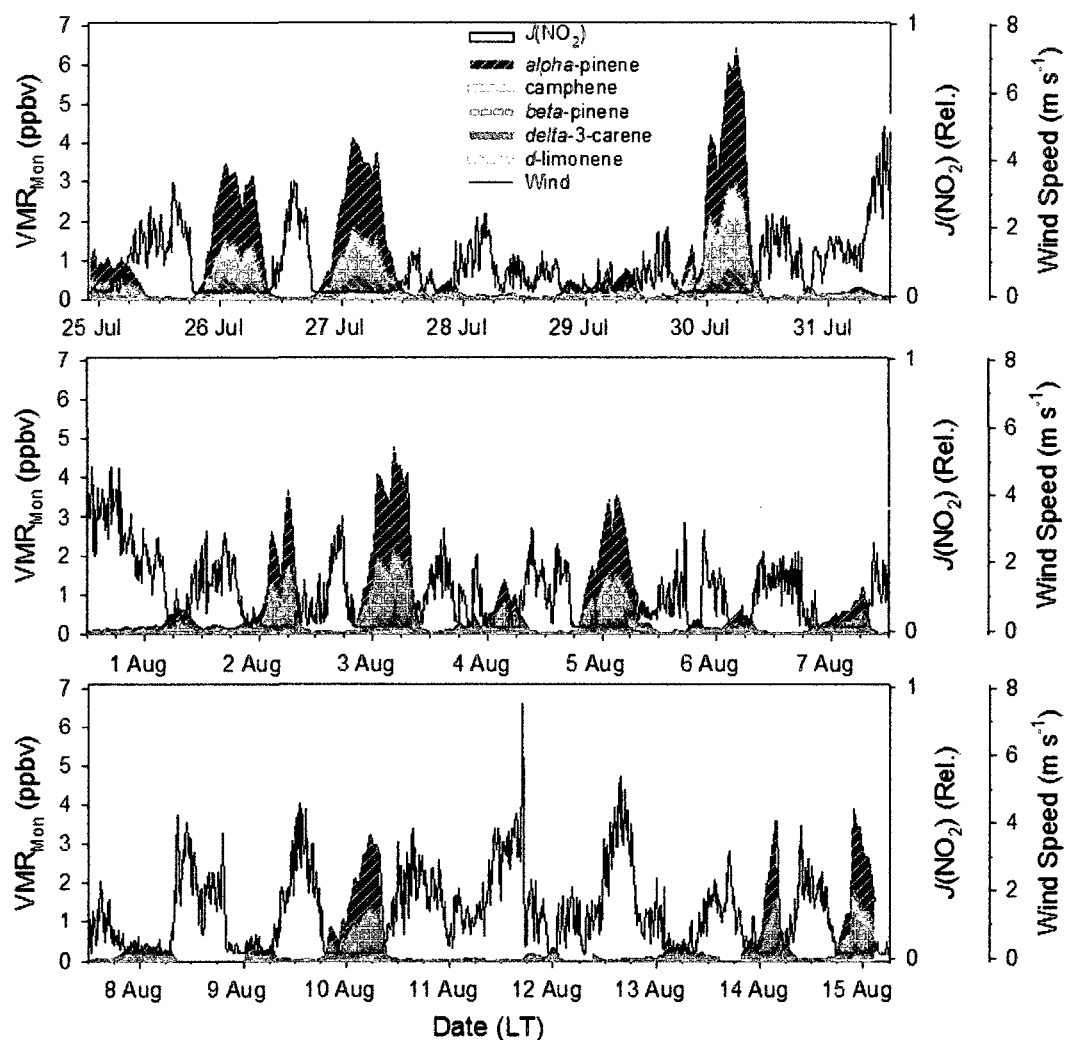
11. Portion of a chromatogram from the THF GC system primary working standard. Compounds that eluted between nonane and undecane on the VF-5ms column are identified. The temperature program employed was 35 °C for 2 min, 10 °C min⁻¹ to 115 °C, 7 °C min⁻¹ to 200 °C for 5 min. Abbreviations: TMB, trimethylbenzene; DEB, diethylbenzene.



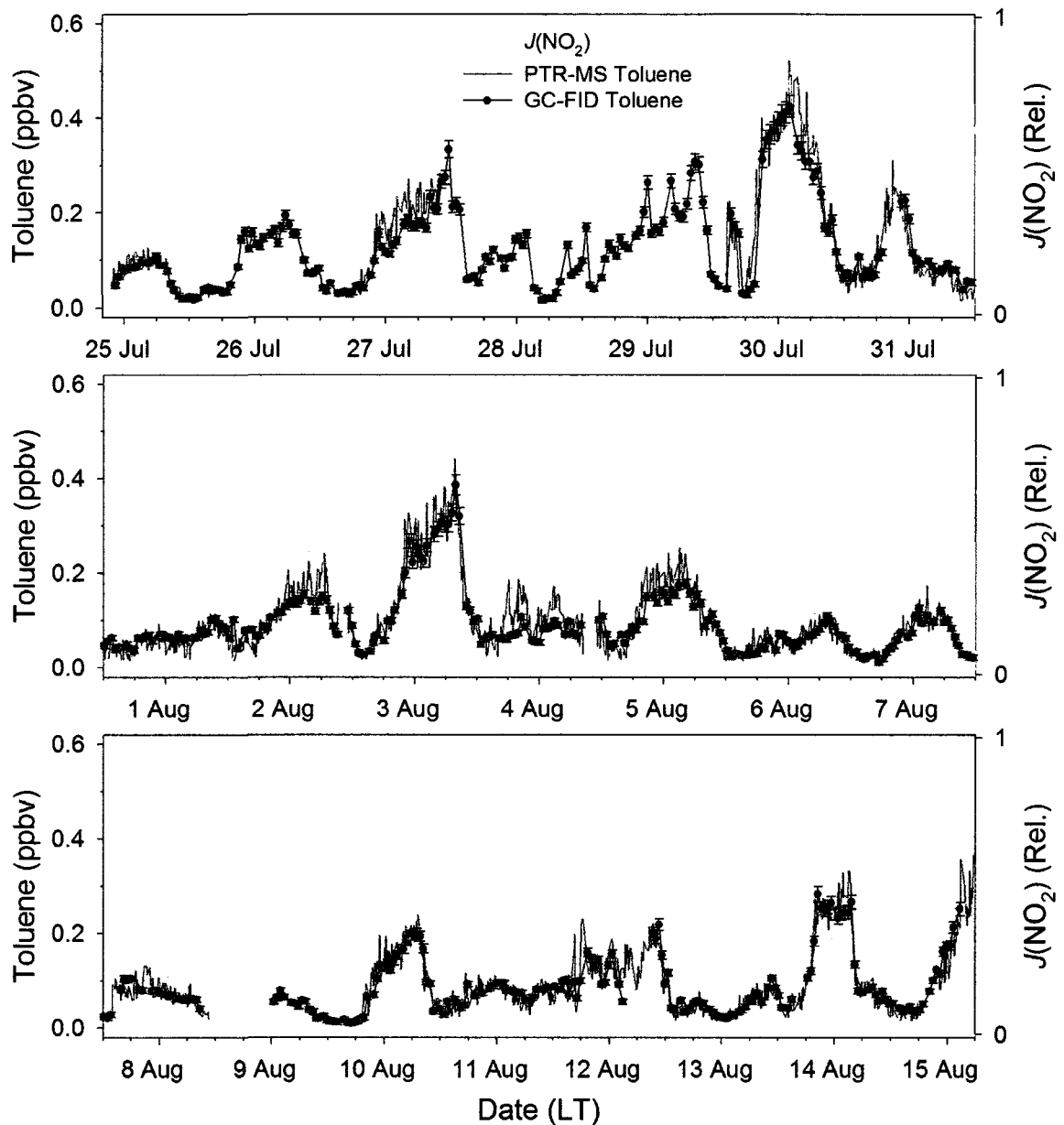
12. Portion of a chromatogram recorded at THF at 04:23 on August 3 during a period of enhanced monoterpene mixing ratios.



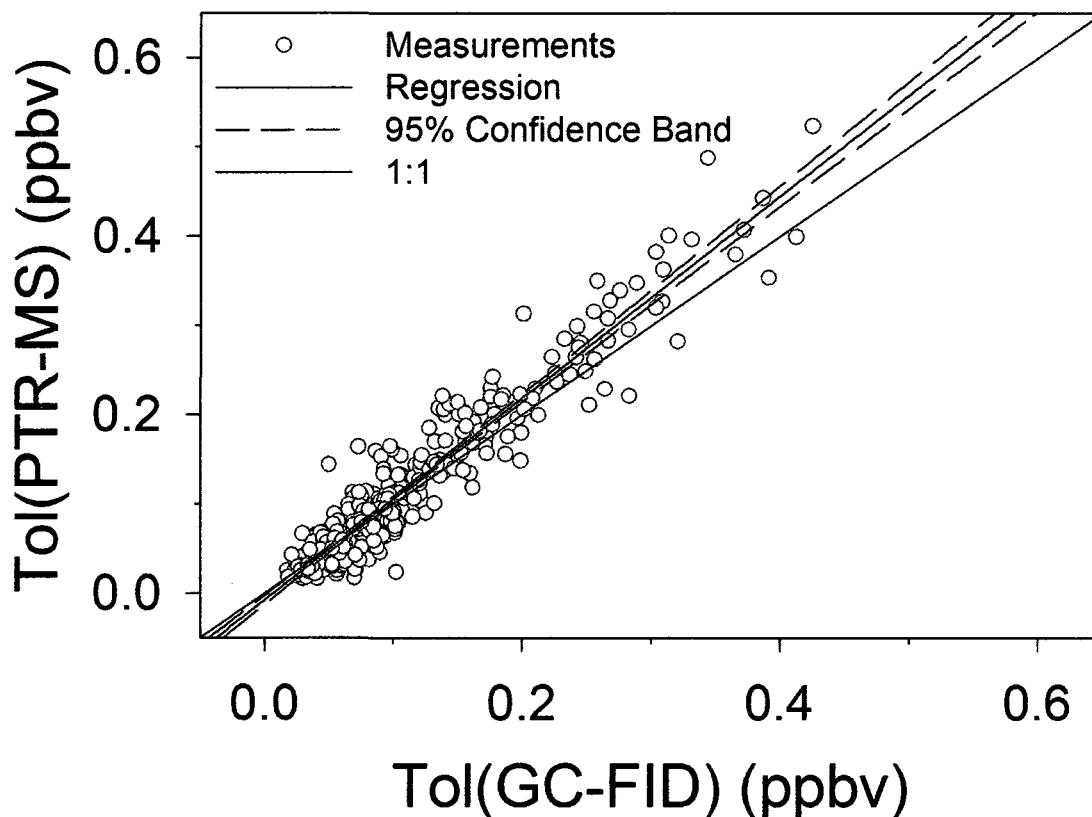
13. Comparison of trends in the mixing ratios of α -pinene and an unidentified (UnID) compound (assumed to be C_{10}) during the period from 12:00 on August 2 to 12:00 on August 3. (a) Time series of relative mixing ratios; (b) linear regression of absolute mixing ratios. The $J(\text{NO}_2)$ data in (a) are 10 min averages and delineate daytime and nighttime periods. In (b) the correlation between the d -limonene and α -pinene mixing ratios is shown for comparison. The coefficients of determination (r^2) for the regression lines were 0.97 and 0.95 for d -limonene and UnID, respectively. Error bars represent the greater of the measurement precision or LOD. Mixing ratios below the LOD were set to $0.5 \times \text{LOD}$ in (a) and were excluded from the regression in (b).



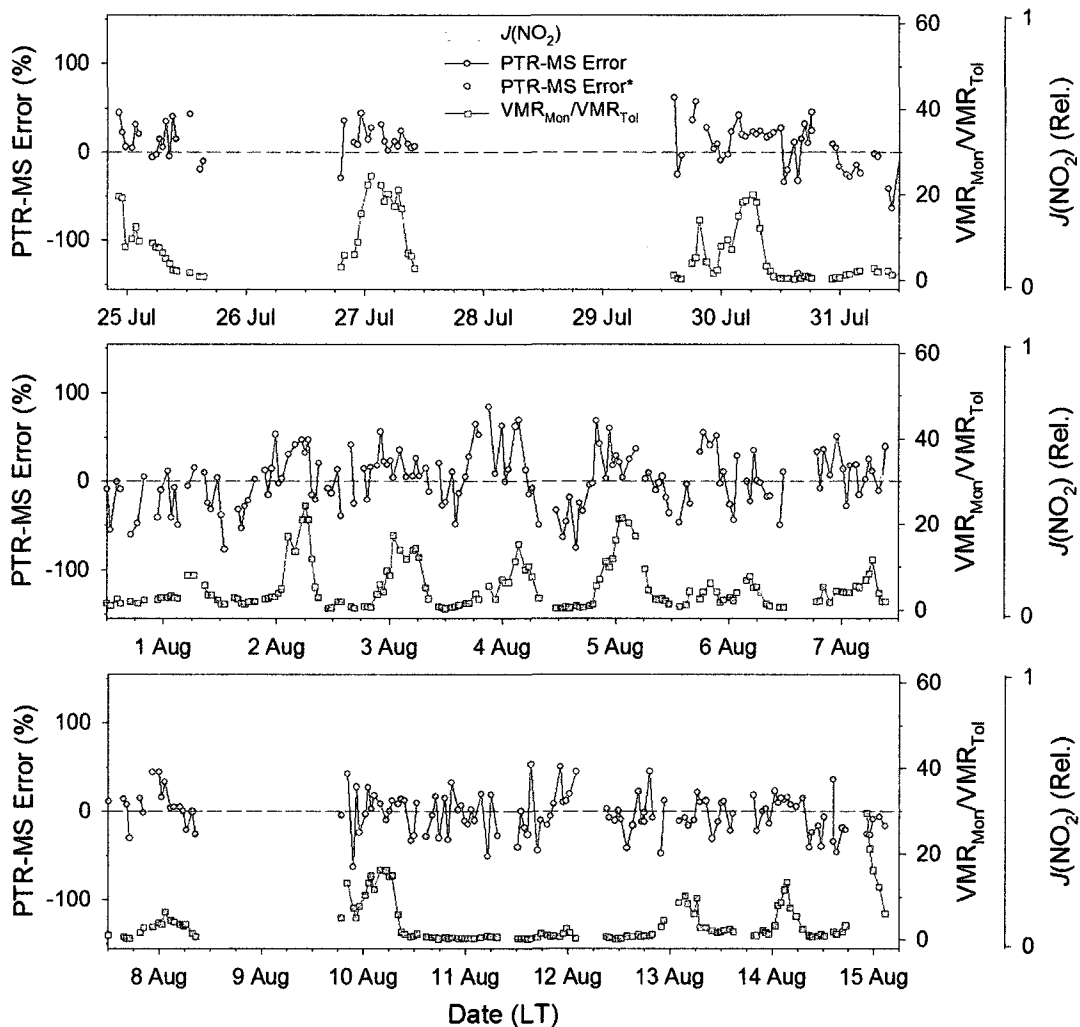
14. Time series of monoterpenes, $J(\text{NO}_2)$ and wind speed measured at THF from 22:00 on July 24 to 06:00 on August 15. Values of $J(\text{NO}_2)$ and wind speed are 10 min averages. The former are given as relative to the summertime maximum and illustrate daytime and nighttime periods. Mixing ratios below the LOD were set to $0.5 \times \text{LOD}$.



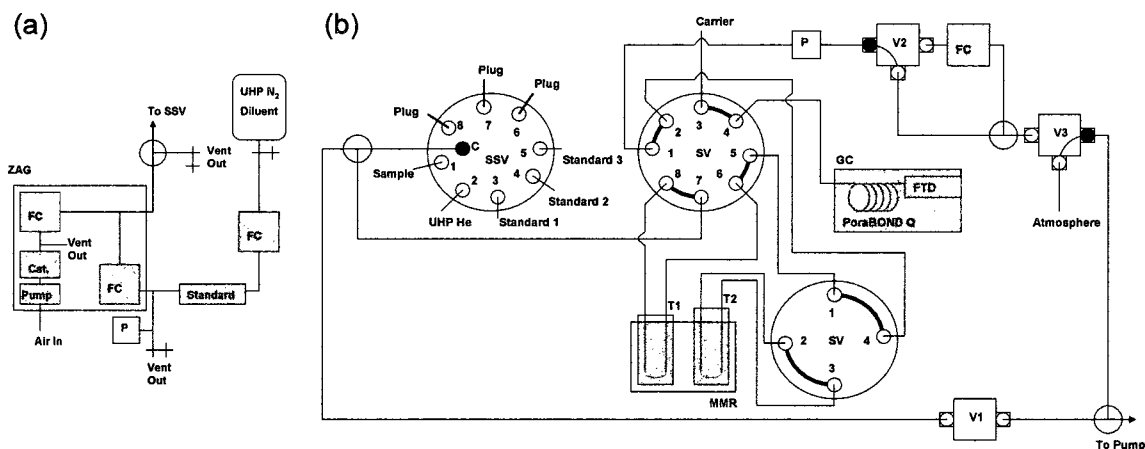
15. Time series of toluene measured by GC-FID and PTR-MS during the period between 22:00 on July 24 and 06:00 on August 15. Values of $J(\text{NO}_2)$ are show as in Figure 14. Errors in the GC-FID and PTR-MS data are the greater of the 1σ measurement precision or LOD.



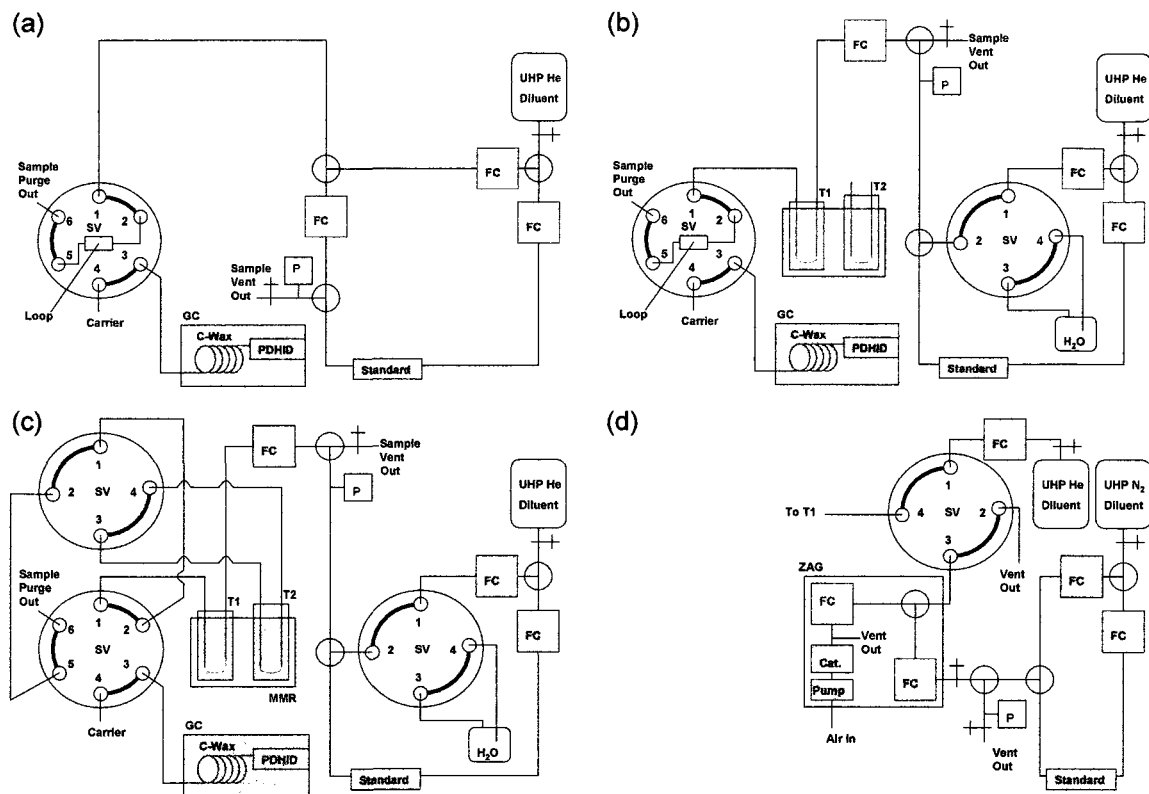
16. Linear correlation between toluene measurements by GC-FID and PTR-MS. The regression line and its confidence band were derived from a simple least squares analysis. The regression parameters are given in Table 7.



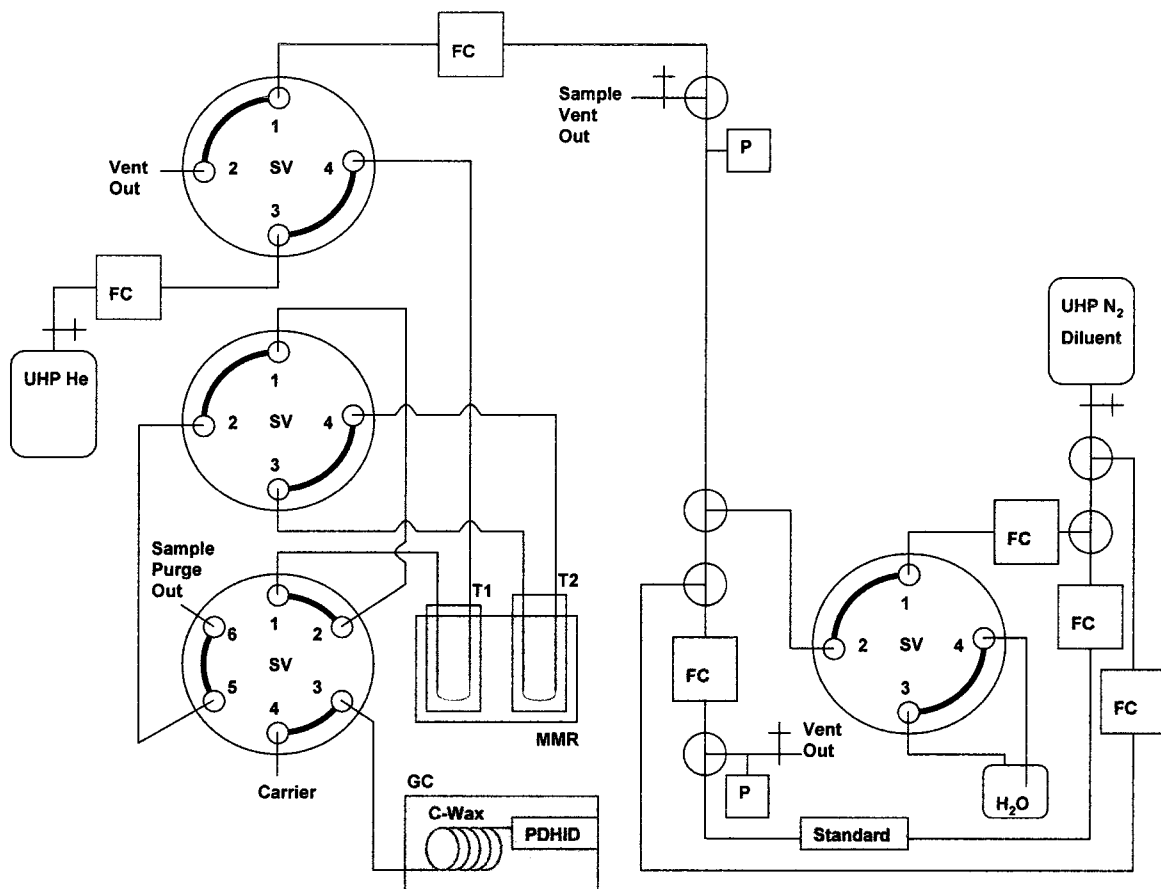
17. Comparison between values of $\epsilon_{\text{PTR-MS}}$ and Δ_{Mon} for merged GC-FID, PTR-MS data for the period from 22:00 on July 24 to 06:00 on August 15. Values of $J(\text{NO}_2)$ are show as in Figure 5. *Open symbols correspond with times when the toluene measurements did not agree quantitatively within the combined precisions of the two instruments. The dotted line represents perfect agreement.



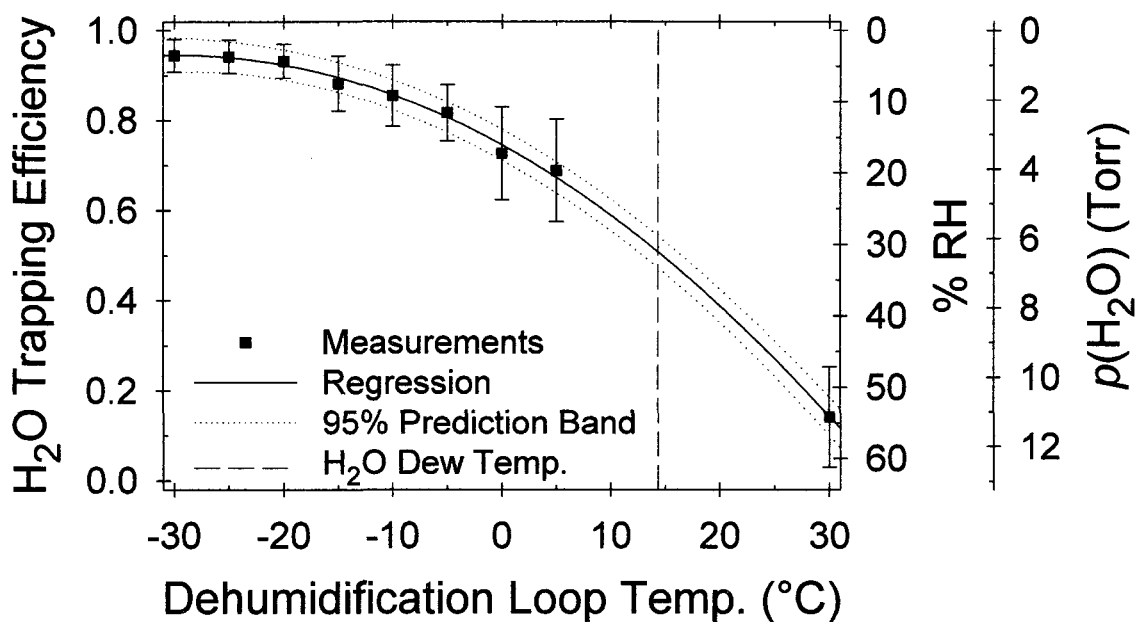
18. Schematic of the GC-FTD system. System segregated into (a) standard dilution, (b) sample capture and analysis components. Configuration in (b) shows 8-port SV in position A and 4-port SV in position B (for sample desorption). Components: SV, switching valve; SSV, stream select valve; V, solenoid valve; P, pressure gauge; FC, flow controller; T1, sample dehumidification chamber; T2, sample enrichment chamber; ZAG, zero air generator.



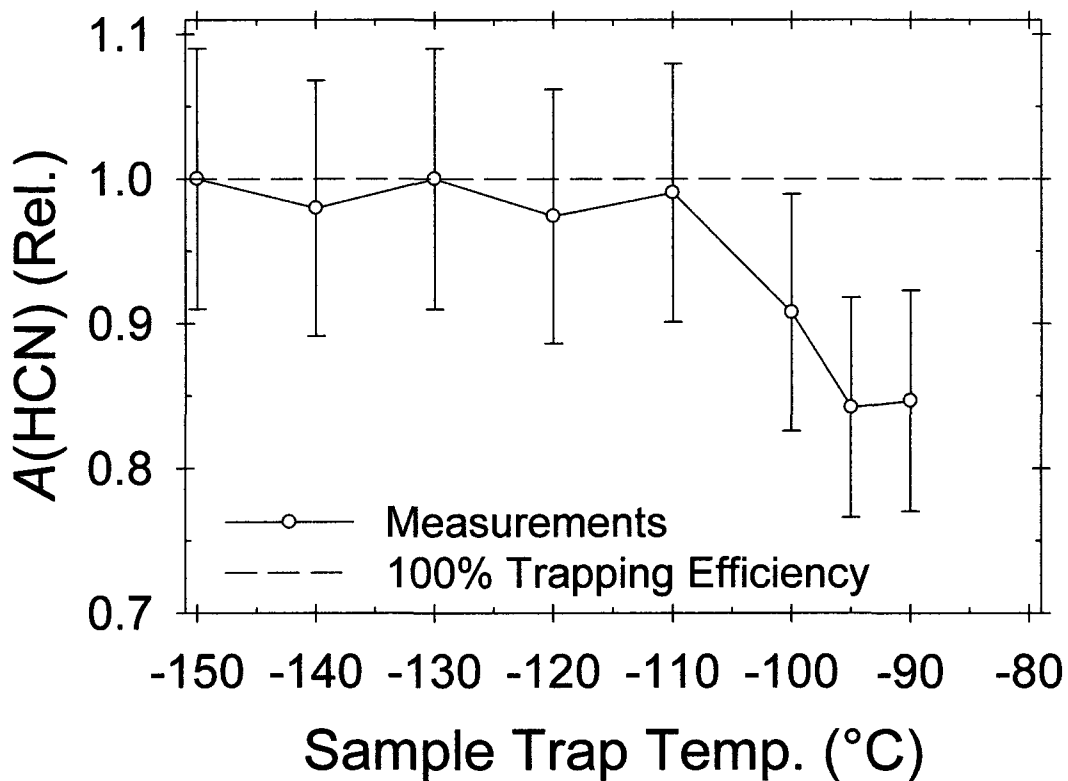
19. Schematic of the instrument configurations employed for development of HCN sampling and detection schemes. Configurations are shown for (a, b) direct loop injection, (c) sample concentration, and (d) preparing standards in N₂ and zero air. Components as in Figure 18, except: H₂O, water bubbler.



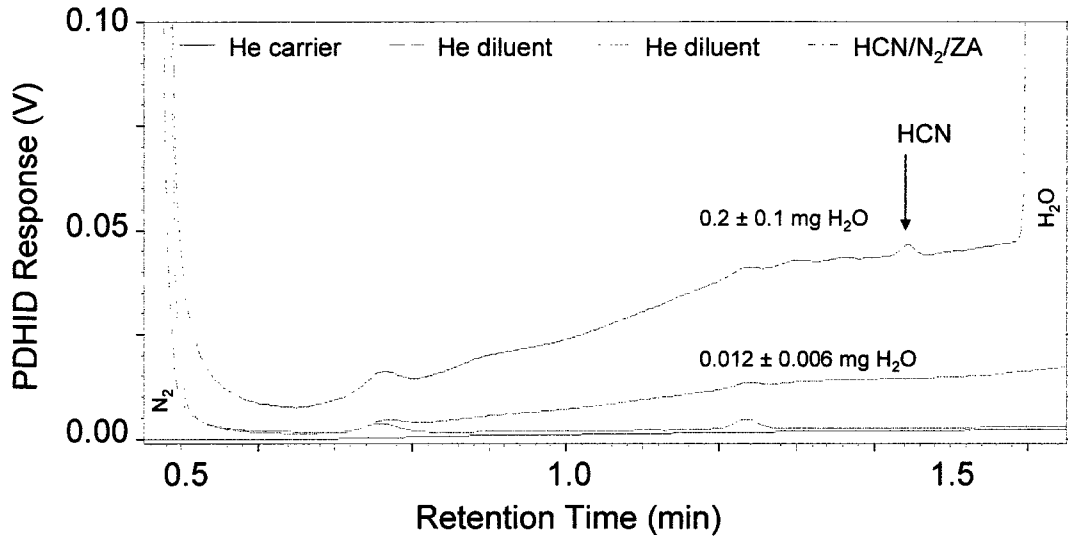
20. Schematic of the instrument configuration used for preliminary testing of both the PDHID and FTD. Components labeled as in Figures 18 and 19.



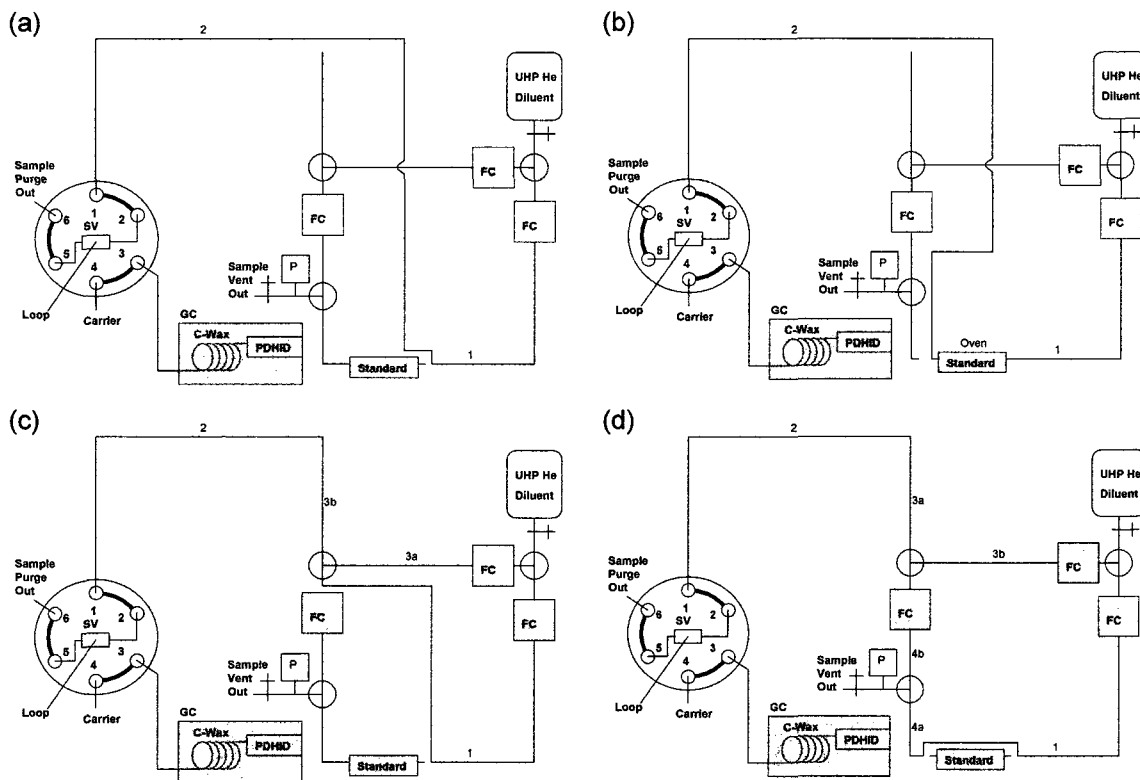
21. Water vapor trapping efficiency in the sample dehumidification loop as a function of T1 temperature. The error bars correspond with the trapping efficiency values and represent contributions from the measured and calculated humidity ($\pm 4\%$ and $\pm 7\%$, respectively). The regression line is a quadratic fit to the data, where $a = -2.2 \pm 0.1$, $b = -0.0134 \pm 0.0002$ and $c = 0.745 \pm 0.006$.



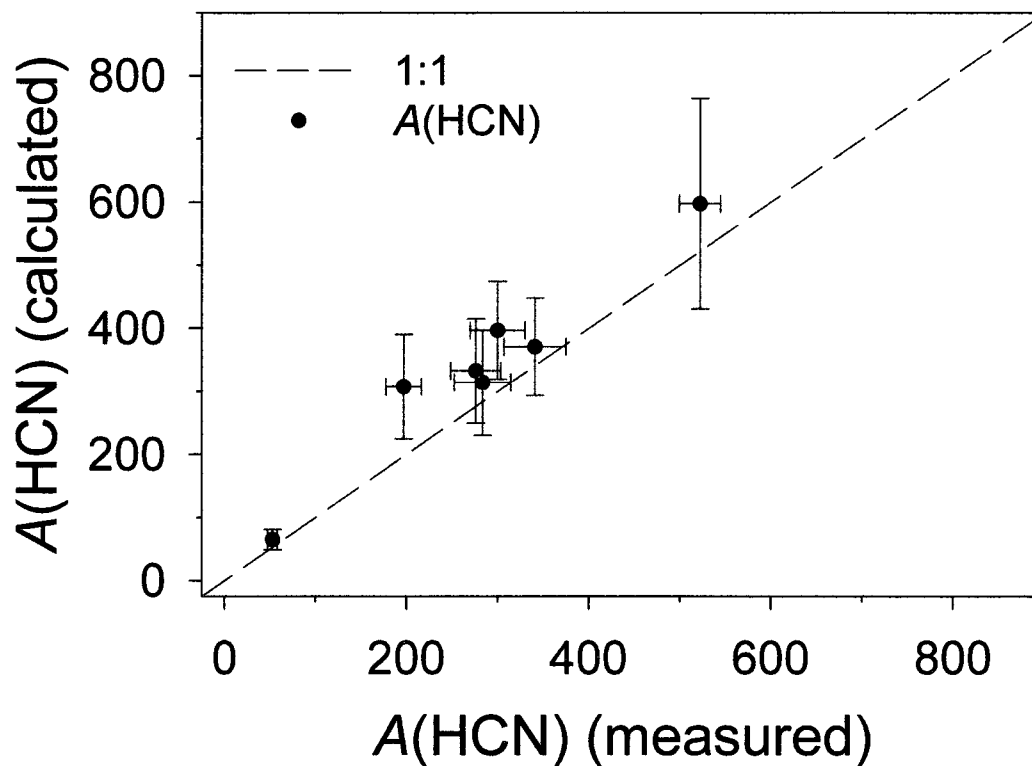
22. HCN trapping efficiency as a function of sample enrichment loop temperature. Temperature program: 30 °C for 0.6 min, 80 °C min⁻¹ to 80 °C, 30 °C min⁻¹ to 100 °C, 60 °C min⁻¹ to 200 °C for 4 min. The carrier flow rate at the initial column temperature was estimated at 17 ± 2 cm³ min⁻¹ from the N₂ RT and the volume of the system components between the sample enrichment loop and the GC column.



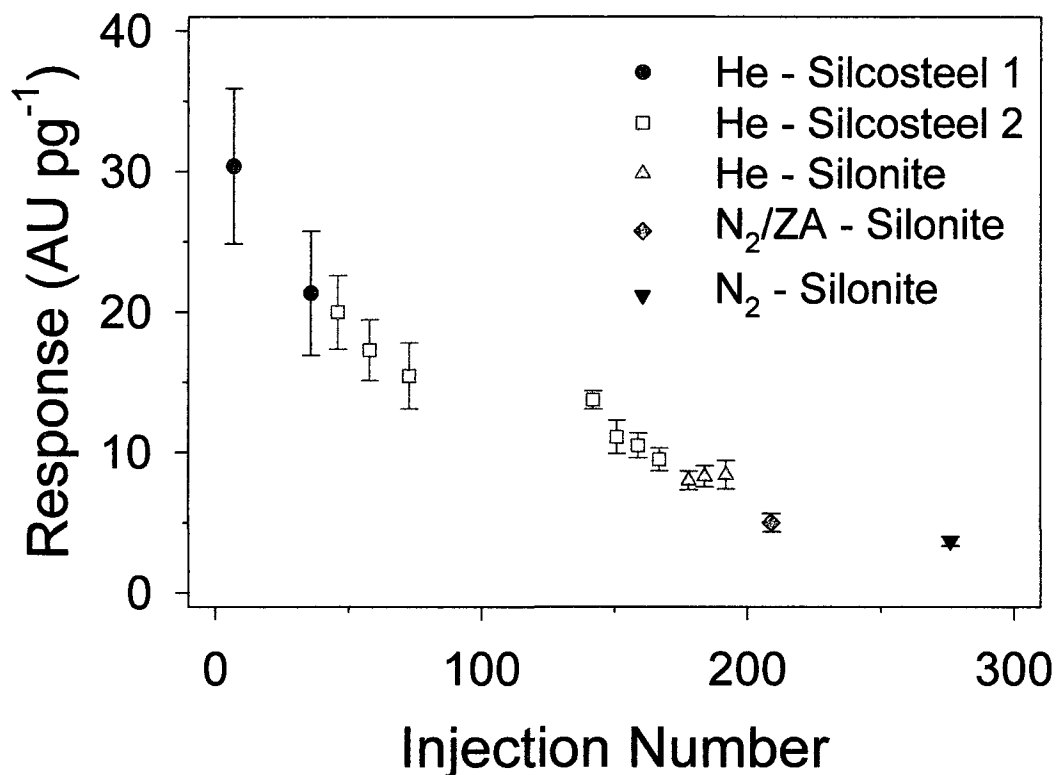
23. Chromatograms recorded with the PDHID for blank and standard samples prepared with the Cryofocus System. The instrument configurations were as in Figure 19c, d. The bottom trace shows the detector baseline response to the He carrier gas; the second and third traces were for 200 STP cm³ samples of UHP He; the uppermost trace was for a 200 STP cm³ standard sample of HCN (0.58 ± 0.04 ng) in UHP N₂/zero air. Peaks for HCN, N₂ and H₂O are labeled. The chromatograms were recorded on two separate days. Approximate H₂O masses in the preceding samples are shown for traces 3 and 4. The temperature program was the same as that give in Figure 22.



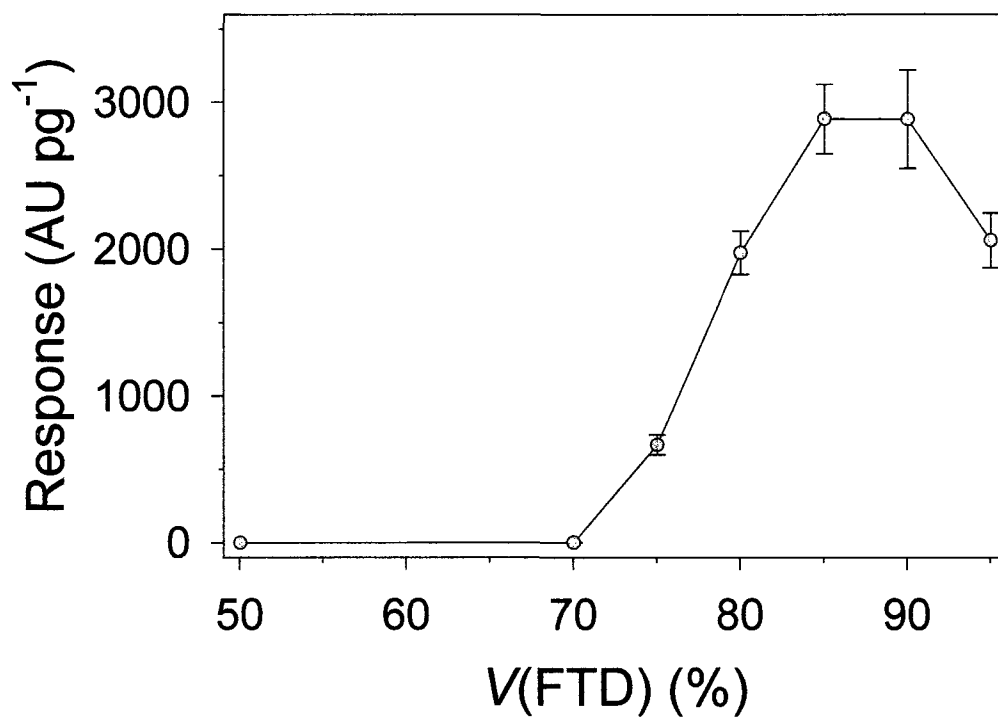
24. Configurations of standard dilution system used for blank response attribution. Isolated components include (a) oven FC outlet (line 1), standard dilution system outlet (line 2) and downstream components; (b) oven and components in (a); (c) outlet of secondary dilution FC (lines 3a and 3b) and components in (a); (d) oven outlet (lines 4a and 4b), downstream FC and components in (c).



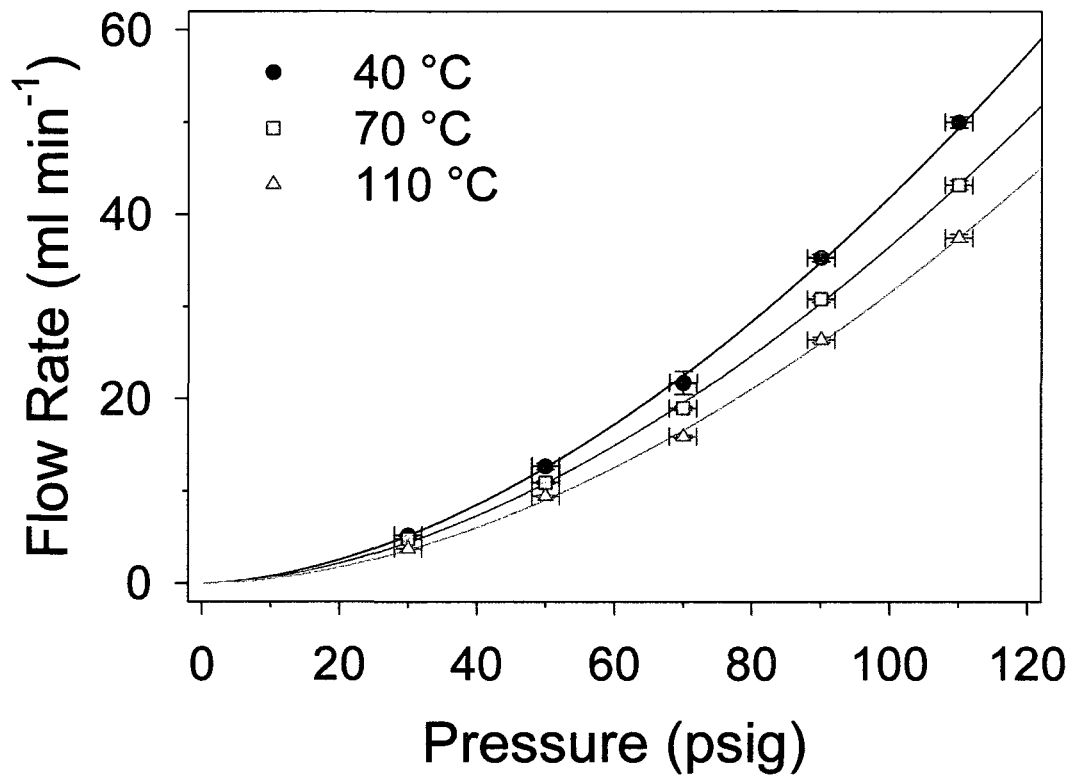
25. Comparison of measured blank HCN chromatographic peak areas with those calculated using an HCN desorption model. Error bars represent the measurement precision (5–10%) and uncertainties associated with estimated HCN surface emission rates and diluent flow rates through the standard dilution system.



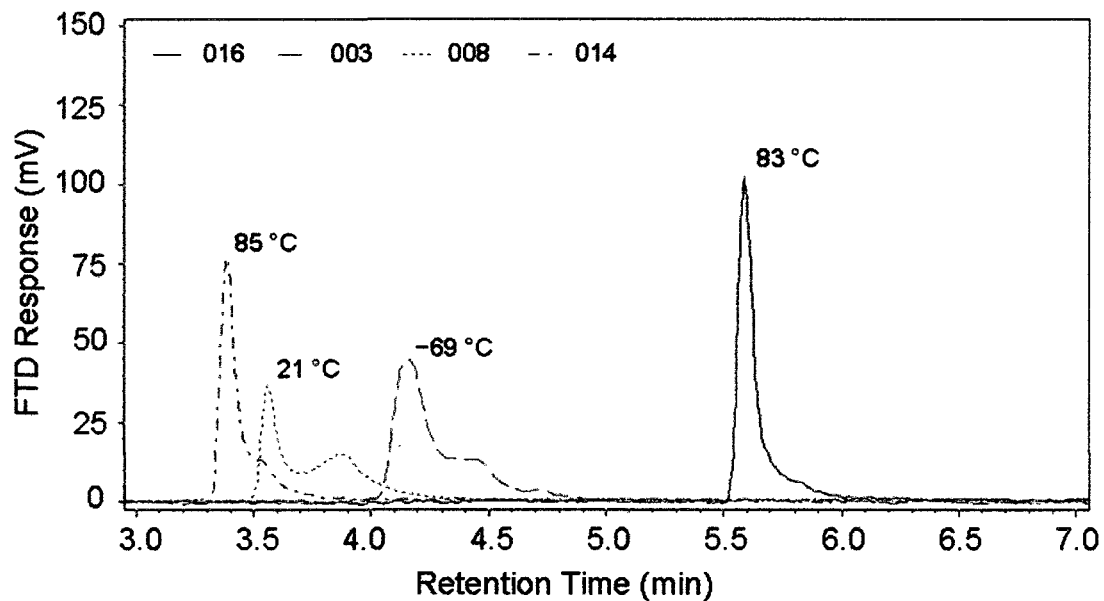
26. Observed variation in PDHID response as a function of sample injection number. Values represent daily average responses ($n = 2-10$) at the daily median injection number and were corrected for measured response to diluent blanks; errors, ranging from 5% to 20%, were determined from the measurement precision and uncertainties associated with quantifying the mass of HCN delivered. Data are labeled by diluent gas and sample loop, where ZA stands for zero air; Silcosteel 1 and Silcosteel 2 stand for 5 cm³ and 15 cm³ Silcosteel loops, respectively, at room temperature; Silonite stands for the glass bead-packed Silonite loop in the Cryofocus System.



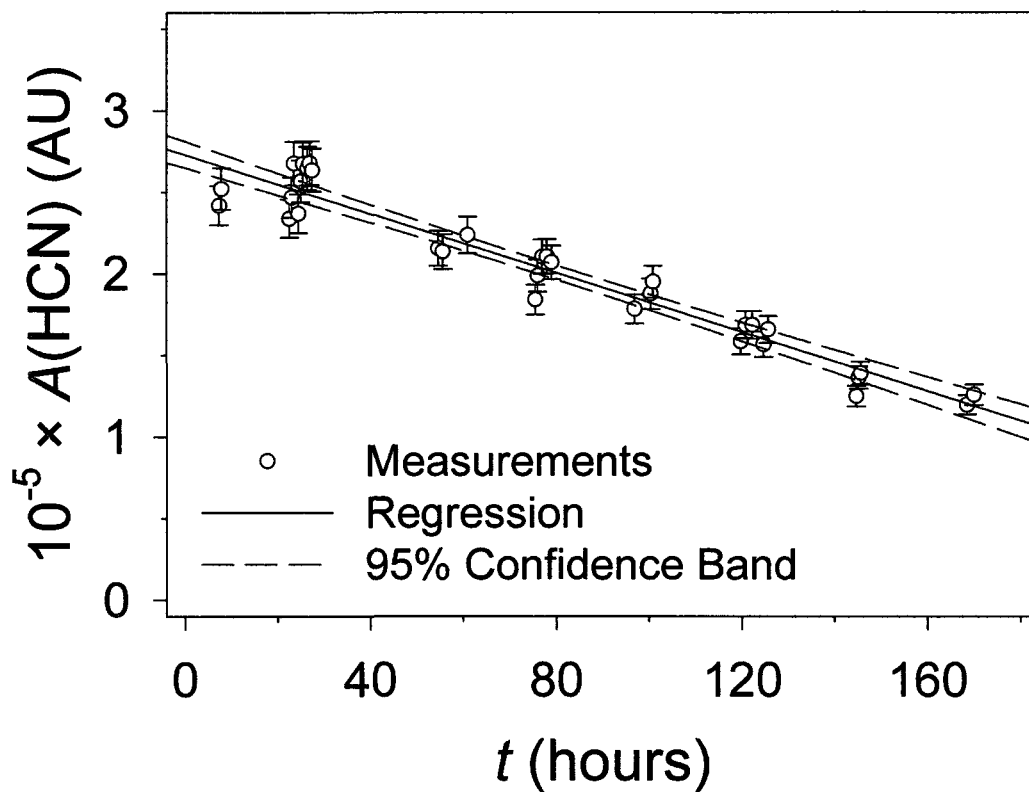
27. Response of the FTD to HCN as a function of bead voltage. Values at $V(\text{FTD}) = 50$, 75 and 95% are from single determinations, while the remaining values represent averages of replicate measurements ($n = 2-5$). Error bars represent contributions from the measurement precision and the sampled HCN mass.



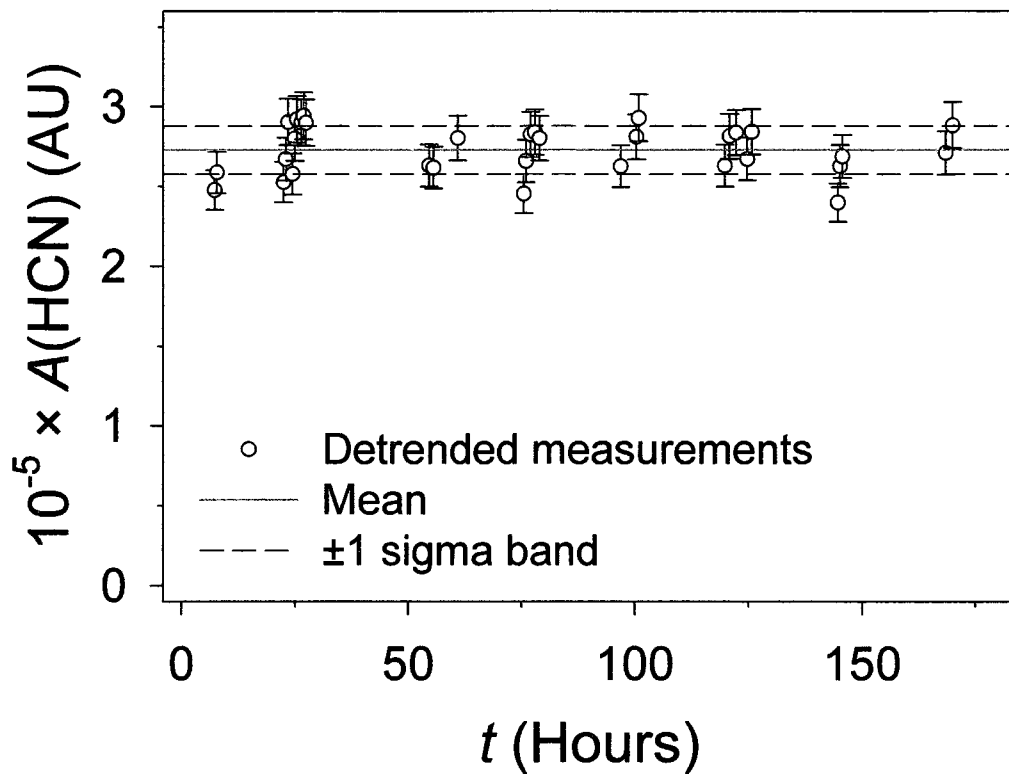
28. Carrier gas flow rate measurements. Data points are averages of 4–6 measurements. Errors are 2 psig and the standard deviation (<6%) of the average flow rate at each value of P and T . Lines fit to the data are two parameter power series functions, $y = a \cdot x^b$.



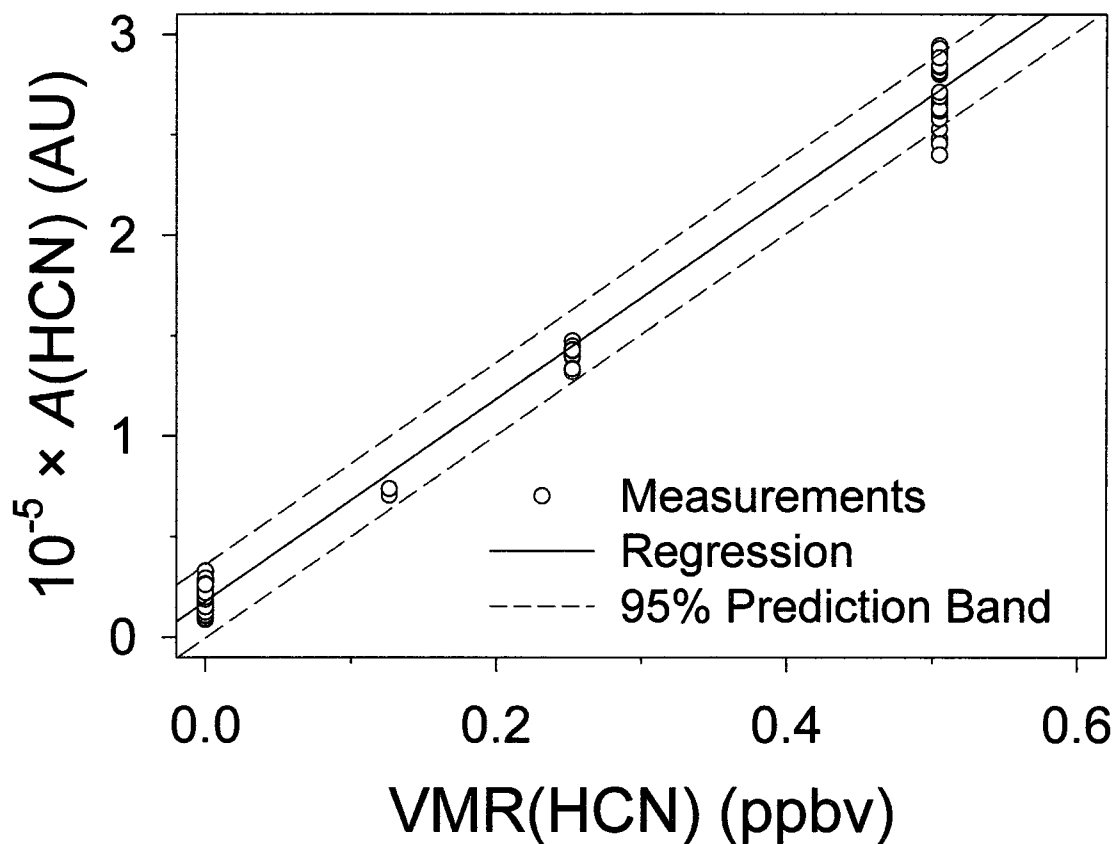
29. Comparison between standard chromatograms recorded over a range of injection temperatures. Peaks are labeled by injection temperature. For the sample injected at 83 °C (sample 016) the sample enrichment loop was isolated during desorption; the chromatogram is offset by 2 min for clarity. Temperature program: 40 °C for 7.5 min, 15 °C min⁻¹ to 150 °C, hold for 4 min.



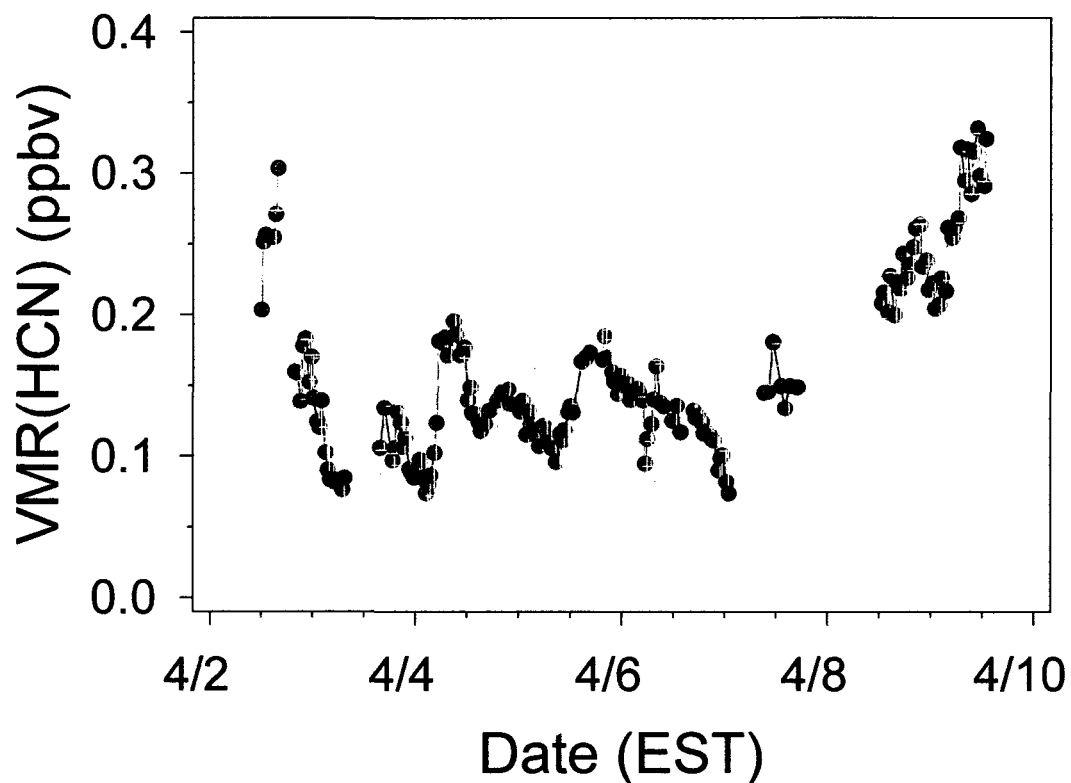
30. Chromatographic peak areas measured for standard samples analyzed during a period of continuous operation between April 2 and 9, 2009.

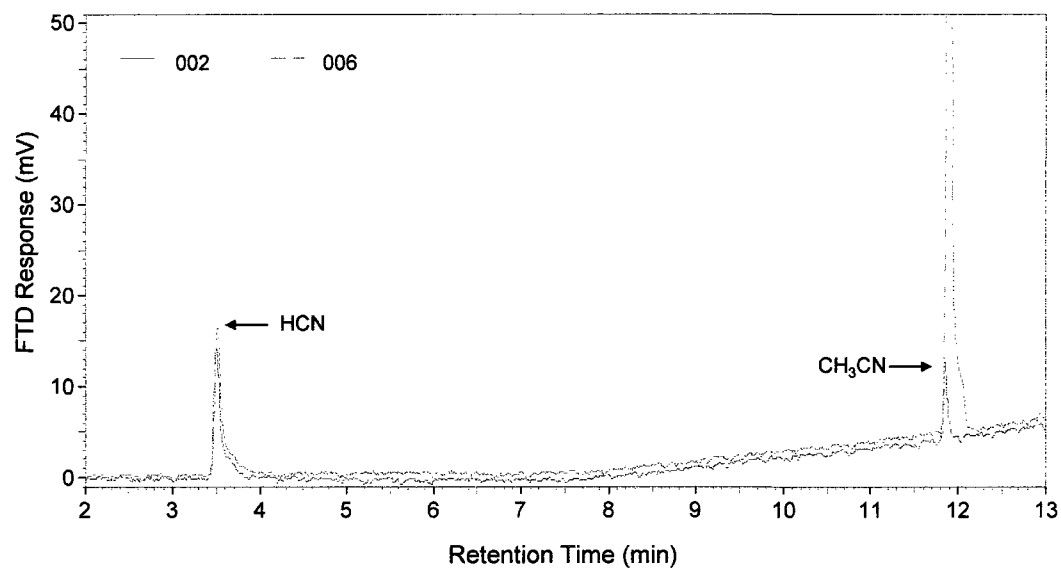


31. De-trended measurements from Figure 30.



32. Calibration curve constructed from de-trended standard and blank measurements made between April 2 and 9, 2009.





34. Qualitative identification of CH₃CN in ambient air. Chromatograms recorded for ambient air samples before (002) and after (006) introducing a small volume of diluted pure CH₃CN liquid headspace vapor into the ambient air inlet stream of the instrument shown in Figure 18.

LIST OF REFERENCES

- Aikman, K., D. Bergman, J. Ebinger, and D. Seigler (1996), Variation of cyanogenesis in some plant species of the Midwestern United States, *Biochem. Syst. Ecol.*, *24*, 637–645.
- Aldener, M., et al. (2006), Reactivity and loss mechanisms of NO₃ and N₂O₅ in a polluted marine environment: Results from in situ measurements during New England Air Quality Study 2002, *J. Geophys. Res.*, *111*, D23S73, doi:10.1029/2006JD007252.
- Alicke, B., U. Platt and J. Stutz (2002), Impact of nitrous acid photolysis on the total hydroxyl radical budget during the Limitation of Oxidant Production/Pianura Padana Produzione di Ozono study in Milan, *J. Geophys. Res.*, *107*, doi:10.1029/2000JD000075.
- Allan, B. J., N. Carslaw, H. Coe, R. A. Burgess, and J. M. C. Plane (1999), Observations of the nitrate radical in the marine boundary layer, *J. Atmos. Chem.*, *33*, 129–154.
- Allan, B. J., G. McFiggans, J. M. C. Plane, H. Coe, and G. G. McFadyen (2000), The nitrate radical in the remote marine boundary layer, *J. Geophys. Res.*, *105*, 24,191–24,204.
- Ambrose, J. L., H. Mao, H. R. Mayne, J. Stutz, R. Talbot, and B. C. Sive (2007), Nighttime nitrate radical chemistry at Appledore Island, Maine during the 2004 International Consortium for Atmospheric Research on Transport and Transformation, *J. Geophys. Res.*, *112*, D21302, doi:10.1029/2007JD008756.
- Andreae, M. O., and P. Merlet (2001), Emission of trace gases and aerosols from biomass burning, *Global Biogeochem. Cy.*, *15*, 955–966.
- Apel, E. C., J. G. Calvert, J. P. Greenberg, D. Riemer, R. Zika, T. E. Kleindienst, W. A. Lonneman, K. Fung, and E. Fujita (1998), Generation and validation of oxygenated volatile organic carbon standards for the 1995 Southern Oxidants Study Nashville Intensive, *J. Geophys. Res.*, *103*, 22,281–22,944.
- Apel, E. C., J. G. Calvert, T. M. Gilpin, F. Fehsenfeld, and W. A. Lonneman (2003b), Nonmethane hydrocarbon intercomparison experiment (NOMHICE): Task 4, ambient air, *J. Geophys. Res.*, *108*(D9), 4300, doi:10.1029/2002JD002936.
- Apel, E. C., A. J. Hills, R. Leub, S. Zindel, S. Eisele, and D. D. Riemer (2003a), A fast-GC/MS system to measure C₂ to C₄ carbonyls and methanol aboard aircraft, *J. Geophys. Res.*, *108*(D20), 8794, doi:10.1029/2002JD003199.
- Atkinson, R. (1989), Kinetics and mechanisms of the gas-phase reactions of the hydroxyl radical with organic compounds, *J. Phys. Chem. Ref. Data Monogr.*, *1*, 1–246.
- Atkinson, R. (1991), Kinetics and mechanisms of the gas-phase reactions of the NO₃ radical with organic compounds, *J. Phys. Chem. Ref. Data*, *20*, 459–507.

- Atkinson, R. (1994), Gas-phase tropospheric chemistry of organic compounds, *J. Phys. Chem. Ref. Data Monogr.*, 2, 1–216.
- Atkinson, R. (1997), Gas-phase tropospheric chemistry of volatile organic compounds: 1. alkanes and alkenes, *J. Phys. Chem. Ref. Data*, 26, 215–290.
- Atkinson, R. (2000), Atmospheric chemistry of VOCs and NO_x, *Atmos. Environ.*, 34, 2063–2101.
- Atkinson, R., and J. Arey (2003), Gas-phase tropospheric chemistry of biogenic volatile organic compounds: a review, *Atmos. Environ.*, 37(S2), S197–S219.
- Atkinson, R., D. L. Baulch, R. A. Cox, R. F. Hampson, J. A. Kerr, M. J. Rossi, and J. Troe (1997), Evaluated kinetic, photochemical, and heterogeneous data for atmospheric chemistry: Supplement V, *J. Phys. Chem. Ref. Data*, 26, 521–1011.
- Atkinson, R., D. L. Baulch, R. A. Cox, R. F. Hampson, J. A. Kerr, M. J. Rossi, and J. Troe (1999), Evaluated kinetic and photochemical data for atmospheric chemistry, organic species: Supplement VII, *J. Phys. Chem. Ref. Data*, 28, 191–393.
- Atkinson, R., D. L. Baulch, R. A. Cox, J. N. Crowley, R. F. Hampson, R. G. Hynes, M. E. Jenkin, M. J. Rossi, and J. Troe (2004), Evaluated kinetic and photochemical data for atmospheric chemistry: Vol. I – gas phase reactions of O_x, HO_x, NO_x, and SO_x species, *Atmos. Chem. Phys.*, 4, 1461–1738.
- Atkinson, R., D. L. Baulch, R. A. Cox, J. N. Crowley, R. F. Hampson, R. G. Hynes, M. E. Jenkin, M. J. Rossi, and J. Troe (2006), Evaluated kinetic and photochemical data for atmospheric chemistry: Volume II – gas phase reactions of organic species, *Atmos. Chem. Phys.*, 6, 3625–4055.
- Atkinson et al. (2009), Evaluated Kinetic Data, IUPAC Subcommittee for Gas Kinetic Data Evaluation, <http://www.iupac-kinetic.ch.cam.ac.uk>, Cambridge University, UK.
- Barry, E. F. (2004), Columns: packed and capillary; column selection in gas chromatography, in *Modern Practice of Gas Chromatography*, edited by R. L. Grob and E. F. Barry, pp. 65–191, John Wiley and Sons, Inc., Hoboken, New Jersey.
- Bartram, R. J. (2004), Gas management systems for gas chromatography, in *Modern Practice of Gas Chromatography*, edited by R. L. Grob and E. F. Barry, pp. 491–543, John Wiley and Sons, Inc., Hoboken, New Jersey.

- Baum, M., J. A. Moss, S. H. Pastel, and G. A. Poskrebyshv (2007), Hydrogen cyanide exhaust emissions from in-use motor vehicles, *Environ. Sci. Technol.*, *41*, 857–862.
- Becidan, M., Ø. Skreiberg, and J. E. Hustad (2007), NO_x and N₂O precursors (NH₃ and HCN) in pyrolysis of biomass residues, *Energy and Fuels*, *21*, 1173–1180.
- Blake, R. S., P. S. Monks, and A. M. Ellis (2009), Proton-Transfer Reaction Mass Spectrometry, *Chem. Rev.*, *109*, 861–896.
- Brasseur, G., and D. Schimel (1999), Atmospheric chemistry and the Earth system, in *Atmospheric Chemistry and Global Change*, edited by G. P. Brasseur et al., pp. 1–18, Oxford Univ. Press, New York.
- Brasseur, G., et al. (1999), Trace gas exchanges and biogeochemical cycles, in *Atmospheric Chemistry and Global Change*, edited by G. P. Brasseur et al., pp. 159–203, Oxford Univ. Press, New York.
- Brown, S. S., H. Stark, T. B. Ryerson, E. J. Williams, D. K. Nicks Jr., M. Trainer, F. C. Fehsenfeld, and A. R. Ravishankara (2003a), Nitrogen oxides in the nocturnal boundary layer: Simultaneous in situ measurements of NO₃, N₂O₅, NO₂, NO, and O₃, *J. Geophys Res.*, *108*(D9), 4299, doi:10.1029/2002JD002917.
- Brown, S. S., H. Stark, and A. R. Ravishankara (2003b), Applicability of the steady state approximation to the interpretation of atmospheric observations of NO₃ and N₂O₅, *J. Geophys. Res.*, *108*(D17), 4539, doi:10.1029/2003JD003407.
- Brown, S. S., et al. (2004), Nighttime removal of NO_x in the summer marine boundary layer, *Geophys. Res. Lett.*, *31*, L07108, doi:10.1029/2004GL019412.
- Brown, S. S., et al. (2006a), Variability in nocturnal nitrogen oxide processing and its role in regional air quality, *Science*, *311*, 67–70.
- Brown, S. S., et al. (2006b), Nocturnal odd-oxygen budget and its implications for ozone loss in the lower troposphere, *Geophys Res. Lett.*, *33*, L08801, doi:10.1029/2006GL025900.
- Canosa-Mas, C. E., E. S. N. Cotter, J. Duffy, K. C. Thompson, and R. P. Wayne (2001), The reactions of atomic chlorine with acrolein, methacrolein and methyl vinyl ketone, *Phys. Chem. Chem. Phys.*, *3*, 3075–3084.
- Chen, M., R. Talbot, H. Mao, B. Sive, J. Chen, and R. J. Griffin (2007), Air mass classification in coastal New England and its relationship to meteorological conditions, *J. Geophys. Res.*, *112*, D10S05, doi:10.1029/2006JD007687.

- Christian, T. J., B. Kleiss, R. J. Yokelson, R. Holzinger, P. J. Crutzen, W. M. Hao, T. Shirai, and D. R. Blake (2004), Comprehensive laboratory measurements of biomass-burning emissions: 2. First intercomparison of open-path FTIR, PTR-MS, and GC-MS/FID/ECD, *J. Geophys. Res.*, *109*, D02311, doi:10.1029/2003JD003874.
- Cicerone, R. J., and R. Zellner (1983), The atmospheric chemistry of hydrogen cyanide (HCN), *J. Geophys. Res.*, *88*(C15), 10,689–10,696.
- Colón, L. A., and L. J. Baird (2004), Detectors in Modern Gas Chromatography, in *Modern Practice of Gas Chromatography*, edited by R. L. Grob and E. F. Barry, pp. 277–337, John Wiley and Sons, Inc., Hoboken, New Jersey.
- Crouse, J. D., K. A. McKinney, A. J. Kwan, and P. O. Wennberg (2006), Measurement of gas-phase hydroperoxides by chemical ionization mass spectrometry, *Anal. Chem.*, *78*, 6726–6732.
- Custer, T. G., S. Kato, R. Fall, and V. M. Bierbaum (2000), Negative ion mass spectrometry and the detection of carbonyls and HCN from clover, *Geophys. Res. Lett.*, *27*(23), 3849–3852.
- Dagaut, P., P. Glarborg, and M. U. Alzueta (2008), The oxidation of hydrogen cyanide and related chemistry, *Prog. Energy Combust. Sci.*, *34*, 1–46.
- Dalton, I., D. L. Albritton, W. Lindinger, and M. Pahl (1976), Mobilities of CO_2^+ , N_2H^+ , H_3O^+ , $\text{H}_3\text{O}^+\text{H}_2\text{O}$, and $\text{H}_3\text{O}^+(\text{H}_2\text{O})_2$ ions in N_2 , *J. Chem. Phys.*, *65*, 5028–5030.
- de Gouw, J., and C. Warneke (2007), Measurements of volatile organic compounds in the Earth's atmosphere using proton-transfer-reaction mass spectrometry, *Mass. Spectrom. Rev.*, *26*, 223–257.
- de Gouw, J. A., P. D. Goldan, C. Warneke, W. C. Kuster, J. M. Roberts, M. Marchewka, S. B. Bertman, A. A. P. Pszenny, and W. C. Keene (2003a), Validation of proton transfer reaction-mass spectrometry (PTR-MS) measurements of gas-phase organic compounds in the atmosphere during the New England Air Quality Study (NEAQS) in 2002, *J. Geophys. Res.*, *108*(D21), 4682, doi:10.1029/2003JD003863.
- de Gouw, J., C. Warneke, T. Karl, G. Eerdekens, C. van der Veen, and R. Fall (2003b), Sensitivity and specificity of atmospheric trace gas detection by proton-transfer-reaction mass spectrometry, *Int. J. Mass Spectrom.*, *223–224*, 365–382.
- de Gouw, J. A., et al. (2006), Volatile organic compounds composition of merged and aged forest fire plumes from Alaska and western Canada, *J. Geophys. Res.*, *111*, D10303, doi:10.1029/2005JD006175.

- Ehhalt, D. H., and F. Rohrer (2000), Dependence of the OH concentration on solar UV, *J. Geophys. Res.*, *105*, 3565–3571.
- Fehsenfeld, F. C., et al. (2006), International Consortium for Atmospheric Research on Transport and Transformation (ICARTT): North America to Europe – Overview of the 2004 summer field study, *J. Geophys. Res.*, *111*, D23S01, doi:10.1029/2006JD007829.
- Fischer, E., A. Pszenny, W. Keene, J. Maben, A. Smith, A. Stohl, and R. Talbot (2006), Nitric acid phase partitioning and cycling in the New England coastal atmosphere, *J. Geophys. Res.*, *111*, D23S09, doi:10.1029/2006JD007328.
- Folkers, M., T. F. Mentel, A. Wahner (2003), Influence of an organic coating on the reactivity of aqueous aerosols probed by the heterogeneous hydrolysis of N₂O₅, *Geophys. Res. Lett.*, *30*, doi:10.1029/2003GL017168.
- Forsyth, D. S. (2004), Pulsed discharge detector: theory and applications, *J. Chromatogr. A*, *1050*, 63–68.
- Geron, C., R. Rasmussen, R. R. Arnts, and A. Guenther (2000), A review and synthesis of monoterpene speciation from forests in the United States, *Atmos. Environ.*, *34*, 1761–1781.
- Geyer, A., B. Alicke, S. Konrad, R. Shmitz, J. Stutz, and U. Platt (2001), Chemistry and oxidation capacity of the nitrate radical in the continental boundary layer near Berlin, *J. Geophys. Res.*, *106*, 8013–8025.
- Geyer, A., and U. Platt (2002), Temperature dependence of the NO₃ loss frequency: A new indicator for the contribution of NO₃ to the oxidation of monoterpenes and NO_x removal in the atmosphere, *J. Geophys. Res.*, *107*(D20), 4431, doi:10.1029/2002JD002436.
- Glarborg, P., A. D. Jensen, and J. E. Johnsson (2003), Fuel nitrogen conversion in solid fuel fired systems, *Prog. Energy Combust. Sci.*, *29*, 89–113.
- Goldstein, A., and I. Galbally (2007), Known and unexplored organic constituents in the Earth's atmosphere, *Environ. Sci. Technol.*, *40*, 1514–1521.
- Goode, J. G., R. J. Yokelson, D. E. Ward, R. A. Susott, R. E. Babbitt, M. A. Davies, and W. M. Hao (2000), Measurements of excess O₃, CO₂, CO, CH₄, C₂H₄, C₂H₂, HCN, NO, NH₃, HCOOH, CH₃OOH, HCHO, and CH₃OH in 1997 Alaskan biomass burning plumes by airborne Fourier transform infrared spectroscopy (AFTIR), *J. Geophys. Res.*, *105*, 22,147–22,166.

- Guenther, A. B., P. R. Zimmerman, P. C. Harley, R. K. Monson, and R. Fall (1993), Isoprene and monoterpene emission rate variability: model evaluations and sensitivity analyses, *J. Geophys. Res.*, *98*, D7, 12,609–12,617.
- Hakola, H., J. Arey, S. M. Aschmann, and R. Atkinson (1994), Product formation from the gas-phase reactions of OH radicals and O₃ with a series of monoterpenes, *J. Atmos. Chem.*, *18*, 75–102.
- Hallquist, M., D. J. Stewart, J. Baker, and R. A. Cox (2000), Hydrolysis of N₂O₅ on submicron sulfuric acid aerosols, *J. Phys. Chem. A*, *104*, 3984–3990.
- Hallquist, M., D. J. Stewart, S. K. Stephenson, R. A. Cox (2003), Hydrolysis of N₂O₅ on sub-micron sulfate aerosols, *Phys. Chem. Chem. Phys.*, *5*, 3453–3463.
- Hansel, A., A. Jordan, R. Holzinger, P. Prazeller, W. Vogel, and W. Lindinger (1995), Proton transfer reaction mass spectrometry: on-line trace gas analysis at the ppb level, *Int. J. Mass. Spectrom. Ion Proc.*, *149/150*, 609–619.
- Hatakeyama, S., K. Izumi, T. Fukuyama, H. Akimoto, and N. Washida (1991), Reactions of OH with alpha-pinene and beta-pinene in air – estimate of global CO production from the atmospheric oxidation of terpenes, *J. Geophys. Res.*, *96*(D1), 947–958.
- Hayward, S., C. N. Hewitt, J. H. Sartin, and S. M. Owen (2002), Performance characteristics and applications of a proton transfer reaction-mass spectrometer for measuring volatile organic compounds in ambient air, *Environ. Sci. Technol.*, *36*, 1554–1560.
- Heald, C. L., et al. (2009), Total observed organic carbon (TOOC) in the atmosphere: a synthesis of North American observations, *Atmos. Chem. Phys.*, *8*, 2007–2025.
- Heiden, A. C., K. Kobel, M. Komenda, R. Koppmann, M. Shao, and J. Wildt (1999), Toluene emissions from plants, *Geophys. Res. Lett.*, *26*, 1283–1286.
- Heintz, F., U. Platt, J. Flentje, and R. Dubois (1996), Long-term observation of nitrate radicals at the Tor Station, Kap Arkona (Rügen), *J. Geophys. Res.*, *101*(D17), 22,891–22,910.
- Helmig, D., L. F. Klinger, A. Guenther, L. Vierling, C. Geron, and P. Zimmerman (1998), Biogenic volatile organic compound emissions (BVOCs) I. Identifications from three continental sites in the U.S., *Chemosphere*, *38*, 2163–2187.
- Holzinger, R., C. Warneke, A. Hansel, A. Jordan, and W. Lindinger (1999), Biomass burning as a source of formaldehyde, acetaldehyde, methanol, acetone, acetonitrile, and hydrogen cyanide, *Geophys. Res. Lett.*, *26*, 1161–1164.

- Holzinger, R., L. Sandoval-Soto, S. Rottenberger, P. J. Crutzen, and J. Kesselmeier (2000), Emissions of volatile organic compounds from *Quercus ilex* L. measured by Proton Transfer Reaction Mass Spectrometry under different environmental conditions, *J. Geophys. Res.*, *105*, 20,573–20,579.
- Hurley, M. D., O. Sokolov, T. J. Wallington, H. Takekawa, M. Karasawa, B. Koltz, I. Barnes, and K. H. Becker (2001), Organic aerosol formation during the atmospheric degradation of toluene, *Environ. Sci. Technol.*, *35*, 1358–1366.
- Hurst, D. F., D. W. T. Griffith, J. N. Carras, D. J. Williams, and P. J. Fraser (1994), Measurements of trace gases emitted by Australian savanna fires during the 1990 dry season, *J. Atmos. Chem.*, *18*, 33–65.
- IPCC (2007), *Climate Change 2007: The Physical Science Basis. Contribution of Working Group I to the Fourth Assessment Report of the Intergovernmental Panel on Climate Change*, Cambridge Univ. Press, New York.
- Jenkin, M. E., S. M. Saunders, V. Wagner, and M. J. Pilling (2003), Protocol for the development of the Master Chemical Mechanism, MCM v3 (Part B): tropospheric degradation of aromatic volatile organic compounds, *Atmos. Chem. Phys.*, *3*, 181–193.
- Johnson, W. R., and J. C. Kang (1971), Mechanisms of hydrogen cyanide formation from the pyrolysis of amino acids and related compounds, *J. Org. Chem.*, *36*, 189–192.
- Justice, D., A. K. Deely, and F. Rubin (2002), New Hampshire Land Cover Assessment: Final Report, report, 42 pp., Complex Systems Research Center, University of New Hampshire, Durham, NH.
- Karl, T., E. Apel, A. Hodzic, D. D. Riemer, D. R. Blake, and C. Wiedinmyer (2009), Emissions of volatile organic compounds inferred from airborne flux measurements over a megacity, *Atmos. Chem. Phys.*, *9*, 271–285.
- Karlsson, H. L. (2004), Ammonia, nitrous oxide and hydrogen cyanide emissions from five passenger vehicles, *Sci. Total Environ.*, *334–335*, 125–132.
- Kato, S., Y. Miyakawa, T. Kaneko, and Y. Kajii (2004), Urban air measurements using PTR-MS in Tokyo area and comparison with GC-FID measurements, *Int. J. Mass Spectrom.*, *235*, 103–110.
- Keene, W. C., et al. (2007), Inorganic chlorine and bromine in coastal New England air during summer, *J. Geophys. Res.*, *112*, D10512, doi:10.1029/2006JD007689.
- Kleinböhl, A., G. C. Toon, B. Sen, J.-F. L. Blavier, D. K. Weisenstein, R. S. Strekowski, J. M. Nicovich, P. H. Wine, and P. O. Wennberg (2006), On the stratospheric

chemistry of hydrogen cyanide, *Geophys. Res. Lett.*, *33*, L11806, doi:10.1029/2006GL026015.

- Knighton, W. B., E. C. Fortner, A. J. Midey, A. A. Viggiano, S. C. Herndon, E. C. Wood, and C. E. Kolb (2009), HCN detection with a proton transfer reaction mass spectrometer, *Int. J. Mass. Spectrom.*, *283*, 112–121.
- Kuster, W. C., B. T. Jobson, T. Karl, D. Riemer, E. Apel, P. D. Goldan, and F. C. Fehsenfeld (2004), Intercomparison of volatile organic carbon measurement techniques and data at La Porte during TexAQS2000 Air Quality Study, *Environ. Sci. Technol.*, *38*, 221–228.
- Lavagnini, I., and F. Magno (2006), A statistical overview on univariate calibration, inverse regression, and detection limits: application to gas chromatography/mass spectrometry technique, *Mass Spectrom. Rev.*, *26*, 1–18.
- Lee, A., A. H. Goldstein, M. D. Keywood, S. Gao, V. Varutbangkul, R. Bahreini, N. L. Ng., R. C. Flagan, and J. H. Seinfeld (2006a), Gas-phase products and secondary aerosol yields from the ozonolysis of ten different terpenes, *J. Geophys. Res.*, *111*, D07302, doi:10.1029/2005JD006437.
- Lee, A., A. H. Goldstein, J. H. Kroll, N. L. Ng, V. Varutbangkul, R. C. Flagan, and J. H. Seinfeld (2006b), Gas-phase products and secondary aerosol yields from the photooxidation of 16 different terpenes, *J. Geophys. Res.*, *111*, D17305, doi:10.1029/2006JD007050.
- Li, Q., D. J. Jacob, I. Bey, and R. M. Yantosca (2000), Atmospheric hydrogen cyanide (HCN): biomass burning source, ocean sink?, *Geophys. Res. Lett.*, *27*(3), 357–360.
- Li, Q. B., et al. (2003), A global three-dimensional model analysis of the atmospheric budget of HCN and CH₃CN: constraints from aircraft and ground measurements, *J. Geophys. Res.*, *108*(D21), 8827, doi:10.1029/2002JD00375.
- Lide, D. R. (Ed.) (2008), *CRC Handbook of Chemistry and Physics*, 88th ed., CRC Press, Boca Raton, FL.
- Lindinger W., A. Hansel, and A. Jordan (1998), On-line monitoring of volatile organic compounds at pptv levels by means of proton-transfer-reaction mass spectrometry (PTR-MS) – Medical applications, food control and environmental research, *Int. J. Mass Spectrom.*, *173*, 191–241.
- Liu, Y., S. Consta, F. Ogeer, Y. J. Shi, and R. H. Lipson (2007), Geometries and energetics of methanol-ethanol clusters: a VUV laser/time-of-flight mass spectrometry and density functional theory study, *Can. J. Chem.*, *85*, 843–852.

- Lobert, J. M., D. H. Scharffe, T. A. Kuhlbusch, R. Seuwen, and P. J. Crutzen (1991), Experimental evaluation of biomass burning emissions: Nitrogen and carbon containing compounds, in *Global Biomass Burning: Atmospheric, Climatic, and Biospheric Implications*, edited by J. S. Levine, pp. 289–304, MIT Press, Cambridge, MA.
- Mahieu, E., R. Zander, L. Delbouille, P. Demoulin, G. Roland, and C. Servais (1997), Observed trends in total vertical column abundances of atmospheric gases from IR solar spectra recorded at the Jungfraujoch, *J. Atmos. Chem.*, *28*, 227–243.
- Maleknia, S. D., T. L. Bell, and M. A. Adams (2007), PTR-MS analysis of reference and plant-emitted volatile organic compounds, *Int. J. Mass Spectrom.*, *262*, 203–210.
- Mao, H., and R. Talbot (2004), O₃ and CO in New England: Temporal variations and relationships, *J. Geophys. Res.*, *109*, D21304, doi:10.1029/2004JD004931.
- Mao, H., R. Talbot, C. Nielsen, and B. Sive (2006), Controls on methanol and acetone in marine and continental atmospheres, *Geophys. Res. Lett.*, *33*, L02803, doi:10.1029/2005GL024810.
- Martinez, M., D. Perner, E. M. Hackenthal, S. Kulzer, and L. Schutz (2000), NO₃ at Helgoland during the NORDEX campaign in October 1996, *J. Geophys. Res.*, *105*, 22,685–22,695.
- McFarland, M., D. L. Albritton, F. C. Fehsenfeld, E. E. Ferguson, and A. L. Schmeltekopf (1973), Flow-drift technique for ion mobility and ion-molecule reaction rate constant measurements. II. Positive ion reactions of N⁺, O⁺, and N₂⁺ with O₂ and O⁺ with N₂ from thermal to ~2 eV, *J. Chem. Phys.*, *59*, 6620–6628.
- National Data Buoy Center (2004), Station IOSN3 meteorological data, July 2004, NDBC Standard Meteorological Historical Database, Stennis Space Center, Mississippi.
- Ollinger, S. V., J. D. Aber, and C. A. Federer (1998), Estimating regional forest productivity and water yield using an ecosystem model linked to a GIS, *Landscape Ecol.*, *13*, 323–334.
- Orlando, J. J., G. S. Tyndall, E. C. Apel, D. D. Riemer, and S. E. Paulson (2003), Rate coefficients and mechanisms of the reaction of Cl-atoms with a series of unsaturated hydrocarbons under atmospheric conditions, *Int. J. Chem. Kinet.*, *35*, 334–353.
- Osthoff, H. D., S. S. Brown, E. Williams, B. M. Lerner, J. Stutz, S. Trick, H. Stark, A. Pettersson, T. Baynard, and A. R. Ravishankara (2005), Inter-comparison of NO₂, O₃ and NO₃ measurements in the marine boundary layer during NEAQS-ITCT

2004, poster presented at 2005 ICARTT Data Workshop, Durham, New Hampshire, 9–12 August.

- Parrish, D. D., A. Stohl, C. Forster, E. L. Atlas, D. R. Blake, P. D. Goldan, W. C. Kuster, and J. A. de Gouw (2007), Effects of mixing on evolution of hydrocarbon ratios in the troposphere, *J. Geophys. Res.*, *112*, D10S34, doi:10.1029/2006JD007583.
- Pfrang, C., R. S. Martin, A. Nalty, R. Waring, C. E. Canosa-Mas, and R. P. Wayne (2005), Gas-phase rate coefficients for the reactions of nitrate radicals with (Z)-pent-2-ene, (E)-pent-2-ene, (Z)-hex-2-ene, (E)-hex-2-ene, (Z)-hex-3-ene, (E)-hex-3-ene and (E)-3-methylpent-2-ene at room temperature, *Phys. Chem. Chem. Phys.*, *7*, 2506–2512.
- Pikelnaya, O., S. C. Hurlock, S. Trick, and J. Stutz (2007), Intercomparison of multiaxis and long-path differential optical absorption spectroscopy measurements in the marine boundary layer, *J. Geophys. Res.*, *112*, D10S01, doi:10.1029/2006JD007727.
- Pinho, P. G., C. A. Pio, W. P. L. Carter, and M. E. Jenkin (2007), Evaluation of α - and β -pinene degradation in the detailed tropospheric chemistry mechanism, MCM v3.1, using environmental chamber data, *J. Atmos. Chem.*, *57*, 171–202.
- Platt, U., and C. Janssen (1995), Observations and role of the free radicals NO₃, ClO, BrO, and IO in the troposphere, *Faraday Discuss.*, *100*, 175–198.
- Poulton, J. E., and C. P. Li (1994), Tissue level compartmentation of (R)-amygdalin and amygdalin hydrolase prevents large-scale cyanogenesis in undamaged *Prunus* seeds, *Plant. Physiol.*, *104*, 29–35.
- Pszenny, A. A. P., E. V. Fischer, R. S. Russo, B. C. Sive, and R. K. Varner (2007), Estimates of Cl atom concentrations and hydrocarbon kinetic reactivity in surface air at Appledore Island, Maine (USA), during the International Consortium for Atmospheric Research on Transport and Transformation/Chemistry of Halogens at the Isles of Shoals, *J. Geophys. Res.*, *112*, D10S13, doi:10.1029/2006JD007725.
- Reissell, A., S. M. Aschmann, R. Atkinson, and J. Arey (2002), Products of the OH radical- and O₃-initiated reactions with myrcene and ocimene, *J. Geophys. Res.*, *107*(D12), 4138, 10.1029/2001JD001234.
- Rinne, J., T. M. Ruuskanen, A. Reissell, R. Taipale, H. Hakola, and M. Kulmala (2005), On-line PTR-MS measurements of atmospheric concentrations of volatile organic compounds in a European boreal forest ecosystem, *Boreal Env. Res.*, *10*, 425–436.

- Rinsland, C. P., E. Mahieu, R. Zander, P. Demoulin, J. Forrer, and B. Buchmann (2000), Free tropospheric CO, C₂H₆, and HCN above central Europe: Recent measurements from the Jungfraujoch station including the detection of elevated columns during 1998, *J. Geophys. Res.*, 105(D19), 24,235–24,249.
- Rinsland, C. P., A. Goldman, J. W. Hannigan, S. W. Wood, L. S. Chiou, and E. Mahieu (2007), Long-term trends of tropospheric carbon monoxide and hydrogen cyanide from analysis of high resolution infrared solar spectra, *J. Quant. Spectrosc. Radiat. Transfer*, 104, 40–51.
- Roberts, J. M., F. C. Fehsenfeld, S. C. Liu, M. J. Bollinger, C. Hahn, D. L. Albritton, and R. E. Sievers (1984), Measurements of aromatic hydrocarbon ratios and NO_x concentrations in the rural troposphere: Estimates of air mass photochemical age and NO_x removal rate, *Atmos. Environ.*, 18, 2421–2432.
- Roberts, J. M., C. J. Hahn, F. C. Fehsenfeld, J. M. Warnock, D. L. Albritton, and R. E. Sievers (1985), Monoterpene hydrocarbons in the nighttime troposphere, *Environ. Sci. Technol.*, 19, 364–369.
- Rogers, T. M., et al. (2006), On-road measurements of volatile organic compounds in the Mexico City metropolitan area using proton transfer reaction mass spectrometry, *Int. J. Mass. Spectrom.*, 252, 26–37.
- Rohrer, F., and H. Berresheim (2006), Strong correlation between levels of tropospheric hydroxyl radicals and solar ultraviolet radiation, *Nature*, 442, 184–187.
- Schneider, J., V. Bürger, and F. Arnold (1997), Methyl cyanide and hydrogen cyanide measurements in the lower stratosphere: Implications for methyl cyanide sources and sinks, *J. Geophys. Res.*, 102, 25,501–25,506.
- Schofield, K. (2008), The enigmatic mechanism of the flame ionization detector: Its overlooked implications for fossil fuel combustion modeling, *Prog. Energ. Combust.*, 34, 330–350.
- Schoon, N., C. Amelynck, L. Vereecken, and E. Arijs (2003), A selected ion flow tube study of the reactions of H₃O⁺, NO⁺ and O₂⁺ with a series of monoterpenes, *Int. J. Mass Spectrom.*, 229, 231–240.
- Schoon, N., C. Amelynck, L. Vereecken, H. Coeckelberghs, and E. Arijs (2004), A selected ion flow tube study of the reactions of H₃O⁺, NO⁺ and O₂⁺ with some monoterpene oxidation products, *Int. J. Mass Spectrom.*, 239, 7–16.
- Seto, Y., N. Tsunoda, H. Ohta, and T. Shinohara (1993), Determination of blood cyanide by headspace gas chromatography with nitrogen-phosphorous detection and using megabore capillary column, *Anal. Chim. Acta.*, 276, 247–259.

- Schauer, J. J., M. J. Kleeman, G. R. Cass, and B. R. T. Simoneit (2002), Measurement of emissions from air pollution sources. 5. C₁–C₃₂ organic compounds from gasoline-powered motor vehicles, *Environ. Sci. Technol.*, *36*, 1169–1180.
- Shi, Y. J., S. Consta, A. K. Das, B. Mallik, D. Lacey, and R. H. Lipson (2002), A 118 nm vacuum ultraviolet laser/time-of-flight mass spectroscopic study of methanol and ethanol clusters in the vapor phase, *J. Chem. Phys.*, *116*, 6990–6999.
- Shim, C., Y. Wang, H. B. Singh, D. R. Blake, and A. B. Guenther (2007), Source characteristics of oxygenated volatile organic compounds and hydrogen cyanide, *J. Geophys. Res.*, *112*, D10305, doi:10.1029/2006JD007543.
- Shimadzu Corporation (1995), Shimadzu gas chromatograph GC-17A Ver.3 user's manual, Shimadzu Instruments Corporation, Analytical Instruments Division, Kyoto, Japan.
- Shimadzu Corporation (2004), Flame thermionic detector for capillary columns FTD-2014c user's manual, Shimadzu Corporation, Kyoto, Japan.
- Singh, H. B., and P. B. Zimmerman (1992), Atmospheric distribution and sources of nonmethane hydrocarbons, in *Gaseous Pollutants: Characterization and Cycling*, edited by J. O. Nriagu, pp. 177–235, John Wiley & Sons, Inc., New York.
- Singh, H. B., M. Kanakidou, P. J. Crutzen, and D. J. Jacob (1995), High concentrations and photochemical fate of oxygenated hydrocarbons in the global troposphere, *Nature*, *378*, 50–54.
- Singh, H. B., et al. (2003), In situ measurements of HCN and CH₃CN over the Pacific Ocean: sources, sinks, and budgets, *J. Geophys. Res.*, *108*(D20), 8795, doi:10.1029/2002JD003006.
- Sive, B. C. (1998), Atmospheric nonmethane hydrocarbons: Analytical methods and estimated hydroxyl radical concentrations, Ph.D. Thesis, University of California, Irvine, Irvine.
- Sive, B. C., Y. Zhou, D. Troop, Y. Li, W. Little, O. W. Wingenter, R. S. Russo, R. K. Varner, and R. W. Talbot (2005), Development of a cryogen-free concentration system for measurements of volatile organic compounds, *Anal. Chem.*, *77*(21), 6989–6998, doi:10.1021/ac0506231.
- Smith, N., J. M. C. Plane, C.-F. Nien, P. A. Solomon (1995), Nighttime radical chemistry in the San Joaquin Valley, *Atmos. Environ.*, *29*, 2887–2897.
- Španěl, P., and D. Smith (1998), Selected ion flow tube studies of the reactions of H₃O⁺, NO⁺, and O₂⁺ with several aromatic and aliphatic hydrocarbons, *Int. J. Mass Spectrom.*, *181*, 1–10.

- Steeghs, M., H. P. Bais, J. de Gouw, P. Goldan, W. Kuster, M. Northway, R. Fall, and J. M. Vivanco (2004), Proton-transfer-reaction mass spectrometry as a new tool for real time analysis of root-secreted volatile organic compounds in Arabidopsis, *Plant. Physiol.*, *135*, 47–58.
- Stutz, J., B. Alicke, R. Ackermann, A. Geyer, A. White, and E. Williams (2004), Vertical profiles of NO₃, N₂O₅, O₃, and NO_x in the nocturnal boundary layer: 1. Observations during the Texas Air Quality Study 2000, *J. Geophys. Res.*, *109*(D12306), doi:10.1029/2003JD004209.
- Sullivan, R. C., and K. A. Prather (2005), Recent advances in our understanding of atmospheric chemistry and climate made possible by on-line aerosol analysis instrumentation, *Anal. Chem.*, *77*, 3861–3886.
- Talbot, R., H. Mao, and B. C. Sive (2005), Diurnal characteristics of surface level O₃ and other important trace gases in New England, *J. Geophys. Res.*, *110*, D09307, doi:10.1029/2004JD005449.
- Tan, C. Y., and B. Iglewicz (1999), Measurement-methods comparisons and linear statistical relationship, *Technometrics*, *41*, 192–201.
- Tani, A., S. Hayward, and C. N. Hewitt (2003), Measurement of monoterpenes and related compounds by proton transfer reaction-mass spectrometry (PTR-MS), *Int. J. Mass Spectrom.*, *223–224*, 561–578.
- Tani, A., S. Hayward, A. Hansel, and C. N. Hewitt (2004), Effect of water vapor pressure on monoterpene measurements using proton transfer reaction-mass spectrometry (PTR-MS), *Int. J. Mass. Spectrom.*, *239*, 161–169.
- Thornton, J. A., and J. P. D. Abbatt (2005), N₂O₅ reaction on submicron sea salt aerosol: Kinetics, products, and the effect of surface active organics, *J. Phys. Chem. A*, *109*(44), 10,004–10,012.
- Thornton, J. A., C. F. Braban, and J. P. D. Abbatt (2003), N₂O₅ hydrolysis on sub-micron organic aerosols: the effect of relative humidity, particle phase, and particle size, *Phys. Chem. Chem. Phys.*, *5*, 4593–4603.
- Valco Instruments Co., Inc. (1998), Pulsed discharge detector models D-2 and D-2-I instruction manual, Valco Instruments Co., Inc., Houston, TX.
- Vetter, J. (2000), Plant cyanogenic glycosides, *Toxicol.*, *38*, 11–36.
- Vrekoussis, M., N. Mihalopoulos, E. Gerasopoulos, M. Kanakidou, P. J. Crutzen, and J. Lelieveld (2007), Two-years of NO₃ radical observations in the boundary layer over the Eastern Mediterranean, *Atmos. Chem. Phys.*, *7*, 315–327.

- Wahner, A., T. F. Mentel, and M. Sohn (1998), Gas-phase reaction of N_2O_5 with water vapor: Importance of heterogeneous hydrolysis of N_2O_5 and surface desorption of HNO_3 in a large Teflon chamber, *Geophys. Res. Lett.*, *25*, 2169–2172.
- Warneke, C., C. van der Veen, S. Luxembourg, J. A. de Gouw, and A. Kok (2001), Measurements of benzene and toluene in ambient air using proton-transfer-reaction mass spectrometry: calibration, humidity dependence, and field intercomparison, *Int. J. Mass. Spectrom.*, *207*, 167–182.
- Warneke, C., J. de Gouw, W. C. Kuster, P. D. Goldan, and R. Fall (2003), Validation of atmospheric VOC measurements by proton-transfer-reaction mass spectrometry using a gas-chromatographic preseparation method, *Environ. Sci. Technol.*, *37*, 2494–2501.
- Warneke, C., et al. (2004), Comparison of daytime and nighttime oxidation of biogenic and anthropogenic VOCs along the New England coast in summer during New England Air Quality Study 2002, *J. Geophys. Res.*, *109*, (D10309), doi:10.1029/2003JD004424.
- Warneke, et al. (2007), Determination of urban volatile organic compound emission ratios and comparison with an emissions database, *J. Geophys. Res.*, *112*, D10S47, doi:10.1029/2006JD007930.
- Wentworth, W. E., S. V. Vasin, S. D. Stearns, and C. J. Meyer (1992), Pulsed discharge helium ionization detector, *Chromatographia*, *34*, 219–225.
- Wentworth, W. E., H. Cai, and S. Stearns (1994), Pulsed discharge helium ionization detector: Universal detector for inorganic and organic compounds at the low picogram level, *J. Chromatogr. A*, *668*, 135–152.
- White, M. L., et al. (2008), Volatile organic compounds in northern New England marine and continental environments during the ICARTT 2004 campaign, *J. Geophys. Res.*, *113*, D08S90, doi:10.1029/2007JD009161.
- White, M. L., R. S. Russo, Y. Zhou, J. L. Ambrose, K. Haase, E. K. Frinak, R. K. Varner, O. W. Wingenter, H. Mao, R. Talbot, and B. C. Sive (2009), Are biogenic emissions a significant source of summertime atmospheric toluene in the rural Northeastern United States?, *Atmos. Chem. Phys.*, *9*, 81–92.
- Yokelson, R. J., et al. (2007), Emissions from forest fires near Mexico City, *Atmos. Chem. Phys.*, *7*, 5569–5584.
- Zhou, Y., R. K. Varner, R. S. Russo, O. W. Wingenter, K. B. Haase, R. Talbot, and B. C. Sive (2005), Coastal water source of short-lived halocarbons in New England, *J. Geophys. Res.*, *110*, (D21302), doi:10.1029/2004JD005603.

Zhou, Y., H. Mao, R. S. Russo, D. R. Blake, O. W. Wingenter, K. B. Haase, J. Ambrose, R. K. Varner, R. Talbot, and B. C. Sive (2008), Bromoform and dibromomethane measurements in the seacoast region of New Hampshire, 2002–2004, *J. Geophys. Res.*, *113*, D08305, doi:10.1029/2007JD009103.